Uncovering the Potential for Oxidized Phosphatidylcholines as Unique Drivers of Asthma Pathobiology

by

Jigneshkumar Vaghasiya

A thesis submitted to the Faculty of Graduate Studies of
The University of Manitoba
in partial fulfilment of the requirements of the degree of

Doctor of Philosophy

Department of Physiology & Pathophysiology
University of Manitoba
Winnipeg, Manitoba, Canada

Table of Contents

Abstract

Asthma pathobiology is characterized by persistent oxidative stress in the lungs that causes oxidative damage in the cell membrane and extracellular phospholipids. This damage results in the accumulation of oxidized phosphatidylcholines (OxPC), potent mediators of oxidative stress. We recently discovered that allergen challenge causes OxPC accumulation in the lungs of human participants that correlates with airway hyperresponsiveness (AHR). OxPC also play a significant role in the pathophysiology of human airway smooth muscle (HASM) cells. The research projects outlined in this thesis aimed to elucidate the functional effects of OxPC on HASM cells, and to identify the downstream effector(s) and/or signaling pathway(s) mediating these effects. Furthermore, we investigated the potential impact of OxPC on the pathophysiologic hallmarks of allergen-induced 'asthma' in a murine model.

Our findings demonstrate that OxPC directly induce airway narrowing in murine thin-cut lung slices (TCLS) and activate the contractile machinery within HASM cells. OxPC mediate both transient and sustained cytosolic Ca^{2+} flux through two distinct pathways: intracellular ryanodine receptors and plasma membrane transient receptor potential ankyrin 1 (TRPA1) channels. These pathways are interdependently required for OxPC-induced HASM contraction and airway narrowing. Next, we demonstrated that OxPC selectively attenuate HASM relaxation in response to bronchodilators (β_2-adrenergic receptor (β_2AR) agonists; isoproterenol, albuterol) using both *ex vivo* (murine tracheal rings and TCLS) and *in vivo* models. These effects correlate with a diminished cyclic-adenosine-monophosphate (cAMP) signaling cascade within HASM cells. The results from this study revealed that OxPC uncouple β_2AR signaling from downstream effectors via activation of protein kinase-C (PKC), a mechanism contributing to the development of bronchodilator insensitivity. Furthermore, we characterized the exacerbation of oxidative burden

within the lungs of a murine model of allergic asthma, observing a concomitant increase in OxPC accumulation. In this model, we showed that immuno-pharmacological neutralization of OxPC using intranasal E06 monoclonal antibody can prevent allergen-induced airway inflammation and AHR.

Collectively, our results indicate that bioactive OxPC are pivotal mediators of oxidative stress-associated allergic lung pathophysiology. These molecules directly contribute to airway contraction and induce bronchodilator insensitivity by modulating airway smooth muscle function, an implication for the phenotype of poorly controlled asthma.

Acknowledgements

I would like to first express my profound gratitude to my supervisor Dr. Andrew J. Halayko whom without his support, guidance, and mentorship along this journey I would never have seen the potential of earning the doctorate, a passion of my professional life. The completion of these studies wouldn't have been possible without the sheer support of Dr. Halayko who has guided me in every step of my PhD journey and openly endorsed my ideas. I expressed my heartfelt gratitude for this opportunity given by him in the middle of my career. Next, I would like to acknowledge my academic committee members Dr. Ian Dixon, Dr. Shyamala Dakshinamurti and Dr. Abdel Soussi Gounni for their constant guidance, critical review and insight.

I next would like to acknowledge not only for technical support but also general help that I received from, both past and present Halayko lab colleagues, Dr. Chris Pascoe, Dr. Aruni Jha, Sujata Basu, Dr. Thomas Mahood, Jacquie Shwartz, Gerald Stelmack, Dr. Anurag Sikarwar, Azadeh Dalvand, and Dheer Pandey. I would also like to recognize the contributions made by undergraduate summer students in the research project; Nathan Varghese, Alaina Bagan, Divleen Mangat, Yuchuan Li, Katarina Kowatsch, Angela Duaqui, Sparshita Mishra, Mirna Ragheb, and Siwon Jengsuksavat. I enjoyed supervising their summer projects and it was fun training and mentoring diverse young talents during my PhD journey. I would also like to acknowledge our collaborator Dr. Amir Ravandi, who brought valuable expertise to the success of my project.

I would like to convey special thanks to the former and present department head, Drs. Peter Cattini and Ian Dixon, respectively, administrative staff at the Dept. of Physiology, Gail McIndless, Judith Olfert, and Jenna Trupish as well as administrative staff at the Children's Hospital Research Institute of Manitoba (CHRIM), Nichola Wigle, Debbie Korpesho, and Lana Peters for their constant support and guidance in administrative issues. I would like to acknowledge Dr. Abdel Soussi Gounni and his lab for providing training on flow cytometry, and our international collaborators, Dr. Raymond B. Penn (Thomas Jefferson University) and Dr. J. L. Witztum (University of California (San Diego)) for their help with technical aspects of this project. I must also thank Dr. Dedmer Schaafsma (Science Impact) for his editorial work that improved the current thesis immensely.

I would also like to acknowledge the financial assistance from: Research Manitoba, Children's Hospital Research Institute of Manitoba (CHRIM), Rady Faculty of Health Sciences, Faculty of Graduate Studies and Department of Physiology and Pathophysiology, University of Manitoba, Canadian Respiratory Research Network, Canadian Lung Association, and American Thoracic Society.

Finally, I could not thank my family, wife Saroj, son Dhyey and daughter Ruhi, enough times for tirelessly supporting me through my entire PhD journey, especially for being the reason to smile during the demanding times of my PhD journey. Without them, this journey would have been merely a dream. I would like to specially acknowledge my friends who I met for the first time in Winnipeg,

Rajendra, Rakesh, Aruni, Sujata and Prajwal for their generous help during my first-time arrival in the middle of winter and thereafter setting up family life here. Those relations are now continuing as family relations. Last but not least, I must also thank my parents and my brothers who always supported me in all my endeavors in life.

Dedication

Dedicated to my wonderful wife "SAROJ", who has always been a source of inspiration and pillar of support ever since she came into my life... thank you for being there to support my passion!!!

Dedicated to my lovely son "DHYEY" and beautiful daughter "RUHI", who always been a source of joy and delight to my family ever since they were born!!!

Dedicated to my parents and brothers for their untiring love and endless blessings ...thank you for making me what I'm today!!!

Lists of Figures

Lists of Tables

Lists of Copyright Material (Permission obtained)

List of Abbreviations

AC	Adenylate cyclase
Ach	Acetylcholine
AHR	Airway hyperresponsiveness
AITC	Allyl isothiocyanate (oil of mustard)
Alb	Albuterol
ALI	Acute lung injury
AM	Alveolar macrophages
ApoA-I	Apolipoprotein A-I
ASM	Airway smooth muscle
ATP	Adenosine triphosphate
AP-1	Activated protein-1
BAL	Bronchoalveolar lavage
BALF	Bronchoalveolar lavage fluid
DAG	Diacylglycerol
DAMP	Damage-associated molecular pattern
DCs	Dendritic cells
cADDis	cAMP difference detector in situ
cADPR	Cyclic adenosine diphosphate ribose
cAMP	Cyclic adenosine monophosphate
CD38	Cluster of differentiation 38
COPD	Chronic obstructive pulmonary disease
COX	Cyclooxygenase
CPI-17	Protein kinase C-potentiated inhibitor protein of 17 kDa
CTS	Canadian Thoracic Society
E06 mAb	E06 mouse monoclonal IgM antibody
E06-scFv	Single-chain variable fragment of E06
ECM	Extra cellular matrix
EGF	Epidermal growth factor
Eos	Eosinophils
ESC	Embryonic stem cells
EPAC	Exchange proteins activated by cAMP
FACS	Fluorescence activated cell sorting
FeNO	Fractional exhaled nitric oxide
FEV1	Forced expiratory volume in 1 second
G	Peripheral tissue damping
Gd^{3+}	Gadolinium chloride
GINA	Global Initiative for Asthma
GRs	Glucocorticoid receptors
GRE	Glucocorticoid response element
H	Tissue elastance

HA	Hemagglutinin
HASM	Human airway smooth muscle
HBSS	Hanks Balanced Salt Solution
HDL	High density lipoproteins
HDM	House dust mite
HEK-293	Human embryonic kidney-293
HEPES	4-(2-hydroxyethyl)-1-piperazineethanesulfonic acid
HO-1	Heme oxygenase 1
HRP	Horseradish peroxidase
i.n.	Intranasal
i.p.	Intraperitoneal
I/R	Ischemia/Reperfusion
ICS	Inhaled corticosteroids
ILC2	Innate lymphoid type-2 cells
IM	Interstitial macrophages
IP_3	Inositol 1,4,5-triphosphate
Iso	Isoproterenol
K-H	Krebs-Henseleit bicarbonate buffer
LABA	Long-acting β2 adrenergic receptor agonist
LP-PLA2	Lipoprotein-associated phospholipase A2
LTRA	Leukotriene receptor antagonist
Mch	Methacholine
MDA	Malondialdehyde
MLC	Myosin light chain
MLCK	Myosin light-chain kinase
MLCP	Myosin light-chain phosphatase
Neu	Neutrophils
NFE2L2	Nuclear factor erythroid 2-related factor 2 or NRF2
NF-κB	Nuclear factor-κB
NLRP3	Nucleotide-binding domain, leucine-rich–containing family, pyrin domain–containing-3
NMDA-R	N-methyl-D-aspartate receptor
NPS	Neuronal precursor cell
OSEs	Oxidation specific epitopes
OxPAPC	Oxidized 1-palmitoyl-2-arachidonoyl-sn-glycero-3-phosphocholine
OxPC	Oxidized phosphatidylcholines
OxPL	Oxidized phospholipids
PAF-AH	Platelet-activating factor-acetylhydrolase
PAPC	1-palmitoyl-2-arachidonoyl-sn-glycero-3-phosphocholine
PC20	Provocative concentration (causes 20% fall in FEV1)
PEIPC	1-palmitoyl-2-(5,6)-epoxyisoprostane E2-sn-glycero-3-phosphocholine
PFA	Paraformaldehyde
PGPC	1-palmitoyl-2-glutaroyl-sn-glycero-3-phosphocholine

PIP_2	Phosphatidylinositol 4,5-bisphosphate
PKA	Protein kinase A
PKC	Protein kinase C
PLC	Phospholipase C
PM	plasma membrane
p-MLC	Phosphorylated Myosin light chain
POVPC	1-palmitoyl-2-(5-oxovaleroyl)-sn-glycero-3-phosphocholine
PRRs	Pattern recognition receptors
PSPC	1-palmitoyl-2-stearoyl-sn-glycero-3-phosphocholine
PUFA	Polyunsaturated fatty acids
p-VASP	Phosphorylated vasodilator-stimulated phosphoprotein
ROC	Receptor-operated Ca^{2+} channels
ROCK	Rho-associated protein kinase
ROS	Reactive oxygen species
Rrs	Respiratory resistance (total)
RyR	Ryanodine receptors
SABA	Short-acting β2 adrenergic receptor agonist
SERCA	Sarcoplasmic/endoplasmic reticulum Ca^{2+}-ATPase
SOC	Store-operated Ca^{2+} channels
SOD	Superoxide dismutase
SR	Sarcoplasmic reticulum
TCLS	Thin-cut lung slices
TGF-β	Transforming Growth Factor-β
TLR	Toll-like receptors
TNF	Tumor necrosis factor
TPA	12-O-tetradecanoylphorbol-13-acetate
TRP	Transient receptor potential
TRPA1	Transient receptor potential ankyrin 1
TRPC	Transient receptor potential canonical
TSLP	Thymic stromal lymphopoietin
VASP	Vasodilator-stimulated phosphoprotein
VGC	Voltage-gated Ca^{2+} channels
β_2AR	β_2 adrenergic receptor
βARA	β_2 adrenergic receptor agonist
$[Ca^{2+}]_i$	Intracellular Ca^{2+} concentration
4-HNE	4-hydroxynonenal
8-Br-cADPR	8-bromo-cyclic adenosine diphosphate ribose
8oxodG	8-oxo-2′-deoxyguanosine

Chapter 1: Introduction

1.1 Asthma

Asthma is a chronic lung disease of the conductive airways marked by persistent airway inflammation with episodes of wheezing, bronchial spasms, and airway hyperresponsiveness (AHR) to inhale allergic and non-allergenic stimuli [1]. Sir John Foyer was first to identify difficulty in breathing due to constriction of the airways as described in his treatise published in 1698 [2]. In 1860, Henry Hyde Salter defined asthma as "paroxysmal dyspnoea of a peculiar character with intervals of healthy respiration between attacks" to differentiate it from other causes of breathlessness [3], and he was first to describe airway hyperreactivity and identify some immune cells in sputum from asthmatics. Approximately 30 years later, Sir William Osler in his first edition of "*The principles and practice of medicine*" published in 1892, defined many features that are currently associated with asthma, including a special form of airway inflammation [4]. Airway "hyperresponsiveness" and "inflammation", as first described by Salter and Osler respectively in the early 19th century, are still clinically considered the "hallmark features of asthma" in the modern concept of disease pathophysiology. Asthma is now recognized as a disease that can exhibit heterogeneous phenotypes with various underlying etiologies [5]. According to the Global Initiative for Asthma (GINA) [6], the consensus definition of asthma is standardized as "a heterogeneous disease, usually characterized by chronic airway inflammation. Asthma is defined by the history of respiratory symptoms such as wheeze, shortness of breath, chest tightness and cough that vary over time and in intensity, together with variable expiratory airflow limitation."

1.2 Prevalence and burden of asthma

According to the Global Burden of Disease Study 2019, asthma affected an estimated 262 million people globally [7], making it one of the most common chronic lung diseases and causing significant morbidity [7, 8]. Asthma prevalence varies from 1% to 29% across different geographical regions (Figure 1.1) [9-11]. It affects all age groups from both sexes but is influenced by age and gender (Figure 1.1 and 1.2) [8, 9, 11]. For instance, asthma is more prevalent in males than females during childhood, a trend that reverses in adulthood (Figure 1.2). Asthma prevalence peaks between the ages of 5 and 9 years followed by a declining trend up to the 25-29 years age range, after which it continuously increases with age (Figure 1.2). The direct healthcare as well as indirect economic burden (e.g., because of school or work absenteeism) associated with asthma is substantial [12, 13]. For instance, the aggregate direct healthcare and indirect costs was amounted to $81.9 billion in the United States alone in 2013 [14]. Despite the availability of advanced therapy, there is a substantial unmet medical need for uncontrolled asthma [15]. For the next 20 years, the total economic burden of asthma is estimated to be $963.5 billion for the United States only, of which $300.6 billion is for direct health care [13]. Therefore, there is a need for preclinical proof-of-concept demonstrating a novel mechanism(s) of disease pathobiology that could eventually support development of new therapy and/or improvement in efficacy of the conventional therapy, in order to improve quality of life for patients and lessen economic burden on society.

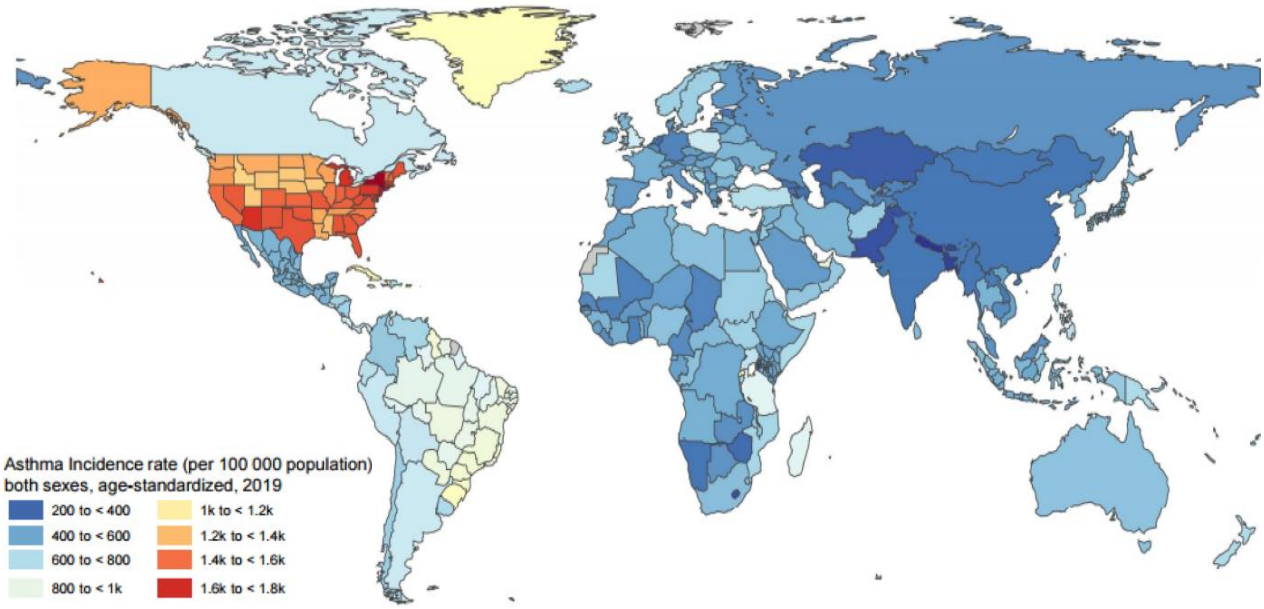

Figure 1.1: Global distribution of the asthma prevalence rate.
Color on the global map shows the age-standardized rate (per 100,000 population) of both sexes in 2019. Reproduced with permission from John Wiley and Sons via Copyright Clearance Center from previously published article [8].

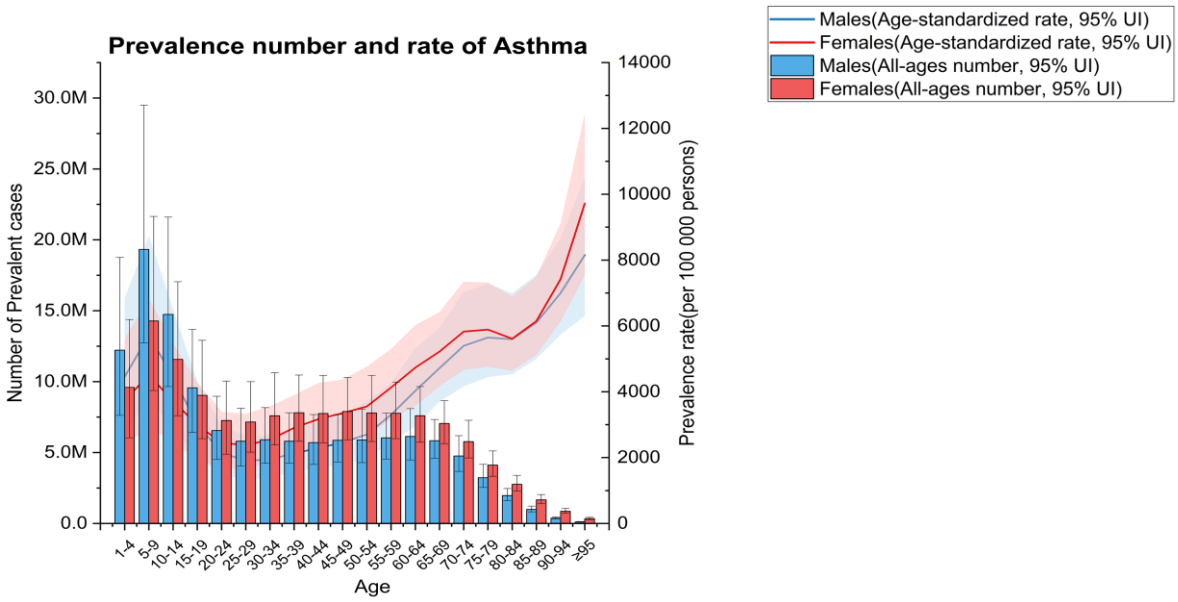

Figure 1.2: Global asthma prevalent cases and rates by age in 2019.
Reproduced with permission from John Wiley and Sons via Copyright Clearance Center from the published article [8].

1.3 Pathophysiology of asthma

Airway hyperresponsiveness (AHR) of the conductive airways is a cardinal feature of asthma and at least in part due to inflammation. Airway inflammation is a complex immunological process that involves various immune cells and inflammatory mediators within the airways, playing a central role in disease pathogenesis. Chronically inflamed airways are typically subject to various structural changes of the airway wall; these are collectively referred to as airway remodeling, a process linked to the development of persistent AHR and progressive lung function decline.

1.3.1 Airway inflammation and immunology

Airway inflammation in asthma is a highly complex process and plays a central role in disease pathogenesis. Asthma is often triggered by exposure to specific allergens, (non-specific) irritants, or respiratory infections. For example, allergens such as house dust mite, mold, pollen, or animal dander can lead to an allergic response in susceptible individuals, while non-allergic irritants like smoke and other air pollutants can also trigger asthma symptoms [16]. In response to these triggers, the immune system reacts in a bi-phasic manner with early and late phase asthmatic responses. The early phase response occurs within minutes of allergen exposure, which is triggered by mast cell degranulation, releasing histamine, prostaglandin D2, leukotriene C4, and mast cell-specific tryptase, leading to bronchoconstriction, airway edema and mucus secretion [17]. At the same time, activated epithelial and dendritic cells (DCs) orchestrate a late-phase adaptive immune response, mainly involving Th2 lymphocytes and type 2 immune response (Figure 1.3). Thus, activated DCs and epithelial-derived alarmin cytokines [Interleukins (IL)-25, IL-33, Thymic stromal lymphopoietin (TSLP)] parallelly initiate the production and migration of Th2 cells to create Th2 cytokine-rich milieu (IL-4, IL-5, IL-13) in local airway tissues, which subsequently drives a cascade of downstream events [18-20]. For example, IL-5 acts on eosinophils to promote

activation, maturation, survival and recruitment into the airways, whereas IL-4 stimulates B cells to produce allergen-specific IgE [21-23]. Recruited eosinophils release additional pro-inflammatory substances that mediate prolonged inflammation, AHR, and goblet cell metaplasia [24, 25]. Recent advances in asthma immunology have revealed a role of type 2 innate lymphoid (ILC2) cells in perpetuating type 2 immunity [26, 27]. Epithelial-derived alarmin cytokines can directly stimulate ILC2 cells to mediate the type 2 immune response and airway eosinophilic inflammation independent of the adaptive immune response (reviewed by Hammad and Lambrecht) [26]. Activated eosinophils in the airway release a meshwork of DNA fibers, granule proteins, reactive oxygen species (ROS), and crystals which cause tissue damage, mucus plugging, and perpetuation of the cycle of innate and adaptive immunity [25, 28, 29].

Additionally, a clinically sub-group of asthma patients exhibits a pre-dominant accumulation of neutrophils in the airway (*i.e.*, a non-type 2 immune response; an asthma phenotype not characterized by a typical Th2 cytokine profile) [30, 31]. Hammad and Lambrecht [27] have reviewed various pre-clinical and clinical studies to reveal potential pathways for neutrophil accumulation in the airway (Figure 1.4). Briefly, these mechanisms include the activation of alveolar macrophages and epithelial cells following exposure to environmental triggers (i.e. smoke, pollutant, or microbial exposure), which results in the release of pro-inflammatory cytokines (IL-1β, IL-6, or IL-8) and, consequently, recruitment and activation of neutrophils in the airways [20, 27]. In addition, activated Th1/Th17 lymphocytes promote neutrophil recruitment and degranulation (Figure 1.4), leading to release of various toxic factors such as neutrophil elastase, myeloperoxidase, or ROS that can cause cellular damage.

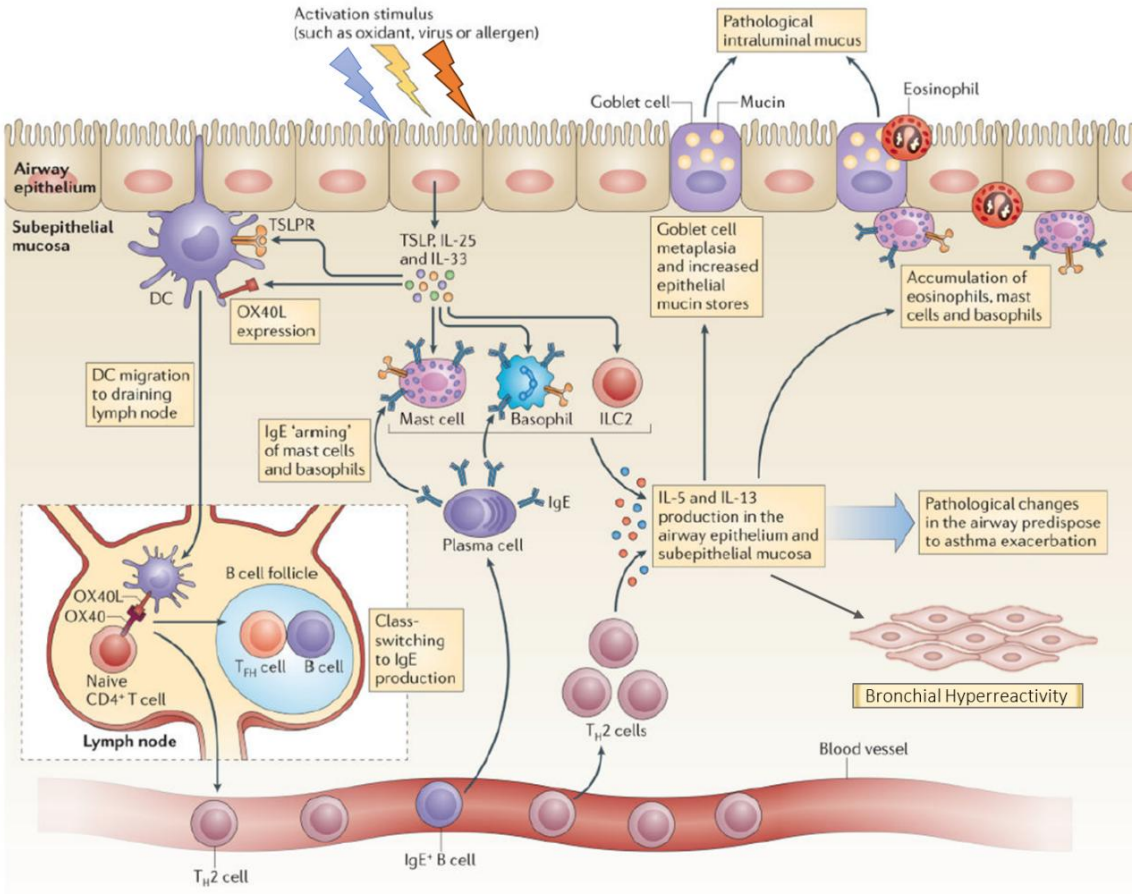

Figure 1.3: Schematic representation of the type 2 immune response in asthma.
The type 2 immune response in the airways is mainly mediated by eosinophils, mast cells, basophils, Th2 cells, group 2 innate lymphoid cells (ILC2) and IgE-producing B cells. Allergen engulfed by dendritic cells (DCs) and/or DCs under the influence of epithelial derived cytokines migrate to the local lymph nodes where they activate Th2 cells production and migration to the airway. Th2 cells produce IL-5, IL-13 and IL-4, of which the later mediates IgE class-switching in B cells. IL-5 and IL-13 mediate eosinophilic inflammation, bronchial hyperreactivity, and mucus production. In parallel, epithelial cytokines (TSLP, IL-25 and -33) can directly stimulate mast cells, basophils, or ILC2 to drive type 2 immune response. Reproduced with permission from Nature Research via Copyright Clearance Center from previously published article [19]. DC: dendritic cells, TSLP: thymic stromal lymphopoietin, ILC2: innate lymphoid cells type 2.

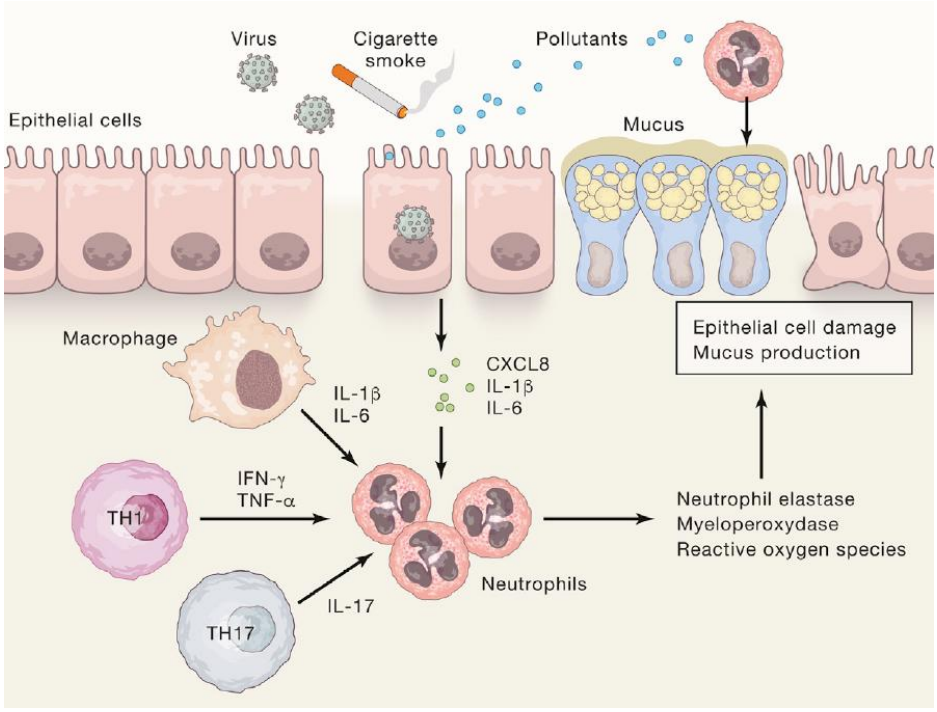

Figure 1.4: Schematic of the none type 2 immune response in asthma.
Certain environmental triggers such as microbes or air pollutants stimulate airway epithelial cells and alveolar macrophages to produce pro-inflammatory cytokines (IL-1β, IL-6); in addition, the epithelium can produce the potent neutrophil attractant CXCL8 (known as IL-8). Th1- and Th17- derived cytokines also promote neutrophil recruitment and activation. Adopted with permission from Elsevier via Copyright Clearance Center from a previously published article [27].

1.3.2 Airway remodeling

Airway remodeling in asthma results from chronic airway inflammation and concomitant tissue injury and/or abnormal repair; it is pathologically characterized by various structural changes in the airway epithelial and subepithelial layer (Figure 1.5) [32]. These include; i) shredding, exudation, and (functional) abnormality of epithelial cells [33-35], ii) goblet cell hyperplasia and increased mucus production [36], iii) basement membrane thickening [37] and extracellular matrix deposition and fibrosis [38-40], and iv) an increase in ASM mass (due to ASM cell hypertrophy and hyperplasia) [41, 42]. Many of these pathological changes in epithelial cells are recapitulated in a recent single-cell RNA sequencing study of airways from asthmatic patients [43]. These structural changes contribute to the overall thickening of the airway wall and baseline airway closure [44]. Conceivably, remodeled airways impose a greater risk for airway flow obstruction when ASM contracts [45].

The continuous lining of the epithelial barrier structure in the airways provides physical protection against inhaled environmental insults. This epithelial barrier is impaired in asthma due to the loss of adherens and tight junction proteins like desmosomes, E-cadherin, β-catenin, ZO-1, and occludin, which results in functional loss and increase permeability [46, 47]. Such structural changes in the epithelium start early in the remodeling process and have been observed in atopic children even before clinical diagnosis of asthma [48]. In asthma, the epithelial layer shows an increase in goblet cells and goblet cell metaplasia as well as decrease in ciliated cells, which collectively causes an increase in mucus production with dysfunctional mucociliary clearance [41]. Inflammatory cytokines such as IL-13 also promote goblet cell metaplasia [49] and can affect epithelial barrier integrity [50]. Stimulated epithelial and infiltrated inflammatory cells release growth factors like epidermal growth factors (EGF) and transforming growth factor-β (TGF-β) [51,

52], which activate fibroblasts and myofibroblasts. This principally contributes to airway wall thickening by induction of excessive ECM deposition in the reticular basement membrane region and submucosa (subepithelial fibrosis), and ASM hypertrophy and hyperplasia [42, 53].

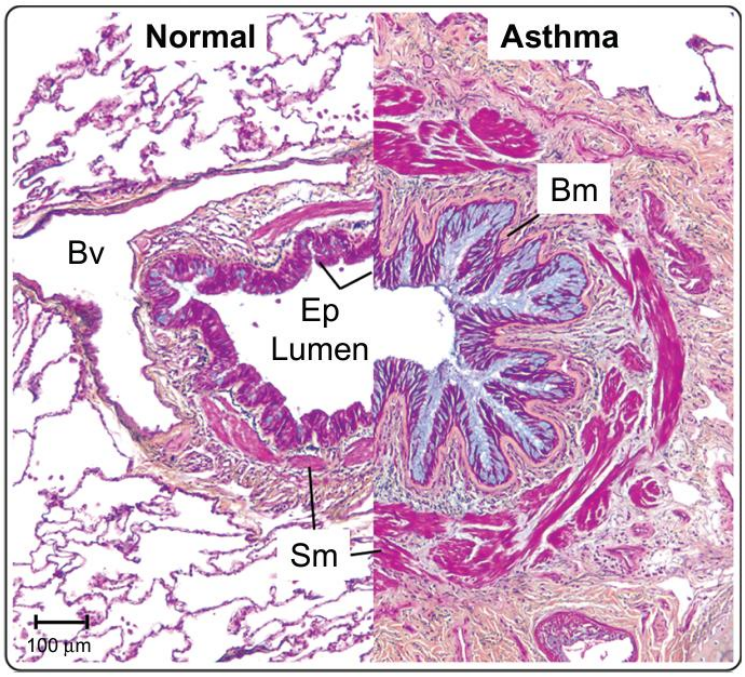

Figure 1.5: The pathological features of airway remodeling in asthmatics.
This image compares a cross-section of a medium-sized airway from a healthy individual (left) and a severe asthma patient (right) donor. Movat's pentachrome staining reveals histopathological changes such as mucus hypersecretion (blue staining in the epithelium (Ep)), basement membrane (Bm) thickening, and an increase in smooth muscle (Sm) in the diseased airway. Scale bar 100 µm; Bv: blood vessel. Adopted from [32] with permission from Dove Medical Press under the Creative Commons Attribution License.

1.3.3 Airway hyperresponsiveness

AHR is a clinically defining characteristic of asthma. ASM cells in the sub-epithelium of the conductive airways constitute the principal cell type responsible for controlling airway diameter and, therefore, airway caliber. AHR is characterized by a tendency of ASM cells to contract in response to nonspecific stimuli (e.g., cold air, exercise) and an exaggerated response to contractile agents (e.g. acetylcholine and histamine) [54]. Clinically, AHR is diagnosed via a bronchoprovocation test with inhaled methacholine (an acetylcholinesterase resistant analog of acetylcholine); this is the only chemical challenge approved for human use in North America [55]. The increase in airway resistance in response to methacholine challenge is quantified by estimating the volume of air exhaled within the first second of a forced expiration (FEV_1). Assessment of the methacholine provocative concentration causing a 20% fall in FEV_1 ($[PC_{20}]$) is the current diagnostic standard. Asthma patient with AHR generally exhibit a PC_{20} <8 mg/mL of methacholine depending on disease severity (i.e. lower PC_{20} indicates a higher degree of AHR), while PC_{20} values exceed 16 mg/mL in most healthy individuals (Figure 1.6) [54].

Although AHR is an integral part of asthma disease, the mechanisms underpinning AHR in asthma remain incompletely understood. *In vivo* measurements of airway responsiveness reflects various interacting factors and AHR is now recognized to be present in two components, episodic and persistent AHR, based on underlying disease pathobiology [56, 57]. Episodic AHR is a more likely consequence of direct exposure to asthma triggers and mediators released during early inflammation, whereas persistent AHR has been increasingly associated with the permanent structural and/or pathophysiological changes in the airway wall observed under conditions of chronic inflammation [56]. ASM is considered the primary effector of AHR, which is supported by the underlying pathophysiology of airway inflammation and remodeling [58]. There are

additional factors such as genetic predisposition and environmental interaction [54, 59] that can also contribute to AHR as well.

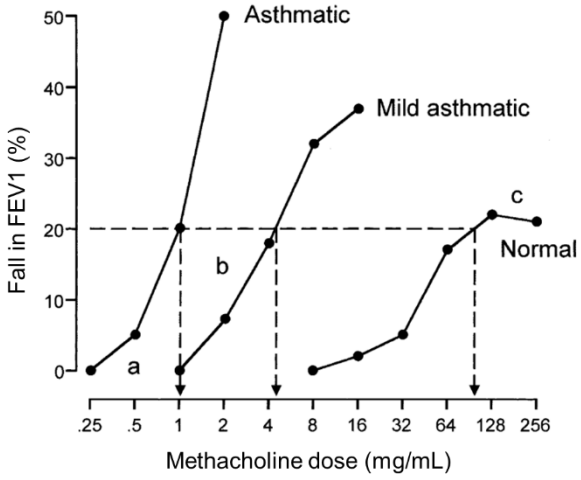

Figure 1.6: Illustration of AHR in asthmatics as assessed by a methacholine provocation test.
The curves compare % fall in FEV1 from baseline in response to increasing methacholine doses in patients with mild and severe asthma vs healthy individuals. The PC_{20} is calculated by interpolating a 20% fall in FEV1 to the log-linear dose-response curve for each individual (dash lines). Asthmatic subjects have a reduced threshold response (a) indicating increased airway sensitivity. An increased slope (b) represents enhanced airway reactivity, whereas (c) represents the maximal (plateau) response; the latter is typically not achieved in patients with AHR as it would be fatal. Adopted from a previously published article [54] with permission from Elsevier and Copyright Clearance Center Inc. FEV1: forced expiratory volume in 1 second.

1.3.3.1 Airway smooth muscle (ASM) in airway hyperresponsiveness

The contractile function of ASM surrounding the airways is to regulate airway diameter; therefore, it can be envisioned that abnormalities of ASM function may directly affect muscle tone and contributes to AHR. Indeed, mathematical modeling has shown that the ASM layer within the structure of airway wall is a major contributor to the airway closure and AHR development in severe asthma [60, 61]. Chapman and Irvin have extensively reviewed various intrinsic or extrinsic factors in [59] that are associated with ASM abnormality. Intrinsic factors favoring excessive ASM contractility include an increase in ASM mass within the airway wall, increased expression of contractile proteins (α-smooth muscle actin and desmin) in the ASM layer, enhanced cellular myosin light-chain kinase (MLCK) activity, and altered shortening velocity of ASM in the diseased state [42, 62-64]. Furthermore, lung elasticity is compromised in asthma [65], which reduces the elastic force against which ASM contracts, thereby indirectly increasing ASM shortening velocity [66].

Extrinsic factors such as pro-inflammatory cytokines and mediators released by inflammatory cells can cause exaggerated ASM responsiveness. Some pro-inflammatory cytokine TNF (Tumor necrosis factor) and Th2 cytokines (IL-4 and IL-13) directly act on ASM to enhance the response of contractile agonists [67-69]. Degranulation of accumulated mast cells within the ASM layer can also induce ASM contraction by releasing pro-contractile mediators like histamine, prostaglandin D2, and cysteinyl leukotrienes [70]. Toxic granules released by eosinophils in the proximity of nerve endings in the airway wall stimulate parasympathetic nerves, which also leads to increased irritant sensitivity and exaggerated airway responsiveness [71]. Airway epithelial damage is another extrinsic factor that likely contributes to AHR; damaged epithelial barrier increases penetration of contractile mediators that directly interact with ASM. Additionally, local injury to

epithelial cells results in the release of soluble mediators that can act as triggers for global ASM contraction [72].

In summary, intrinsic factors typically increase ASM maximum contractility and shift the contractile dose-response curve upwards, whereas extrinsic factors generally sensitize ASM to contractile stimuli and help to shift the contractile dose-response curve leftwards (as described in Figure 1.6). Collectively, these factors are instrumental to the development of AHR in asthma [73].

1.4 Airway smooth muscle

The primary role of ASM is active force generation and cell shortening. Under healthy conditions, ASM fine-tunes basal airway tone and caliber. However, in asthma, its functional involvement appears to be amplified [74] as indicated by studies showing that mechanical ablation of the ASM layer by thermoplasty can suppress symptoms in patients with severe disease state and significantly improve quality of life [75]. An increased functional role for ASM under pathophysiological conditions is supported by an ever-growing body of evidence showing that ASM has various pathobiological roles, including the production of pro-inflammatory cytokines, chemokines, growth factors, ECM production, and has the ability to undergo phenotype and mechanical plasticity [76]. The principal (intra)cellular mechanisms driving ASM contraction and relaxation are described below.

1.4.1 Mechanism of ASM contraction

An increase in the intracellular Ca^{2+} concentration ($[Ca^{2+}]_i$) is the primary trigger for the initiation of ASM contraction, and that is coordinated by Ca^{2+} release from intracellular stores and Ca^{2+} influx via plasma membrane channels as depicted in Figure 1.7 [77]. Gq protein-coupled receptors such as the muscarinic (M)3, histamine (H)1, and cysteinyl leukotriene (CLT) 1 receptors are expressed on the surface of ASM cells and play a prominent role in contraction [78]. Spasmogens, including acetylcholine from parasympathetic nerve endings and mediators (*e.g.*, histamine, leukotrienes, and prostaglandins etc.) released by inflammatory cells, are able to activate their specific Gq protein-coupled receptors on ASM. This leads to the downstream activation of phospholipase C (PLC), an enzyme that converts phosphatidylinositol 4,5-bisphosphate (PIP_2) into inositol 1,4,5-trisphosphate (IP_3) and 1,2-diacylglycerol (DAG). Next, IP_3 in cytoplasm activates IP_3 channel of the sarcoplasmic reticulum (SR) to induce cytoplasmic Ca^{2+} flux. This is followed

by subsequent Ca^{2+} -mediated opening of ryanodine receptors (RyR) to provide an additional pool of SR Ca^{2+} (known as Ca^{2+}-induced Ca^{2+} release) [77, 79]. The sarco/endoplasmic reticulum Ca^{2+}ATPase (SERCA) on the SR pumps Ca^{2+} back into SR [80]; at the same time, SR Ca^{2+} store are also replenished by store-operated Ca^{2+} channels (e.g. Orai1, TRPC). This repeated release and re-uptake of Ca^{2+} by SR causes cytoplasmic Ca^{2+} oscillations. The cationic channels (e.g., Transient receptor potential ankyrin 1 (TRPA1), N-methyl-D-aspartate receptor (NMDA-R)) and voltage-gated channels (VGC) also provide an additional pool of Ca^{2+} influx [81-83]. Of note, intracellular RyR on the SR can also be independently activated by CD38/cADPR to cause Ca^{2+} release from the SR [84]. Overall, ASM expresses multiple functional Ca^{2+} handling proteins which help to maintain elevated $[Ca^{2+}]_i$ under stimulated conditions.

This cytosolic-free Ca^{2+} binds to calmodulin and the Ca^{2+}-calmodulin complex activates myosin light chain kinase (MLCK), which is a key regulatory enzyme in ASM contraction. MLCK phosphorylates the 20 kDa regulatory myosin light chain (MLC20) enabling the interaction between myosin and actin filaments ("cross-bridge cycling") to generate force and cause muscle contraction [85]. On the other side, myosin light chain phosphatase (MLCP) dephosphorylates MLC, thereby counteracting MLCK activity to inhibit contraction [85]. The relative balance of activity between MLCK and MLCP determines the degree of MLC phosphorylation and contractile state of ASM [85]. Two main (parallel) pathways have been shown to interfere with this equilibrium by inhibiting the activity of MLCP, which leads to prolonged MLC phosphorylation (and contraction) without requiring an additional increase in $[Ca^{2+}]_i$. The first pathway involves RhoA/Rho-kinase (ROCK) signaling, and the second is driven by DAG/protein kinase C (PKC)-mediated CPI-17 (protein kinase C-potentiated inhibitor protein of 17 kDa) phosphorylation as illustrated in Figure 1.7 [86, 87]. The enhancement of MLC phosphorylation

at a fixed $[Ca^{2+}]_i$ is referred to as "Ca^{2+} sensitization", a process that has been linked to AHR in (models) of allergic asthma [88, 89].

1.4.2 Mechanism of ASM relaxation

ASM expresses several Gs-coupled receptors, including well-known β_2-adrenergic receptor (β_2AR) that play a crucial role in ASM relaxation by inhibiting the contractile machinery in ASM (as shown in Figure 1.7) [78]. When an agonist (e.g., adrenaline) binds to β_2AR, Gs uncouples from receptor and activates its effector adenylyl cyclase to convert cytoplasmic adenosine triphosphate (ATP) into cyclic adenosine 3′, 5′-monophosphate (cAMP) [78]. The intracellular cAMP has a multifunctional role in ASM relaxation via its effector proteins, protein kinase A (PKA) and exchange protein activated by cAMP (EPAC) [90]. However, cAMP/PKA is the predominant signaling pathway involved in ASM relaxation, while independent role of EPAC in ASM relaxation is not well-understood yet [91, 92]. PKA phosphorylates the IP_3 receptor (reducing its affinity for IP_3) to inhibit Ca^{2+} mobilization and inhibits the activity of various contractile proteins such as Gq, MLCK, and PLC [78]. Simultaneously, PKA also activates Ca^{2+}-gated potassium (K^+) channels on the plasma membrane to induce membrane hyperpolarization and further promote relaxation [93].

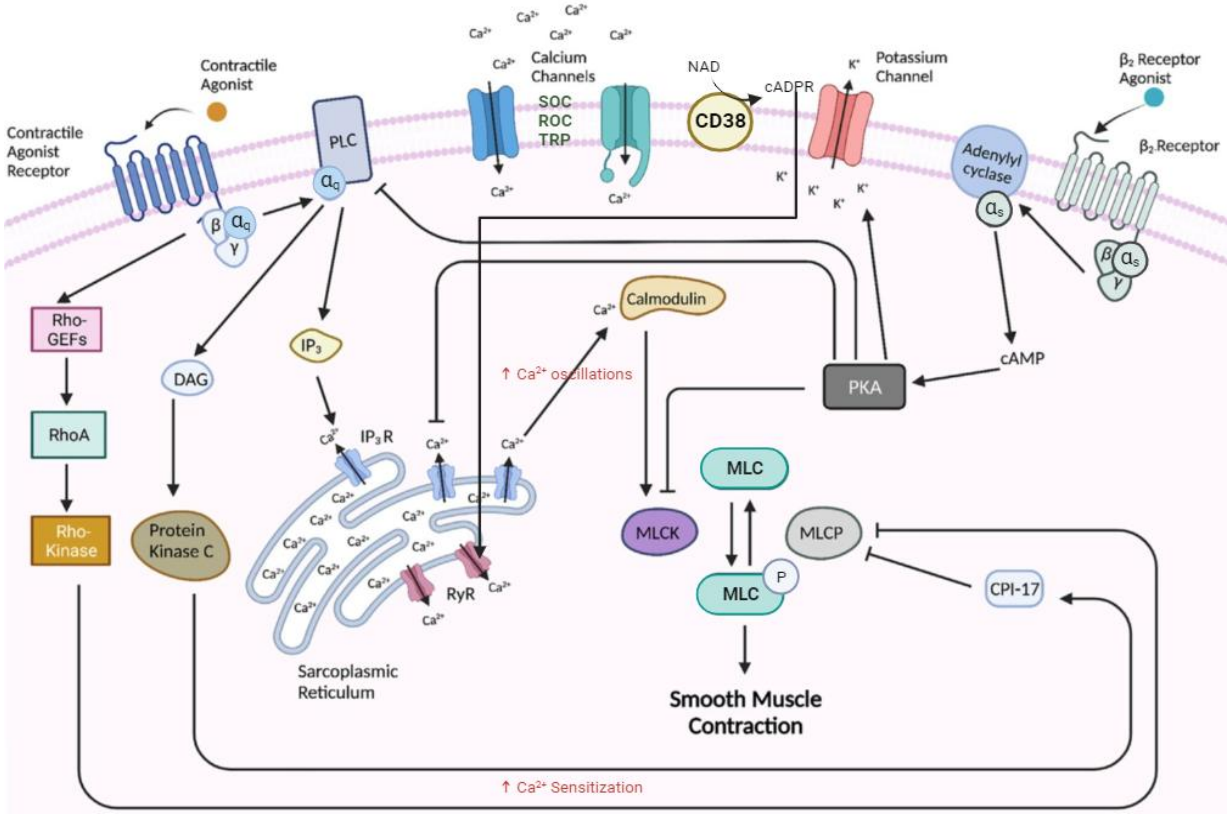

Figure 1.7: Primary intracellular pathways underlying ASM contraction and relaxation.
Binding of contractile agonists to Gq protein-coupled receptors activated PLC that leads to IP_3 and DAG generation. IP_3 causes Ca^{2+} mobilization via IP_3 receptors and RyR channels on the SR to rapidly increase the intracellular Ca^{2+} concentration ($[Ca^{2+}]_i$). SERCA actively pumps Ca^{2+} backs into SR (not shown here). This repeated release and uptake of Ca^{2+} leads to cytoplasmic oscillation. Alternatively, Ca^{2+} influx via plasma membrane channels such as store operated channels (SOC) or receptor operated channels (ROC) can provide additional pool of Ca^{2+} influx. All possible mechanisms for Ca^{2+} influx in not included here. A rise in $[Ca^{2+}]_i$ initiates contractile machinery of ASM. DAG/PKC and ROCK kinase pathways increase contraction by increasing Ca^{2+} sensitivity through inhibition of MLCP. Conversely, activation of Gs protein-coupled receptors by relaxants induces the cAMP/PKA pathway which leads to inhibition of the contractile machinery and ASM relaxation. Reproduced with permission from Frontiers under the Creative Commons Attribution License from previously published article [94].
Legend: GEF: guanine nucleotide exchange factors, RhoA: ras homolog family member A, DAG: diacylglycerol, PLC: phospho lipase C, IP_3:inositol trisphosphate, SOC: store-operated channels, ROC: receptor-operated channels, TRP: transient receptor potential channels, NAD: nicotinamide adenine dinucleotide, cADPR: cyclic adenosine diphosphate ribose, PKA: protein kinase A, cAMP: cyclic adenosine monophosphate, MLC: myosin light chain, MLCK: myosin light chain kinase, MLCP: myosin light chain phosphatase, RyR: ryanodine receptor, SR: sarcoplasmic reticulum, SERCA: Sarcoendoplasmic Reticulum Calcium ATPase

1.5 Asthma treatment and advances

Asthma is a chronic heterogeneous disease that cannot be cured completely. The main goal of conventional therapy is to control symptoms, avoid future exacerbations, and improve the quality of life. The Canadian Thoracic Society (CTS) 2021 guideline recommends four core strategies for better management of asthma symptoms [95]: regular assessment of asthma control and risk of exacerbation, implementation of a written action plan, evaluation of triggers and environmental control, and pharmacological therapy. Current approved pharmacology therapies for asthma are divided into three broad categories: reliever, controller, and add-on [19, 95, 96].

Reliever therapy comprises bronchodilators, which provide immediate but temporary relief from bronchospasm by relaxing ASM. Clinically, the most commonly used bronchodilators are β2 adrenergic receptor agonists (βARAs), and sometimes anticholinergics (M3 receptor antagonists) are prescribed as needed [95]. βARAs act on the β2 adrenergic receptor and prompt ASM relaxation via mechanisms as shown in Figure 1.7 to open up constricted airways and restore normal breathing. These bronchodilators are classified into short- (SABA) and long-acting (LABA) agonists [92]. Albuterol and terbutaline constitute the most widely used inhaled SABAs with up to 4 hours duration of effect, while the inhaled LABAs salmeterol and formoterol are effective for up to 12 hours [92]. A review of multiple randomized control trials revealed that LABAs perform better than SABAs for overall control of asthma in both adults and children [97]; in addition, more frequent SABA usage is associated with increased risk of exacerbations and asthma-related death [98]. Thus, SABA is recommended only for acute symptom relief as needed [95]. Tiotropium, a long-acting M3 receptor antagonist, is an additional reliever for patients with difficult-to-control asthma or those who are βARA intolerant. It inhibits ASM contraction by blocking the contractile M3 receptor on ASM [99].

The gold standard for controller therapy is the inhaled corticosteroids (ICS), which are able to control underlying airway inflammation in the majority of asthma patients. Clinically approved ICS includes fluticasone, beclomethasone, budesonide, ciclesonide, and mometasone [95]. These ICS are all effective in controlling asthma symptoms, but vary in their potency and side effects profile. For instance, fluticasone is the most potent ICS, while new approved ciclesonide and mometasone have comparatively lesser side effects [100]. ICS act by binding to the glucocorticoid receptors (GRs) in the cytoplasm which stimulates GR translocation to the nucleus. Here, it binds to glucocorticoid-response elements (GRE) in the promoter region to transactivate anti-inflammatory genes. In addition, activated nuclear GRs suppress pro-inflammatory effects of various transcription factors (e.g., Nuclear factor-κB (NF-κB) and activated protein-1 (AP-1)) [100]. Treatment with ICS leads to significant reductions in pro-inflammatory cytokines/chemokine levels, immune cells infiltration, mucus production, and AHR [100]. A second line of controller therapy is leukotriene receptor antagonists (LTRAs) (e.g., montelukast and zafirlukast), but they are less effective than ICS and can cause neuropsychiatric side effects [95, 101]. Oral corticosteroids (e.g., prednisone) are recommended in severe disease stage when ICS in combination with an additional controller are ineffective; however, this approach increases the risk of systemic steroid side effects [102].

With a growing understanding of the immunopathology of asthma, novel biologics as add-on therapy have emerged for patients with severe asthma. Anti-IgE (omalizumab) and anti-IL5 (mepolizumab, reslizumab, and benralizumab) monoclonal antibodies are currently approved therapies in this category [96]. Omalizumab directly binds to IgE and reduces its action on multiple targets. Anti-IL-5 antibodies act by blocking IL-5 bioactivity or IL-5α receptor [103]. Of note, these treatments are only recommended for patients with high levels of specific biomarkers such

as sputum and blood eosinophils count, serum IgE, and/or FeNO (fraction of exhaled nitric oxide) [96]. Likewise, anti-IL-4 (dupilumab) and anti-TSLP (tezepelumab) are new therapeutic class recently developed [104, 105]. Although these therapies are effective in reducing exacerbation rate and improving asthma control in specific sub-group of patients, they have limited effect on baseline airflow limitation and AHR, and are therefore considered as add-on only [19]. Additionally, these novel therapy are not approved for children [96]. Macrolide antibiotics (*e.g.*, azithromycin and clarithromycin) represent another class of add-on therapies recommended in the CTS position statement for patients with severe asthma. These compounds have anti-microbial as well as immunomodulatory properties and help reduce exacerbation risk independent of the inflammatory profile; however, their exact mechanism of action in the lungs is still unclear [106]. Lastly, bronchial-thermoplasty is an invasive treatment strategy that uses radiofrequency energy in a controlled manner to selectively ablate ASM from the airway wall, thereby eliminating potential ASM abnormalities and excessive bronchoconstriction [107]. Although it is recognized as a treatment option, international guidelines strongly suggest the application of thermoplasty for clinical research purposes only because of the (present) lack of long-term benefit to risk assessments [108].

In summary, ever since their respective first-time approval in 1969 and 1974, inhaled βARAs and ICS remain the gold standard for the treatment of asthma in the majority of patients. Current guidelines recommend using combination therapy of reliever and controller in a single inhaler because of their synergistic effects on efficacy and low future risk of exacerbation [19, 95, 109, 110].

1.5.1 Limitation of current asthma therapy

i) There is a lack of effective controller therapy for asthmatics with type-2 low inflammation characteristics, which represent a large sub-group of total asthma patients [111, 112]. Mechanisms underpinning type-2 low inflammation are not well characterized, explaining the paucity of clinically proven targets to treat type-2 low inflammation [19, 27, 113]. Additional subsets of patients in severe disease stage with underlying type-2 high inflammation often remain refractory to ICS therapy as reviewed by Hammad and Lambrecht in [27]. This lack of ICS responsiveness is clinically defined as "steroid resistance" or "steroid insensitivity".

ii) A significant number of asthma patients exhibit sub-optimum response to βARAs bronchodilator therapy [114, 115], which is clinically characterized as "bronchodilator insensitivity". Multiple factors have been identified to (potentially) contribute to bronchodilator insensitivity and include environmental exposure to allergens or air pollution [116], prolonged βARA usage-induced receptor desensitization, and genetic polymorphisms in the β_2AR gene [117, 118]. Additionally, these therapies are insufficient in reversing or protecting against severe exacerbation [119] and persistent airway obstruction caused by airway-wall remodeling [120]. Thus, targeting prevention or reversal of airway remodeling is an important avenue for future treatments.

iii) Neither ICS nor LABAs target oxidative stress or its mediators in the lungs that are involved in asthma pathogenesis. Oxidative stress plays a significant role in the pathogenesis of asthma and has been implicated in therapy resistance [121, 122]. Therefore, oxidative stress and its mediators represent potential targets for the development of novel therapeutic strategies for the treatment of asthma.

Taken together, these shortcomings of current therapies and the critical impact of oxidative stress in disease development support the rationale for pursuing a detailed understanding of oxidative stress mediators in asthma pathobiology in order to ultimately improve the overall effectiveness of asthma therapy.

1.6 Oxidative stress in asthma

Oxidative stress occurs due to a redox imbalance stemming from the overproduction of reactive oxygen species (ROS) [123]. Under physiological conditions, components of endogenous antioxidant systems, such as superoxide dismutase (SOD) and catalase, counteract endogenous ROS production and protect against cellular damage caused by ROS [124]. In fact, low levels of oxidative stress under surveillance of an antioxidant system are crucial for certain cellular processes and host-defense [123]. However, pathophysiological conditions may result in redox imbalance due to increased ROS production coupled with a low level of antioxidant activity leading to harmful level of ROS exposure. These ultimately modify cellular molecules such as proteins, DNA and lipids, resulting in protein carbonylation, DNA oxidation or lipid peroxidation, respectively [124, 125]. The stable end products of these structural modification, including bromotyrosine, nitrotyrosine, 8-oxo-2′-deoxyguanosine (8oxodG), malondialdehyde (MDA), 4-hydroxy-2-nonenal (4-HNE), isoprostanes, and oxidized phospholipids (OxPL) have been identified as biomarkers of oxidative stress in various diseases [126]. Most importantly, several lipid peroxidation end products such as MDA, 4-HNE, and choline-head group containing OxPL (oxidized phosphatidylcholines, OxPC) are not just biomarkers of oxidative stress but also act as self-modified epitope, known as oxidation specific epitopes (OSEs), that are recognized by innate or adaptive immunity and involved in chronic inflammation [127, 128].

Oxidative stress in asthma is evidenced by excessive ROS generation by inflammatory cells (i.e. eosinophils and neutrophils) and epithelial cells with concurrent loss of antioxidants in the lungs [129-131]. Oxidative stress in the lung can be further amplified by direct environmental exposure to allergens, pollutants, microbes, or smoke [129]. This persistent nature of oxidative stress in the lungs could be reflected by observed higher levels of oxidative stress markers (e.g., H_2O_2, MDA,

and isoprostanes) in plasma and/or exhaled breath condensates of asthmatics, which correlates with disease severity [132-134]. Similarly, elevated levels of bromotyrosine in urine or nitrotyrosine in exhaled breath condensates have been associated with asthma exacerbations [135, 136]. Recently, I published a section on "current understanding of oxidative stress in asthma" in a collaborative review article (section # 5 in [137]); Here is an excerpt: "The fundamental function of lungs is to facilitate gas exchange between the environment and bloodstream. Therefore, the lung is highly susceptible to oxidative stress from direct exposure to environmental oxidants. Chronic inflammatory diseases such as asthma are inextricably linked with the overproduction of ROS and reactive nitrogen species (RNS) that can overwhelm endogenous anti-oxidant systems. There is substantial literature showing that ongoing oxidative stress is linked with the pathobiology of asthma including airflow obstruction, airway hyperreactivity, and remodeling. However, the cause-and-effect relationship between oxidative stress and asthma is unsettled and its potential as a therapeutic target remains controversial. Previous attempts to use antioxidants as interventions in asthma were unsuccessful. This could be due to a lack of information on the cause-effect relationship between oxidative stress and asthma, the role of oxidation specific epitopes (OSEs) in mediating this effect, and the point in the cycle of oxidative stress-driven pathology that interventions have targeted. Production of ROS is multifaceted and is required for appropriate immune regulation and tolerance. OSEs, on the other hand, are produced when ROS is unconstrained, and they directly disrupt cellular functions promoting inflammation and tissue damage. OSEs therefore may be a more specific marker of localized stress where they function as direct effectors of excessive ROS. In this way, OSEs provide a more tangible target for limiting the damage caused by excessive ROS while potentially preserving the beneficial effects of low-level ROS. Therefore, treatments targeting the OSEs generated by oxidative damage rather than

targeting ROS themselves, could be effective in managing asthma symptoms [137].” OxPC are well-known OSEs that accumulate in and contribute to various disease pathologies [127].

1.7 Formation of oxidized phosphatidylcholines (OxPC)

Phosphatidylcholine phospholipids are highly abundant in plasma membranes [138] as well as circulating lipoproteins [139], and constitute a key component of airway surfactant fluid [140]. Phosphatidylcholines that contain polyunsaturated fatty acid molecules at the sn-2 position (e.g., arachidonic acid or linoleic acid) are a major target for nonenzymatic or enzymatic oxidation, resulting in the generation of fragmented and non-fragmented bioactive oxidized phosphatidylcholines (OxPC) moieties [141]. For instance, 1-palmitoyl-2-arachidonoyl-sn-glycero-3-phosphocholine (PAPC) is a naturally occurring phosphatidylcholine consisting of saturated palmitate (16:0) moiety at sn-1 position and polyunsaturated arachidonate moiety (20:4) at sn-2 position, a site highly prone to oxidation. ROS oxidize the arachidonate moiety into peroxyl radical, which further undergoes fragmentation or cyclization to generate hundreds of OxPC moieties [141] as well as secondary cleavage products like MDA or 4-HNE (Figure 1.8) [142]. These bioactive OxPC moieties can bind to structural components of the plasma membrane or circulating proteins, and participate as OSEs in various disease pathogenesis [127]. Of note, circulating OxPC moieties are particularly abundant in apoB-containing lipoproteins such as low-density lipoprotein and lipoprotein(a) [143].

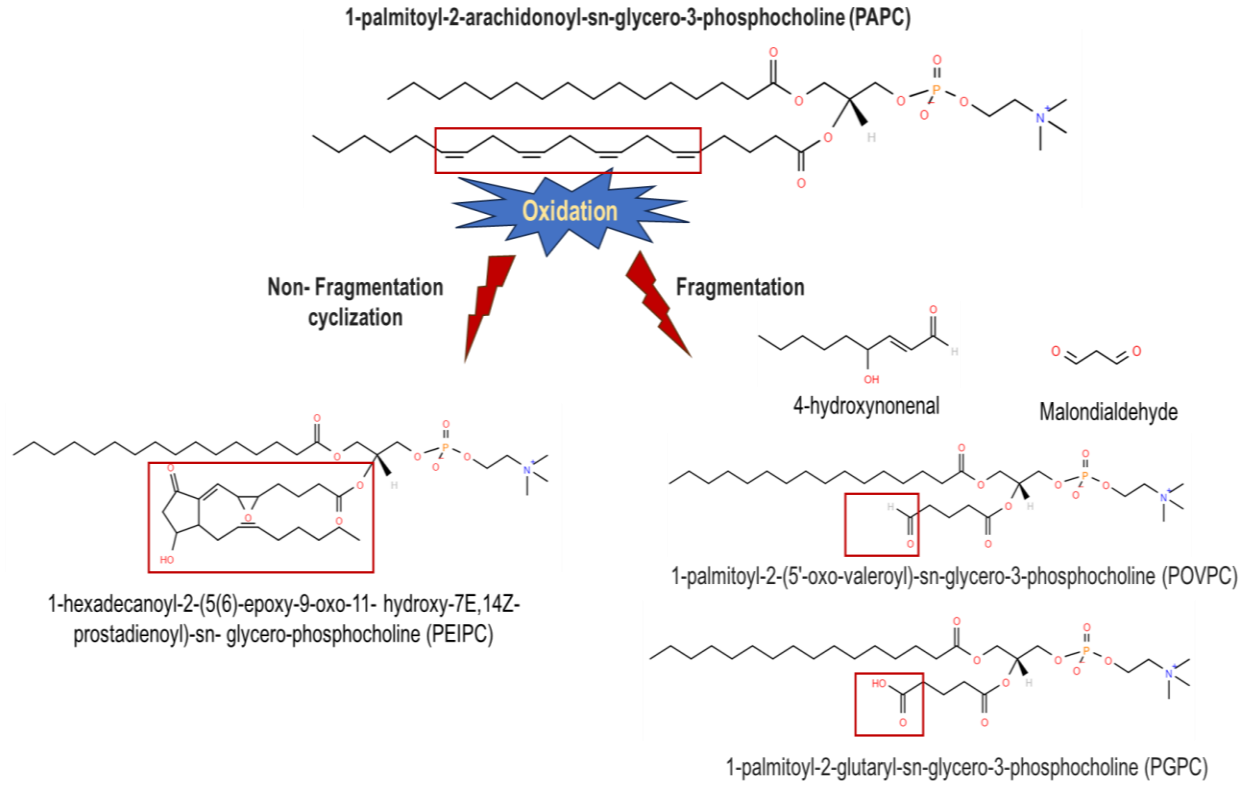

Figure 1.8: Oxidation of PAPC generates fragmented and non-fragmented OxPC moieties. ROS target membrane or circulating phospholipids such as PAPC, leading to the production of various bioactive OxPC moieties. This schematic highlights several representative moieties (not all possible OxPC moieties are shown). Reproduced with permission from MDPI under the Creative Commons Attribution License from previously published article [144].

1.8 OxPC and pathophysiology

The oxidation of PC containing polyunsaturated fatty acids (PUFA) at the sn-2 position produces hundreds of OxPC moieties; thus, it is not surprising that these structurally diverse OxPC exert pleiotropic biological effects. Bochkov and colleagues have extensively reviewed various biological activities of OxPC [141, 145], and describe them as initiators of inflammation involving induction of cytokines, chemokines and adhesion molecules in endothelial cells, as well as the accumulation and activation of macrophages and neutrophils. Additionally, they act as effectors in inflammation by inducing oxidative stress in endothelial cells, NLRP3 (Nucleotide-binding domain, leucine-rich–containing family, pyrin domain–containing-3) inflammasome activation in macrophages, toxic molecule release from neutrophils, and coagulation [145, 146]. Paradoxically, OxPC also exert beneficial anti-inflammatory and endothelial barrier protecting effects at physiological concentrations [145]. Comprehensive studies conducted by Birukov and others (review in [147]) showed that the beneficial effects of OxPC are mainly limited to unfragmented moieties (e.g., PEIPC) while fragmented OxPC products (e.g., POVPC, PGPC) induce harmful effects. These pleiotropic activities of OxPC can be attributed to the diverse receptor and non-receptor mediated effects of OxPC as elegantly reviewed in [141, 145]. Receptors and other targets that have thus far been identified for OxPC include scavenger receptors (CD36, scavenger receptor BI), pattern recognition receptors (PRRs) (TLR2, TLR4, TLR6), G-protein coupled receptors (platelet-activating factor receptor and prostaglandin EP2/DP2 receptor), soluble PRRs (C-reactive protein, complement component H) and natural antibodies [127, 145]. Furthermore, TRPA1, TRPC5, or GRP78 can be directly activated by OxPC [145]. Because of their multifaceted effects, OxPC have been linked to the pathophysiology of a broad range of diseases (depicted in Figure 1.9).

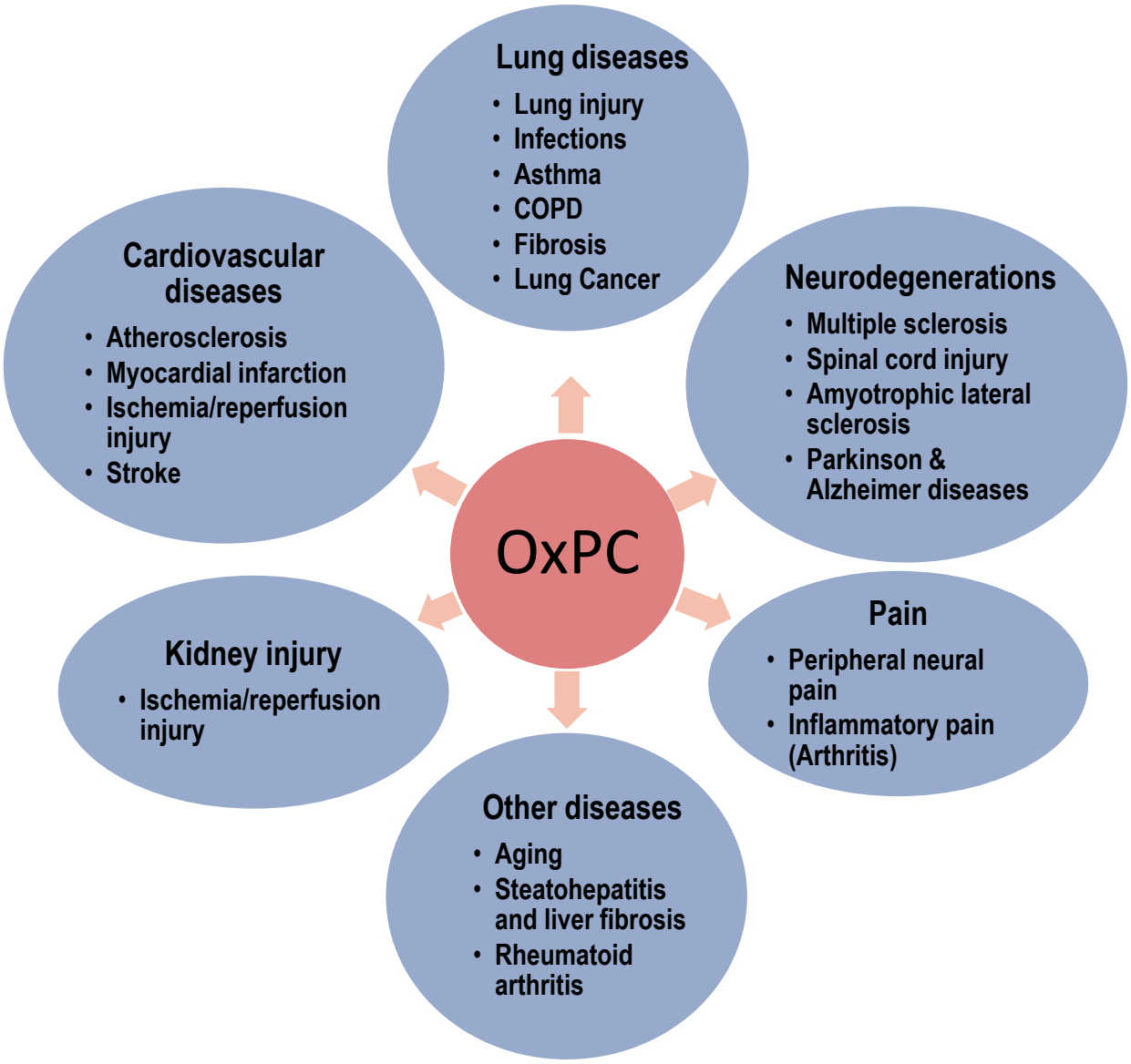

Figure 1.9: OxPC contribute to the pathophysiology of various diseases.
This illustration highlights the impact of OxPC on a broad range of pathophysiological features, affecting numerous physiological systems (of note, all known effects of OxPC are not included for clarity purposes). Relevant highlights were depicted by J. Vaghasiya based on human and animal studies from the following articles: [137, 141, 146, 148-151]. OxPC: oxidized phosphatidylcholines, COPD: chronic obstructive pulmonary disease.

Historically, OxPC were first characterized in atherosclerosis and a substantial body of literature indicates pro-inflammatory and pro-thrombotic roles of OxPC in endothelial cells, vascular smooth muscle cells, monocytes/macrophages, and platelets (review in [141, 145, 146]). OxPC-induced foam cell formation via activation of CD36 on macrophages and subsequent inflammation and cellular migration is a "hallmark process" of atherosclerosis and related complications [152-154]. OxPC also modulate phenotype plasticity of vascular smooth muscle cells and promote angiogenesis [141, 146]. Furthermore, OxPC participate in atherosclerotic plaque development and instability which leads to further downstream cardiovascular complications such as ischemia, myocardial infarction, and stroke [146]. OxPC levels are increased within a few hours in plasma and at the site of myocardial ischemia/reperfusion (I/R) injury as demonstrated in both human [155, 156] and animal studies [157, 158]. Interestingly, OxPC could also serve as biomarker to help predict long-term risk for cardiovascular events and stroke outcomes [159, 160]. Similarly, bioactive OxPC species are associated with acute renal injury following I/R injury [161]. The second most characterized effect of OxPC are in the lung which is described in a separate section below (section 1.9).

Animal studies show OxPC requirement in the pathogenesis of various diseases such as atherosclerosis, nonalcoholic fatty liver disease, I/R injury, rheumatoid arthritis, and osteoporosis [146, 148, 162]. OxPC have also been reported to drive neurodegenerative disorders like multiple sclerosis, dementia, spinal cord injury, and amyotrophic lateral sclerosis [149, 163]. Recently, OxPC are found to increase at the site of inflammatory pain in animal models, and they have been identified as therapeutic target for pain [164, 165].

1.9 OxPC and lung diseases

In mouse lungs, acid aspiration or influenza infection promotes OxPC generation and participation in acute lung injury (ALI) [166]. Similarly, exposure to lethal lung pathogens like anthrax, Y. pestis, or monkeypox can trigger OxPC formation in multiple animal species [166]. Interestingly, aged mice exhibit higher basal levels of OxPC in the lungs, which may underpin exaggerated lung injury in these mice after induction of ALI [168]. OxPC are generated in the lungs upon environmental exposure to air pollutants such as diesel exhaust and allergens in humans [169] or cigarette smoke in mice [170]. Other preclinical studies show OxPC accumulation in the alveolar macrophages after bleomycin, silica dust, or nitrogen mustard exposure, which further promotes macrophage-to-foam cell transition and lung fibrosis [171-174]. Similarly, foam cell like features have been observed in cigarette smoke-exposed mice as they exhibit lipid accumulation in macrophages and followed by pro-inflammatory cytokine IL-1α-mediated inflammation [151]. Of note, OxPC levels are significantly increased in both plasma and within tumor tissues of patients with non-small-cell lung cancer [175].

Our recent work showed that OxPC are increased in the bronchoalveolar lavage (BAL) fluid of mild asthma patients in response to allergens exposure [176]. We also observed distinct profiles of OxPC in a cohort of patients with AHR without clinically diagnosed asthma. In support of this observed association between decline in lung function and OxPC accumulation, my recent research shows that OxPC can directly induce airway narrowing in murine thin-cut lung slices and that is mediated via triggering ASM contraction [177]. Additional experiments in this study also showed pro-inflammatory effects of OxPC in cultured ASM cells as they cause secretion of the pro-inflammatory cytokines (IL-6, IL-8, and GM-CSF) and mediators (oxylipins) [176]. Overall, our recent work is the first to provide experimental evidence to suggest that accumulation of OxPC

correlates with a decline in lung function, and that this may be linked to their pro-contractile and pro-inflammatory roles in ASM cells. Additionally, we also demonstrated that OxPC cause multiple functional defects in epithelial cells including compromised barrier integrity, inhibition of proliferation, and mitochondrial dysfunction [178]. These observations suggest that OxPC can impact lung health by affecting multiple cells in the lungs, including ASM and epithelial cells, which likely contributes to disease severity and progress.

1.10 Mechanisms of OxPC clearance

Oxidation of PUFAs at the sn-2 position of PC brings a conformation shift within the cell membrane, protruding the oxidized side chain into the extracellular aqueous compartment [179, 180]. This structural shift due to OxPC formation is recognized by both cellular and soluble PRRs as a damage-associated molecular pattern (DAMP)[128]. Soluble PRRs such as C-reactive protein and annexin A5, or scavenger receptors of macrophage and natural antibody T15/E06 are involved in the clearance of OxPC [127, 128, 137]. These help to minimize excessive OxPC exposure and associated harmful effects. However, uncleared OxPC at the site of generation simultaneously engage inflammatory PRRs and prevent resolution of inflammation [127, 128, 137]. Under pathophysiological conditions of aberrant OxPC accumulation, this endogenous clearance system is overwhelmed or functionally impaired (e.g., low abundance or decreased binding capacities of soluble PRRs), which further favors OxPC accumulation and promotes sustained inflammation. As an example of the pathophysiological importance of proper clearance, compromised OxPC clearance in aged mice was associated with exaggerated lung injury in a model of lipopolysaccharides-induced ALI [168].

Circulating platelet-activating factor acetylhydrolase (PAF-AH), also known as lipoprotein associated phospholipase A2 (LP-PLA2), recognizes and neutralizes truncated OxPC from cell

membrane or lipoproteins [181-184]. High density lipoprotein (HDL)-associated hydrolase comprises LP-PLA2 along with other two enzymes, paraoxonase-1 (PON1) and lecithin-cholesterol acyl transferase (LCAT), which play an important role in OxPC clearance by hydrolyzing the short acyl chain at the sn-2 position of OxPC [185]. Apart from these enzymes, HDL also harbors apolipoprotein A-I (ApoA-I) which plays a predominant role in converting bioactive OxPC into their inactive hydroxide forms and in the functioning of HDL-associated hydrolases [185]. Additionally, HDL can electrochemically interact with and inhibit OxPC bioactivities by integrating electrophilic OxPC within its phospholipid monolayer [186, 187]. Thus, HDL is critical in the removal of bioactive OxPC via multiple mechanisms. Importantly, dysfunctional HDL itself but not HDL levels affect the intrinsic property of HDL-mediated OxPC inactivation in chronic diseases [187-189]. Thus, in addition to increased OxPC generation, impaired OxPC clearance also contributes to an excessive and chronic presence of OxPC in the system. Collectively, these disturbed dynamics in the management of OxPC abundance may promote disease pathogenesis [127, 128, 137].

1.11 OxPC as therapeutic targets in lung diseases?

Emerging evidence shows that OxPC are important mediators of oxidative stress that not only accumulate during but also actively contribute to the pathogenesis of various diseases. Thus, OxPC represent a tangible therapeutic target that could help to more effectively treat many diseases with oxidative stress as a central pathophysiological mechanism. In this regard, pharmacological neutralization of OxPC using either ApoA-I mimetic peptide or natural IgM antibody has been widely explored. ApoA-I mimetic peptide has a high affinity for OxPC and can inhibit their biological effects [190, 191]. This peptide has demonstrated anti-inflammatory, antioxidant, and other beneficial effects in a wide variety of disease models, such as atherosclerosis and related cardiovascular diseases, pneumonia, diabetes, hepatic fibrosis, Alzheimer's disease, arthritis, and renal inflammation (extensively reviewed in [190]). Currently, multiple ApoA-I mimetic peptides are in the clinical trial stage for the evaluation of their atheroprotective actions [190]. Similarly, ApoA-I mimetics have also shown therapeutic promise in multiple animal models of lung diseases such as acute lung injury, asthma, emphysema, cancer, pulmonary fibrosis, and pneumonia [192]. Additionally, it can also control inflammatory pain in the animal models [150, 164].

T15/E06 is a murine monoclonal IgM antibody first developed by Dr. Witztum (University of California, San Diego) using apolipoprotein E knock-out mice. It specifically reacts with the choline head group of OxPC but not with intact unoxidized PCs [193-195]. Dr. Witztum and his group also successfully generated transgenic (TG) mice (using an apoE promoter with $Ldlr^{-/-}$background) that can produce endogenous single-chain variable fragments of E06 (E06-scFv). E06-scFv is secreted into the plasma, mainly from the liver and macrophages, in a quantity (20-30 μg/mL) sufficient to neutralize the bioactivities of OxPC [162]. Our recent review of multiple pre-clinical studies in [137] highlights that the E06 mAb, by neutralizing biological

activities of OxPC, has several therapeutic benefits (summarized in Table 1.1). Taken together, this suggests that humanized E06 antibody has many potential therapeutic benefits in patients. However, therapeutic benefits of humanized E06 antibody remains to be validated in the clinic; currently no such trials are ongoing. In asthma, unlike the proven therapeutic value of ApoA-I mimetic peptide in the murine model of allergic asthma [196], the therapeutic benefit of E06 is yet to be investigated in preclinical studies. Most importantly, our recent groundbreaking work shows that intranasal delivery of statins abrogates OxPC accumulation in BAL fluid and may have superior efficacy than gold standard ICS therapy in a murine model of allergic asthma [197, 198]. The mechanisms for these effects are currently under investigation, but statins do have pleiotropic effects including immunomodulatory, anti-inflammatory, and antioxidant in addition to lowering cholesterol levels [199].

Overall, pharmacological neutralization of OxPC or prevention of OxPC accumulation (by interfering with generation and/or stimulation of clearance) are likely to have diverse therapeutic benefits in the treatment of various (inflammatory) diseases, including asthma.

Table 1.1. Pharmacological neutralization of OxPC by natural IgM (E06 mAb)

Pre-clinical models	E06 expression/ E06 mAb IgM treatment	Noteworthy observations	References
Hypercholesterolemia/ hyperlipidemia induced inflammation in mice	• Ldlr−/−-E06-scFv-Tg mice express endogenous E06-scFv (20-30 μg/mL, plasma)	E06-scFV by neutralizing OxPC; • Reduces atherosclerosis • Inhibits aortic stenosis • Reduces hepatic steatosis and fibrosis, non-alcoholic steatohepatitis • Reduces osteoporosis	[162, 200-203]
Myocardial ischaemia-reperfusion injury in mice	• Ldlr−/−-E06-scFv-Tg mice express endogenous E06-scFv (20-30 μg/mL, plasma) • E06 mAb IgM (10 μg/mL), myocytes viability assay	• E06-scFv inhibits cardiac infarct development by 65.9% • E06 lowers cytotoxic effects of OxPC	[157]
Porcine model of reperfusion injury	E06 mAb IgM (dose not available)	Intracoronary E06 reduces cardiac infarct by 51.3%	[158]
Hyperoxia-induced lung injury in mice	Ldlr−/−-E06-scFv-Tg mice express endogenous E06-scFv (20-30 μg/mL, plasma & BALF)	E06-scFv ameliorates hyperoxia induced lung injury	[204]
Acute lung injury model using cultured macrophages	EO6 IgM mAb (10 μg/mL)	E06 abrogates OxPAPC induced IL-6 production	[166]
Cigarette smoke exposure in mice	E06 mAb IgM, intranasally (20 μg/mouse, 4 days), 1 hr prior to smoke exposure	E06 enhance lipid clearance by lung macrophages and inhibits IL-1α production	[170]
Cigarette smoke exposure study using a cultured murine macrophage cell line (J774)	EO6 IgM mAb (50 μg/mL)	EO6 inhibits OxPC induced impairment of phagocytosis	[205]
Mechanical and thermal hyperalgesia pain model in rats	EO6 IgM mAb, intraplantar (0.01μg/paw)	• E06 reverses hyperalgesia induced by OxPC • E06 abrogates mechanical hyperalgesia induced by complete freund's adjuvant (CFA) • E06 does not alter thermal hyperalgesia induced by CFA	[164]

Table 1.1. Pharmacological neutralization of OxPC by natural IgM (E06 mAb) ***(Contd…)***

Inflammatory pain model in rats	• EO6 IgM mAb, intraplantar (2µg/paw) • EO6 IgM mAb E06 (3 ng) for HEK-293 Ca^{2+} assay	• E06 ameliorates inflammatory pain mediated by OxPC formation in response to ROS agents • E06 prevents Ca^{2+} influx by OxPC in cells	[206]
Spinal cord injury model and *in vitro* neuronal toxicity	• E06 IgM mAB, spinal cord injection (0.25 µg/mice) • E06 IgM mAB (10 µg/mL) for neurotoxicity assay	• E06 prevents spinal cord injury in mice • E06 prevents neurotoxicity effects of OxPC	[207]

Chapter 2: Thesis Rationale, Hypothesis, Objectives, and Impact

Rationale: Oxidative stress in the lungs is increasingly recognized as a common hallmark of asthma and strongly linked with features of disease pathophysiology, including airflow obstruction, AHR, and remodeling [129-131, 208]. The cause–effect relationship between oxidative stress and asthma pathobiology is unsettled. Thus far, attempts to use systemic antioxidants as broad interventions to overcome oxidative stress and improve asthma control have been unsuccessful [209, 210], leaving the potential of oxidative stress as a therapeutic target controversial [211]. Considering the large body of experimental evidence to support the involvement of oxidative stress in asthma and indications of its contribution to the development of conventional therapy resistance [212, 213], in-depth investigations elucidating how oxidative stress and its mediators drive asthma pathogenesis and progression are warranted.

Recently, we made groundbreaking advances showing that inhalation of allergens by human asthmatics leads to generation of abundant OxPC (as mediator of oxidative stress) in the lungs, and these molecules perpetuate airway inflammation and correlate with the severity of asthma symptoms [176]. Oxidation of unsaturated fatty acid tail dramatically changes the biological activities of PCs, including their role in the regulation of immune responses and inflammation. Thus, OxPC residing in lipid bilayer membranes or circulation form so-called oxidation specific epitopes (OSEs) have been shown to contribute to the pathophysiology of multiple inflammatory diseases, including acute lung injury. Aside from our lab's recent discovery that OxPC accumulate in the airways after allergens challenge, there have been remarkably little focus on OxPC in asthma. To highlight this knowledge gap, I published a collaborative review article discussing OxPC and their potential as important drivers of the disease [137]. Although emerging evidence,

including findings by our group, indicates that OxPC could indeed be novel oxidative-stress mediators in the lungs, our understanding of the specific roles for OxPC in asthma pathogenesis and progression is still limited [137]. The studies described in this thesis were designed to further confirm the impact of OxPC on asthma pathobiology and unravel the mechanisms and signaling pathways involved.

Hypothesis and Objectives: The primary goals of this thesis are to elucidate the direct role(s) of bioactive OxPC in asthma pathophysiology, identify effector pathways that mediate OxPC effects, and delineate the functional effects of OxPC on human ASM. **The main hypothesis is that OxPC can trigger airway inflammation and AHR through direct effects on airway structural cells and concurrently contribute to the loss of effectiveness of conventional asthma therapies**. To test this hypothesis, I have developed three major objectives:

Objective 1: *To assess the direct effects of OxPC on ASM contraction and airway narrowing.* To this aim, we used *in vitro* (cultured human ASM cells) and *ex vivo* (murine thin cut lung slices) experimental models to determine the contractile responses and induction of signaling pathways resulting from OxPC exposure.

Objective 2: *To explore the effects of OxPC on ASM relaxation and bronchodilator (in)sensitivity.* To accomplish this aim, we used *in vitro* (cultured human ASM cells), *ex vivo* (murine thin cut lung slices and tracheal rings) and *in vivo* (murine lung function assessment) approaches to determine the degree of impairment of ASM relaxation by OxPC exposure and the molecular mechanisms involved.

Objective 3: *To determine the pathobiological role(s) of OxPC in airway inflammation and AHR using a murine model of allergic asthma.* For this aim, we used a clinically relevant murine model

of allergic asthma to uncover mechanisms for OxPC accumulation in the lungs, if any, and assess whether immuno-pharmacological neutralization of OxPC holds promise as a future therapeutic strategy for the treatment of asthma.

Significance

The studies described in this thesis utilized various experimental *in vitro*, *ex vivo* and *in vivo* models to study the impact of OxPC on key features of asthma pathobiology, including induction of ASM contraction (leading to *airway hyperresponsiveness*) and impairment of ASM relaxation (*i.e.*, reduced responses to bronchodilators that is clinically characterized as *bronchodilator insensitivity*). This work will be the first to conclusively establish the direct role(s) of OxPC as mediators of oxidative stress, providing novel insights into how OxPC contribute to the pathobiology of asthma. This is important as no current asthma therapies specifically target oxidative stress or associated bioactive mediators like OxPC. Our pre-clinical assessment of the therapeutic impact of targeting OxPC will facilitate the development of more efficient and/or new treatment options for asthma.

Chapter 3: General Materials and Methods

This chapter provides details of all the chemicals, reagents, and antibodies as well as a description of common cell culture and generalized techniques used in the studies described in this thesis. Study-specific methods/protocols are outlined in the individual chapters.

3.1 Chemicals and reagents

- - Acetylcholine, albuterol sulfate, allyl isothiocyanate (AITC), caffeine, forskolin, indomethacin, isoproterenol, methacholine, ryanodine, and TRPA1 inhibitor (HC-030031): Sigma (Oakville, ON, Canada).
  - Xestospongin C: Abcam (Toronto, ON, Canada).
  - 8-bromo-cyclic-adenosine di-phosphate-ribose (8-Br-cADPR): Cayman chemical (Ann Arbor, MI, USA).
  - Gadolinium chloride (Gd^{3+}) and GF-109203X (PKC inhibitor): Tocris Bioscience (Toronto, ON, Canada).
  - 12-O-tetradecanoylphorbol-13-acetate (TPA): Cell Signaling Technology (Danvers, MA, USA).
- Stock solutions of ryanodine, HC-030031, xestospongine C, forskolin, GF-109203X, indomethacin, and TPA were prepared in DMSO, and all other chemicals were directly dissolved in media/buffer as specified.
- HEPES-buffered Hanks balanced salt solution (HBSS) containing Ca^{2+} (1.26 mM Ca^{2+}) was prepared in-house with the following ingredients: [composition in mM: 1.26 $CaCl_2$, 0.493 $MgCl_2$-$6H_2O$, 0.407 $MgSO_4$-$7H_2O$, 5.33 KCl, 0.441 KH_2PO_4, 4.17 $NaHCO_3$, 137.93 NaCl, 0.338 Na_2HPO_4 (anhydrous), 5.56 Dextrose, and 20 HEPSES] and the pH was adjusted to 7.4. Nominally zero Ca^{2+} HEPES-HBSS buffer (0 mM Ca^{2+}) was prepared similarly without adding $CaCl_2$.
- The Krebs-Henseleit bicarbonate buffer (K-H buffer) was prepared in-house with the following ingredients: [composition in mM: 118 NaCl, 23.5 $NaCO_3$, 4.69 KCl, 1.18 KH_2PO_4, 1.00 $MgCl_2$, 2.50 $CaCl_2$ and 5.55 dextrose) and the pH was adjusted to 7.4.

- House dust mite (HDM) lyophilized powder (Lot no. 371590, 11375 endotoxin units per vial) was procured from Greer Laboratories Inc (Lenoir, NC, United States). HDM stock solution (2.5 mg/mL) was prepared by dissolving HDM lyophilized powder in saline. On treatment day, each mouse was administered intranasally (i.n.) with 25 µg of HDM diluted into 35 µL of saline.
- Pentobarbital sodium injection was procured from Bimeda-MTC Animal Health Inc., (Cambridge, ON, Canada).
- The mouse monoclonal (mAb) IgM natural antibody E06 was a generous gift from Dr. JL Witztum (University of California (San Diego).

Table 3.1. Summary of inhibitors and their properties

Inhibitor	Concentration used	Effective concentration	Mechanism of inhibition	References
Gadolinium (Gd^{3+})	500 µM	100% inhibition of Ca^{2+} flux >100 µM	Non-specific plasma membrane Ca^{2+} channels blocker	[214]
HC-030031	50 µM	IC_{50} =6.2 µM	Selective TRPA1 channel blocker	[214-216]
Xestospongin	5 µM	IC_{50} = 358 nM	Reversible, membrane permeable inhibitor of IP_3 receptor-mediated Ca^{2+} release	[217, 218]
Caffeine	25 mM	>10 mM	Non-specific inhibitor (high concentration) of RyR-mediated Ca^{2+} release	[219-221]
Ryanodine	100 µM	>10 µM	Semi-selective ryanodine receptor blocker at high concentrations	[219-222]
8-Br-cADPR	100 µM	IC_{50} =1.7 µM	Membrane-permeable cADPR antagonist	[222]
GF-109203X	10 µM	IC_{50} < 5.8 µM	Selective PKC inhibitor	[176]
Indomethacin	10 µM	IC_{50} 0.97 µM for COX-2	Non-selective COX inhibitor	[176]
E06 IgM	1-10 µL	-	Selective monoclonal antibody against OxPC	[193]

3.2 Antibodies

- Primary antibodies:
  - Rabbit polyclonal antibodies for MLC (Myosin light chain-2), p-MLC (phospho-myosin light chain-2 (Thr18/Ser19) or (Ser19)), and phospho-PKC (pan) (βII Ser660): Cell Signaling Technology (Danvers, MA, USA).
  - Rabbit polyclonal antibody for β-actin and monoclonal antibody for vimentin: Abcam (Cambridge, UK).
  - Mouse monoclonal antibody for TRPA1: Santa Cruz Biotechnology (Dallas, Texas, USA).
  - Mouse monoclonal antibody for vasodilator-stimulated phosphoprotein (VASP): BD Biosciences (Franklin Lakes, NJ, USA).
- Secondary antibodies:
  - Antibodies (for immunoblotting) Goat anti-rabbit IgG-peroxidase conjugate and goat anti-mouse IgG-peroxidase conjugate: Sigma-Aldrich (Saint Louis, MO, USA).
  - Antibodies (for immunofluorescence) Cy3-conjugated donkey anti-mouse IgG and Cy5-conjugated donkey anti-rabbit IgG: Jackson ImmunoResearch (West Grove, PA, USA).
  - Horseradish peroxidase (HRP)-conjugated chicken polyclonal anti-HA-tag antibody: Abcam (Cambridge, UK).

- The following antibodies (Table 3.2) were used for flow cytometry-based immunophenotyping of mouse bronchoalveolar lavage fluid (BALF):

Table 3.2. Panels of antibodies for flow cytometry

Panel	Antibodies	Concentration (ng/µL)	Source
Compensation	PE anti-mouse CD4	2.0	BioLegend, San Diego, CA, USA
	APC anti-mouse CD4	2.0	
	FITC anti-mouse CD4	5.0	
	APC/Cy7 anti-mouse CD4	2.0	
	PerCP/Cy5.5 anti-mouse CD4	2.0	
	PE/Cy7 anti-mouse CD4	2.0	
Granulocytes	PE/Cy7 anti-mouse/human CD11b	5.0	
	PE anti-mouse CD170 (Siglec-F)	5.0	
	FITC anti-mouse CD11c	12.5	
	PerCP/Cy5.5 anti-mouse F4/80	5.0	
	APC anti-mouse Ly-6G	5.0	
Lymphocytes	PE anti-mouse CD3	5.0	
	FITC anti-mouse CD8a	12.5	
	PerCP/Cy5.5 anti-mouse CD4	5.0	
	APC anti-mouse/human CD45R/B220	5.0	
	PE/Cyanine7 anti-mouse CD335 (NKp46)	5.0	
Fc blocker	Anti-mouse CD16/CD32	5.0	Life Technologies Corp, Carlsbad, CA, USA

3.3 Preparation of OxPAPC

Commercial grade 1-palmitoyl-2-arachidonoyl-sn-glycero-3-phosphocholine (PAPC) (Avanti® Polar Lipids, Alabaster, AL, USA) was oxidized at room air for four days, then re-constituted at 1 mg/mL (stock) in chloroform:methanol (2:1), and stored at -20°C until further use. OxPAPC contained a mixture of both fragmented and non-fragmented OxPC as analyzed by LC/MS/MS as described previously [176]. Fully saturated, oxidation-resistant 1-palmitoyl-2-stearoyl-sn-glycero-3-phosphocholine (PSPC, 1 mg/mL stock in chloroform:methanol, 2:1) (Avanti® Polar Lipids, Alabaster, AL, USA) was used as a negative control lipid. Organic solvent was evaporated from the required OxPAPC/PSPC stock aliquots under nitrogen, after which lipids were resuspended in buffer as specified for individual experiments.

3.4 Animals

Female BALB/c mice (6-8 weeks old) were acquired from Charles River Laboratories (Senneville, Quebec, Canada) and acclimatized for one week prior to the start of the experiments. Animals were housed in individually ventilated cage (IVC) system (Techniplast, Italy) with access to standard chow food and water *ad libitum* under 12-hour light/dark cycles. All procedures were carried out as per protocols approved by the institutional ethics committee. Animals were sacrificed at the end of the experiments as specified in the treatment protocol with an intraperitoneal (i.p.) overdose of pentobarbital sodium (Bimeda-MTC Animal Health Inc., Cambridge, ON, Canada).

3.5 Human airway smooth muscle (HASM) cell culture

We used the human telomerase reverse transcriptase gene-expressing HASM cells (passages 6-10), which were prepared as described previously [223, 224] from primary ASM cultures generated from individuals with no airway disease and no smoking history. Primary cultures were

prepared from donated lung tissue following deep endobronchial biopsies from healthy volunteers (Table 3.3) as mentioned in [224-226]. HASM cells were grown in DMEM media (Life technologies, Grand Island, NY, USA) supplemented with 5% fetal bovine serum (FBS) (Life technologies, Grand Island, NY, USA) and 1% penicillin/streptomycin (P/S) (Life technologies, Grand Island, NY, USA) at 37°C (5% CO_2). To promote expression of a contractile ASM phenotype, once cultures were 70-80% confluent they were maintained under serum-free conditions [DMEM, 1% P/S, and 1% ITS (5 g/ml insulin, 5 g/ml transferrin, 5 ng/ml selenium)] (Life technologies, Grand Island, NY, USA) for up to 7 days before performing experiments. Cell culture media was changed every 2-3 days.

Table 3.3. Characteristics of human lung biopsy donors (non-asthmatics; non-smokers)

Donor	Sex	Age
Donor 1	F	21
Donor 2	F	22
Donor 3	F	23
Donor 4	M	22
Donor 5	M	48
Donor 6	M	24

3.6 Immunoblotting

Following treatment as specified, cells were washed with ice-cold HBSS or PBS (as specified) on ice and immediately lysed with ice-cold RIPA buffer (40 mM Tris pH 8.0, 150 mM NaCl, 1% IGEPAL (NP-40), 1% sodium deoxycholate,) supplemented with 1 mM phenylmethylsulphonyl fluoride, 1 mM Na-orthodonavate, and a protease/phosphatase inhibitor cocktail (Sigma Aldrich) unless indicated otherwise. Lysates were sonicated, centrifuged, and supernatant protein concentration was quantified by BCA assay (Bio-Rad DC™ Protein Assay). Samples were mixed in Laemmli loading buffer containing 2-mercaptoethanol.

Equal amounts of protein were loaded into wells of SDS-PAGE gels. After electrophoresis, proteins were transferred to nitrocellulose membranes. Subsequently, membrane were blocked (5% non-fat powdered milk diluted in Tris-buffered saline containing 0.1% Tween-20 (TBS-T)) for 1 hr at room temperature, and incubated overnight at 4 ^{0}C with primary antibody diluted with 1% milk in TBS-T as indicated. Following 3-4 washes with 0.1% TBS-T, membranes were incubated with secondary antibodies (1 hr) and thoroughly washed again with 0.1% TBS-T. Blots were treated with Amersham™ ECL™ reagents (Cytiva Global Life Sciences, Marlborough, MA, USA) and developed using an AFP ImageWorks developer (Elmsford, NY, USA) or ChemiDoc™ imaging system (Bio-Rad, Hercules, CA, USA). Protein bands were quantified as integrated density values by spot densitometry using AlphaEase® FC Software Version 6.0.0 (Alpha Innotech, San Leandro, CA, USA) and normalized to the appropriate loading control(s).

3.7 Murine thin-cut lung slice (TCLS) study procedure

Mice were euthanized with an intraperitoneal (i.p.) overdose of pentobarbital sodium (Bimeda-MTC Animal Health Inc., Cambridge, ON, Canada) and lungs were inflated via a tracheal catheter with ~1.3 mL of 2% low-melting agarose in HBSS (37°C), followed by a 0.2 mL bolus of air to flush agarose to alveoli. Lungs were cooled to 4°C, then lobes were isolated, and sagittal ~180-µm thick serial slices were prepared from lateral to medial planes using an EMS-4000 vibratome (Electron Microscope Sciences, Hatfield, PA, USA). Slices were maintained in DMEM supplemented with 1% P/S (37°C and 5% CO_2) for up to 96 hours. Further details of murine TCLS preparation are described in [83, 227].

Individual TCLS preparations were mounted in a custom-built perfusion chamber. Fresh HBSS buffer was delivered at a constant rate by gravity from a multi-tube manifold controlled by a solenoid valve system. The chamber was mounted on the stage of an inverted phase-contrast

microscope (Nikon Eclipse T*i*, Melville, NY, USA), and video images were recorded through a 10X objective using a CCD camera (Infinity 2, Teledyne Lumenera, Ottawa, ON, Canada). Video Savant 4.0 software (IO Industries, London, ON, Canada) was used for image acquisition and digital recording in time-lapse mode. Captured images were analyzed using the public domain NIH Image-J program (developed at the U.S. National Institutes of Health and available on the Internet at http://rsb.info.nih.gov/nih-image/) equipped with custom-written macros. With this software, images were calibrated using ocular grid lines to enable absolute measurement of airway lumen area (μm^2). For all experiments, airways between 8000 and 45,300 μm^2 (area) were studied. Baseline airway size was recorded under continuous HBSS perfusion, then airway constriction/dilation was induced by stimulants dissolved in HBSS, and airway lumen size was recorded for 3 consecutive minutes for each treatment.

Chapter 4: Oxidized Phosphatidylcholines Trigger TRPA1 and Ryanodine Receptor–Dependent Airway Smooth Muscle Contraction

Jignesh Vaghasiya[1,2], Azadeh Dalvand[1,2], Anurag Sikarwar[1,2], Divleen Mangat[2], Mirna Ragheb[2], Katarina Kowatsch[2], Dheerendra Pandey[1,2], Seyed Mojtaba Hosseini[1,4], Tillie L Hackett[3], Soheila Karimi-Abdolrezaee [1,4], Amir Ravandi[1,5,6], Christopher D Pascoe[1,2] & Andrew J Halayko[1,2,6] on behalf of the Canadian Respiratory Research Network

[1]Dept of Physiology and Pathophysiology, University of Manitoba, Winnipeg, MB, Canada. [2]Biology of Breathing Group, Children's Research Hospital of Manitoba, Winnipeg, MB, Canada. [3]Department of Anesthesiology, Pharmacology & Therapeutics, Centre for Heart Lung Innovation, University of British Columbia, Vancouver, BC, Canada. [4]Manitoba Multiple Sclerosis Research Center, [5]Institute of Cardiovascular Sciences, St. Boniface Hospital Albrechtsen Research Centre, Winnipeg, Manitoba, Canada. [6]Dept of Internal Medicine, Max Rady College of Medicine, University of Manitoba, Winnipeg, MB, Canada.

This research work is published in *American Journal of Respiratory Cell and Molecular Biology*.
Reprinted with permission of the American Thoracic Society.

Vaghasiya J, *et al*. Am J Respir Cell Mol Biol. 2023 Dec;69(6):649-665.
The American Journal of Respiratory Cell and Molecular Biology is an official journal of the American Thoracic Society.

Author Contributions:
Jignesh Vaghasiya: Study design, execution, data analysis, and manuscript writing
Azadeh Dalvand: HASM cells immunofluorescence imaging
Anurag Sikarwar: Assisted with immunoblotting
Divleen Mangat: Assisted with TCLS studies
Mirna Ragheb: Assisted with some Ca^{2+} assays
Katarina Kowatsch: Assisted with immunoblotting
Dheerendra Pandey: Performed RT-PCR
Seyed Mojtaba Hosseini: Neuronal cell culture and imaging
Tillie Hackett: Supplied human lung cryosections
Soheila Karimi-Abdolrezaee: Supervised neuronal cell culture and imaging
Amir Ravandi: Contributed to OxPAPC sample analysis and manuscript review
Christopher Pascoe: Manuscript editing and review
Andrew Halayko: Conceived the project and its design, data plan, and edited manuscript

4.1 Abstract

Asthma pathobiology includes oxidative stress that modifies cell membranes and extracellular phospholipids. Oxidized phosphatidylcholines (OxPC) in lung lavage from allergen-challenged human participants correlate with airway hyperresponsiveness, and induce bronchial narrowing in murine thin cut lung slices (TCLS). OxPC activate many signaling pathways, but mechanisms for these responses are unclear. We hypothesize that OxPC stimulate intracellular free Ca^{2+} flux to trigger airway smooth muscle (ASM) contraction. Intracellular Ca^{2+} flux was assessed in Fura-2 loaded, cultured human airway smooth muscle (HASM) cells. Oxidized 1-palmitoyl-2-arachidonoyl-sn-glycero-3-phosphocholine (OxPAPC) induced ~3-fold increase in 20kDa myosin light chain phosphorylation. This correlated with a rapid peak in intracellular cytoplasmic Ca^{2+} concentration ($[Ca^{2+}]_i$)(143 nM), and a sustained plateau that included slow oscillations in $[Ca^{2+}]_i$. Sustained $[Ca^{2+}]_i$ elevation was ablated in Ca^{2+}-free buffer and by TRPA1 inhibition. Conversely, OxPAPC-induced peak $[Ca^{2+}]_i$ was unaffected in Ca^{2+}-free buffer, TRPA1 inhibition, or by the IP_3 receptor inhibition. Peak $[Ca^{2+}]_i$ was ablated by pharmacologic inhibition of ryanodine receptor (RyR) Ca^{2+} release from sarcoplasmic reticulum. Inhibiting the upstream RyR activator cADPR with 8-Br-cADPR was sufficient to abolish OxPAPC-induced cytoplasmic Ca^{2+} flux. OxPAPC induced ~15% bronchial narrowing in TCLS that could be prevented by pharmacologic inhibition of either TRPA1 or RyR, which similarly inhibited OxPC-induced myosin light chain phosphorylation in cultured HASM. In summary, OxPC mediates airway narrowing by triggering TRPA1 and RyR-mediated mobilization of intracellular and extracellular Ca^{2+} in ASM. These data suggest that OxPC in the airways of allergen challenged subjects, and subjects with asthma may contribute to airway hyperresponsiveness.

4.2 Background

Asthma is marked by persistent airway inflammation linked to episodes of wheezing, bronchial spasm, and airway hyperresponsiveness (AHR) after allergic and non-allergenic exposures [1]. There are limits to effective therapeutic control, with up to 10% of asthmatics having severe disease that accounts for at least 50% of the total healthcare costs, indicating a real need for deeper understanding of pathobiology to meet clinical needs [6, 108, 228]. A substantial pathobiological feature of asthma is oxidative stress in the airways, but how this or its by-products determine disease phenotype and response to therapies is not fully understood [211]. Endogenous anti-oxidant systems in the lungs can be overwhelmed by inhaled environmental oxidants such as allergens, pollutants and smoking, and these factors contribute to chronic lung inflammation [211]. The overproduction of reactive oxygen species (ROS) and reactive nitrogen species (RNS) is associated with therapy-resistant asthma pathophysiology, symptom severity, and persistent lung inflammation [129-131]. ROS and RNS can modify diverse biomolecules, for instance lipids in cell membranes and lung lining fluid. The peroxidation of phospholipids generates new bioactive mediators, including oxidized phosphatidylcholines (OxPC) [229-231]. Our recent report describes a panel of OxPC that are generated after allergen challenge in the airways of participants with atopic asthma, and that correlates with the severity of AHR [176]. Despite this insight, the specific effects of these mediators on the structural cells of the airways have not been investigated until now.

OxPC is abundant in cell membranes, and in extracellular fluids such as bronchoalveolar lavage (BAL) [176] and blood [156]. For instance, multiple oxidized derivatives of 1-palmitoyl-2-arachidonoyl-sn-glycero-3-phosphocholine (OxPAPC) are observed in BAL in association with asthma [176] and as a component of oxidized low-density lipoprotein in association with

atherosclerosis [232-234]. Our recent work has revealed that OxPAPC exposure is sufficient to induce pro-inflammatory cytokine release by cultured HASM cells, airway narrowing in murine thin cut lung slices (TCLS), and disruption of the airway epithelial layer in association with disruption of mitochondrial metabolic activity [176, 178]. OxPAPC can induce elevation of intracellular Ca^{2+} in endothelial cells, activating calcineurin/nuclear factor of activated T cells (NFAT) pathways [235], and it can cause calcium influx into sensory neurons involving inflammatory pain [165]. Notably, mobilization of intracellular Ca^{2+} is the essential trigger for airway smooth muscle (ASM) contraction; however, how OxPAPC might affect intracellular Ca^{2+} in these cells to induce contraction is uninvestigated.

In this study, we assessed whether OxPAPC induces contraction of ASM cells and the mechanisms associated with $[Ca^{2+}]_i$ flux that underpin the contractile response. We used cultured human ASM cells loaded with the Ca^{2+}-sensitive dye, Fura-2, to measure $[Ca^{2+}]_i$ flux, and selective pharmacological inhibitors to investigate the pathways that control changes in $[Ca^{2+}]_i$ in response to OxPAPC. We also validated the role of specific Ca^{2+} pathways involving influx through transient receptor potential cation channel member A1 (TRPA1) and ryanodine receptor (RyR) mediated release from sarcoplasmic reticulum stores in smooth muscle contraction using murine TCLS. Some of the results of this study were previously reported in the form of abstracts [236, 237].

4.3 Materials and methods

4.3.1 Measurement of $[Ca^{2+}]_i$ flux in HASM cells

Real-time quantification of intracellular cytoplasmic Ca^{2+} ($[Ca^{2+}]_i$) was performed as described previously [83, 223], using Fura-2 AM (Life Technologies, Eugene, OR, USA), a Ca^{2+}-sensitive fluorescent dye. Briefly, the cells were loaded with 5 μg/mL Fura-2 AM (37°C, 0.5 h) in HBSS buffer (pH 7.4) with 0.01% pluronic acid, then in HBSS buffer (room temperature, 0.5 h) to facilitate deesterification of Fura-2 AM. The HBSS buffer for this assay contained 0.1% BSA. For all subsequent analyses, cells were maintained in either HBSS buffer (1.26 mM Ca^{2+}) or HBSS buffer (0 mM Ca^{2+}) as specified in individual experiments. An Olympus LX-70 inverted epifluorescence microscope (20X objective) (Olympus, Richmond Hill, ON, Canada) coupled to a Nikon CCD camera controlled by NIS imaging software (NIKON Instruments Inc., Melville, NY, US) was used for measurement of real-time changes in $[Ca^{2+}]_i$. The system was equipped with a Sutter Instruments (Novato, CA, USA) Lambda 10-2 filter wheel and controller with repeated 100-ms excitation at 340 and 380 nm; emission at 510 nm was recorded continuously for up to 3 min after cell stimulation. The ratio of 510 nm emission as excited by 340- and 380-nm, respectively, was converted to $[Ca^{2+}]_i$ from a calibration curve generated using Ca^{2+} standards [238]. After a stable baseline was established for 30 sec, OxPAPC (10 to 80 μg/mL), PSPC (80 μg/mL), or acetylcholine (Ach; 0.1 μM) was added to HASM cells, and the fluorescence intensity was recorded for 3 min. In some studies, cell responses to OxPAPC (10 to 80 μg/mL) were measured in nominally Ca^{2+}-deficient HBSS buffer (0 mM Ca^{2+}). For study to identify cell membrane target for OxPAPC induced Ca^{2+} influx, fura-2 loaded cells in HBSS buffer (1.26 mM Ca^{2+}) were pretreated for 15 min with non-specific plasma membrane Ca^{2+}-channel blocker (Gd^{3+}, 500 μM) or TRPA1 inhibitor (HC-030031, 50 μM) or appropriate vehicle control (HBSS only or 0.5 % DMSO in HBSS buffer) before addition of OxPAPC (80 μg/mL). For experiments to

investigate the source of intracellular Ca^{2+} release, fura-2 loaded HASM cells in HBSS (0 mM Ca^{2+} ex.) were pretreated with inhibitors; inositol 1,4,5-triphosphate (IP3) receptor (Xestospongin C, 5 μM, 30 min), or ryanodine receptor (caffeine, 25 mM, 10 min; or ryanodine, 100 μM, 10 min; or 8-Br-cADPR, 100 μM, 15 min) or appropriate vehicle control (HBSS only or 0.5 % DMSO in HBSS buffer) before addition of OxPAPC (80 μg/mL) or Ach (0.1 μM).

4.3.2 Human neuron cultures from H9 embryonic stem cell (ESC)-derived neural precursor cells (NPC).

Human ESCs (H9 cell line – WAe009-A, catalog # AW09, WiCell) were differentiated to NPCs by dual SMAD inhibition, and then human neurons were generated from NPCs using established protocols [239-241].

4.3.3 Immunoblotting

Seven-day serum starved HASM cells (grown in 100 mm cell culture dish) were equilibrated with HBSS buffer (buffer for assay was containing 0.1% BSA) for 1 hour (37°C), and then treated with control (vehicle- HBSS buffer), PSPC (80 μg/mL), OxPAPC (80 μg/mL), or Ach (0.1 μM) for 2-min at room temperature. After treatment, cells were washed with ice-cold HBSS (without BSA) on ice and immediately lysed with ice-cold RIPA buffer (40 mM Tris pH 8.0, 150 mM NaCl, 1% IGEPAL (NP-40), 1% sodium deoxycholate,) supplemented with 1 mM phenylmethylsulphonyl fluoride, 1 mM Na-orthodonavate, and protease and phosphatase inhibitors cocktail (Sigma Aldrich). The general immunoblotting procedure (as described in section 3.6) was performed for MLC analysis with 20 μg of total protein was loaded into wells of 12% SDS-PAGE gels. After electrophoresis, protein was transferred to nitrocellulose membranes and blocked. Membranes were probed with primary antibody diluted with 1% milk in TBS-T (1:750 anti-p-MLC, 1:1000 anti-MLC or 1:10,000 anti-β-actin) overnight and then with secondary antibody (1:5,000 goat anti-rabbit IgG-peroxidase). Similarly, for TRPA1 immunoblotting, we loaded 50 μg of total protein

from HASM cell cultures of four independent donors, and lysates from human neuron cultures as a positive control for TRPA1 then performed 6% SDS-PAGE before electro-transfer to nitrocellulose membranes. Membranes were probed with mouse anti-TRPA1 antibody (1:500) and then by goat anti-mouse IgG-peroxidase (1:5,000).

4.3.4 Real-time PCR for human TRPA1 mRNA

Confluent cultured of HASM cells or human neurons were lysed in TRIzol™ reagent (Invitrogen, Waltham, Massachusetts, USA) and total RNA was extracted. Normalized total RNA were used for cDNA synthesis with high-capacity cDNA reverse transcription kit (Applied Biosystems, Waltham, Massachusetts, US) followed by qRT-PCR with PowerTrack SYBR Green master mix, Applied Biosystems (Applied Biosystems, Waltham, Massachusetts, US) by using human TRPA1 (*hTRPA1*) primer set, *hTRPA1* forward (5'-CCCCTCTGCATTGTGCTGTA-3') and *hTRPA1* reverse (5'-TGGCTCCTCTCCACATAGCT-3'). Amplification of *hTRPA1* was also confirmed by 2% agarose gel electrophoresis.

4.3.5 Murine thin-cut lung slice (TCLS) studies

First baseline airway size was recorded under HBSS perfusion, then the perfusate was switched to a single concentration of OxPAPC (80 μg/mL) in HBSS with or without Ca^{2+} (1.26 mM and 0 mM, respectively), and airway lumen size was recorded for 3 minutes. To evaluate the impact of inhibitors on airway narrowing, individual TCLS were pre-perfused with inhibitors; ryanodine receptor (caffeine, 25 mM, 10 min; or ryanodine, 100 μM, 10 min;), TRPA1 inhibitor (HC-030031, 50 μM, 15 min) or appropriate vehicle control (HBSS or 0.5 % DMSO in HBSS), before the perfusate was switched to OxPAPC (80 μg/mL) in presence of each inhibitor, and airway lumen size was recorded for 3 minutes. For some studies we used methacholine (Mch, 0.1 μM) as positive control.

4.3.6 Immunocytochemistry

HASM cells were grown to ~60% confluence on pre-cleaned sterile glass coverslips and serum starved for 2-3 days. Cells were washed with cold cytoskeleton buffer (CB) (mM: 10 MES, 150 NaCl, 5 EGTA, 5 MgCl2, and 5 glucose at pH 6.1) then fixed with CB buffer containing 3% paraformaldehyde (PFA) for 15 min at 4°C. Cells were permeabilized with buffer containing 0.3% Triton X-100 for 5 min at 4°C, washed, then blocked with buffer containing 2% BSA (IgG and protease free) and 2% normal donkey serum, for 2 h at room temperature. Subsequently, cells were incubated with primary antibody anti-TRPA1 (1:100) in CB/0.1% Tween 20/ 2% BSA overnight at 4°C. For negative controls, we omitted the primary antibody. Cells were next incubated with Cy3-conjugated donkey anti-mouse IgG (1:1000), and after a buffer rinse, nuclei were counterstained with DAPI (1µg/mL) and coverslips were mounted with Fluoromount-G^{TM} antifade medium (Life Technologies Corp., Carisbad, CA, USA). Fluorescent imaging was performed using both Zeiss epifluorescence and Zeiss LSM700 spectral confocal microscopes and 4-5 fields in cultures from four independent HASM donors.

4.3.7 Immunohistochemistry

To validate studies using cultured HASM cells, we surveyed TRPA1 abundance using fluorescent immunohistology in lung tissue cryosections. These cryosections were prepared from six healthy control subjects (non COPD; non smoker) donated human lung cores (Table 4.1) were provided by the James Hogg Lung Registry (ethics ID: H00-50110) University of British Columbia [242]. Donor lungs inflated with cryomatrix were frozen in liquid nitrogen, and from trans-axial plane samples of the lung, cylindrical cores (15 mm x 20 mm), 5 µM thick cryosections were mounted on slides, then stored at -80ºC. For processing, sections were air dried (10 min, RT), fixed (3% paraformaldehyde-PBS, pH 7.4, 15 min, 4 ºC) and permeabilized (0.3% Triton X-100, PBS, pH

7.4, 10 min, 4ºC). In humidified chamber, slides were blocked (3% normal donkey serum, 3% IgG free BSA, 0.3 M glycine, PBS, pH 7.4, room temperature) for 2.5 hours before overnight incubation at 4°C with primary antibodies – mouse anti-TRPA1 (1:100), rabbit anti-vimentin (1:25), rabbit anti-β-tubulin III (1:750) – diluted in PBS/ 0.1% Tween 20 (PBST). For negative controls, the primary antibody was omitted. Sections were next incubated with Cy3-conjugated donkey anti-mouse IgG (1:500) and Cy5-conjugated donkey anti-rabbit IgG (1:1000) antibodies. Nuclei were counterstained with DAPI (1µg/mL), then mounted with Fluoromount-G™ antifade medium (Life Technologies Corp., Carisbad, CA, USA). Fluorescent imaging was performed with Zeiss epifluorescence and Zeiss LSM700 spectral confocal microscopes.

Table 4.1. Characteristics of human lung donors (non COPD; non smoker)

Donor	Sex	Age	FEV1 (% Predicted)	FEV1/FVC
Donor 1	F	66	121	0.81
Donor 2	F	71	61	0.70
Donor 3	F	69	59	0.86
	Mean±SEM	**68.7±1.5**	**80.3±20.3**	**0.79±0.04**
Donor 4	M	68	90	0.77
Donor 5	M	72	70	0.73
Donor 6	M	69	114	0.79
	Mean±SEM	**69.7±1.2**	**91.3±12.7**	**0.76±0.02**

4.3.8 Statistical analysis

Measurement of $[Ca^{2+}]_i$ was performed in at least 30 cells from four HASM cell lines each derived from 4 independent donors. Assessment of airway narrowing was carried out on at least 18 airways from three different mice. Depending on the design of individual experiments and unless otherwise specified, statistical significance was determined by one-way ANOVA with Dunnets's multiple-comparison tests or multiple t tests with Holm-Sidak's multiple comparisons using GraphPad Prism version 8.4.3 (San Diego, CA, USA). The Ca^{2+} curves were analyzed by nonlinear regression fit with straight-line model to estimate and compare rate (slope) of $[Ca^{2+}]_i$ change over time. Data shown represents mean±SEM unless otherwise specified. $P<0.05$ was considered statistically significant.

4.4 Results

4.4.1 OxPAPC induces $[Ca^{2+}]_i$ flux in HASM cells

Using real time imaging, we measured whether OxPAPC induces changes in $[Ca^{2+}]_i$ in HASM cells. HASM exhibited a rapid increase in $[Ca^{2+}]_i$ in response to OxPAPC. Peak increase in $[Ca^{2+}]_i$ from baseline was 143.0±14.48 nM in response to the highest concentration of OxPAPC (Figure 4.1A and 4.1B). This was comparable to the response induced by 0.1μM Ach (peak increase of 169.23±53.23 nM $[Ca^{2+}]_i$ from baseline) (Figure 4.1A and 4.1B). We used OxPAPC from 10 to 80 μg/mL as this was consistent with OxPC levels in human lung lavage after allergen challenge [176], and because Ca^{2+} influx is induced in cultured mouse dorsal root ganglion cells and TRPA1-expressing HEK293 with OxPAPC 10 to 100 μg/mL. The non-oxidized phospholipid, PSPC (80 μg/mL)(negative control), did not induce a distinct rise in $[Ca^{2+}]_i$, but a trend for a gradual increase in baseline over the 3 minutes was evident (Figure 4.1A and 4.1B). We further assessed the kinetics of $[Ca^{2+}]_i$ change in response to OxPAPC, and we observed that cells heterogeneously exhibit secondary $[Ca^{2+}]_i$ oscillation (Figure 4.1A). To quantify this response, we defined cells as having a repeated response to be the ones that exhibit at least one additional increase of ≥40 nM $[Ca^{2+}]_i$ from baseline after an initial rapid peak response. The percentage of cells that showed repeated responses was concentration dependent, with 80 μg/mL OxPAPC inducing secondary $[Ca^{2+}]_i$ oscillation in 76.0 ± 9.08 % of cells, whereas 10 μg/mL OxPAPC induced secondary $[Ca^{2+}]_i$ oscillation in only 30.5 ± 10.7 % of all cells (Figure 4.1C).

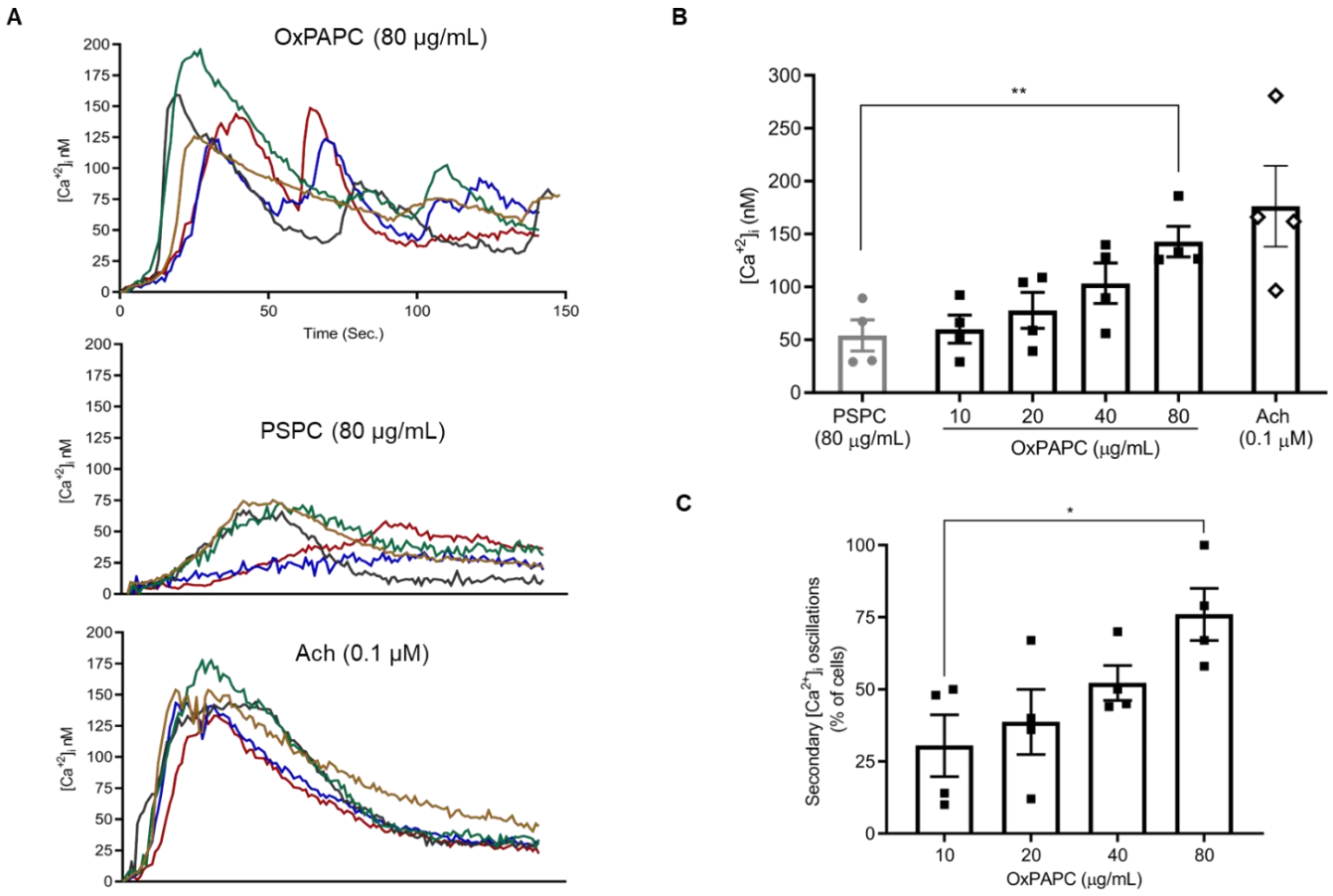

Figure 4.1: OxPAPC induces cytoplasmic Ca^{2+} flux in HASM cells.

Free cytosolic Ca^{2+} concentration ($[Ca^{2+}]_i$) was measured for 3-min by fluorescence microscopy in Fura-2 AM loaded cells. Cells were stimulated with OxPAPC (10-80 µg/mL), PSPC (80 µg/mL) or Ach (0.1 µM/mL). **(A)** Representative temporal tracings showing transient elevation of $[Ca^{2+}]_i$ followed by secondary $[Ca^{2+}]_i$ oscillation in five HASM cells exposed to OxPAPC (80 µg/mL), and comparative tracings of cells exposed to PSPC (80 µg/mL) or Ach (0.1µM). **(B)** Scatter dot plot comparing the increase in peak $[Ca^{2+}]_i$ over baseline in response to PSPC (80 µg/mL), different concentrations of OxPAPC (10-80 µg/mL), and Ach (0.1µM). The bars represent mean±SEM from at least total 30 cells present within the microscopic field (7-10 cells/ cell line) of HASM cultures from four donors. **(C)** Scatter dot plot showing mean±SEM of the percentage of cells exhibiting secondary $[Ca^{2+}]_i$ oscillations in response to OxPAPC (10-80 µg/mL). The data were analyzed by one-way ANOVA with Dunnett's multiple-comparison test; *p<0.05, **p<0.01 compared with respective controls. Ach: acetylcholine

4.4.2 OxPAPC induces myosin light chain phosphorylation in HASM cells

Excitation contraction coupling in HASM cells involved increased $[Ca^{2+}]_i$ that leads to the phosphorylation of myosin light chain (MLC), which is essential for activation of cross bridge cycling. To explore whether the OxPAPC-induced $[Ca^{2+}]_i$ flux was sufficient to induce MLC phosphorylation, we used immunoblotting with an antibody that detects MLC Thr18 and Ser19 phosphorylation. We prepared HASM lysates after 2 minutes exposure to non-oxidizable PSPC (80 μg/mL), OxPAPC (80 μg/mL) and Ach (0.1 μM/mL). We detected low levels of p-MLC protein in control conditions, and consistent with $[Ca^{2+}]_i$ data (Figure 4.1), p-MLC was not significantly increased by PSPC (Figure 4.2A and 4.2B). However, OxPAPC increased p-MLC by 3-fold, an effect that nearly matched that induced by Ach (increased p-MLC by 3.5 fold) (Figure 4.2A and 4.2B). This confirms that OxPAPC-induced $[Ca^{2+}]_i$ flux leads to MLC phosphorylation in HASM cells, which is consistent with our previous report that OxPAPC triggers airway narrowing in murine TCLS [176].

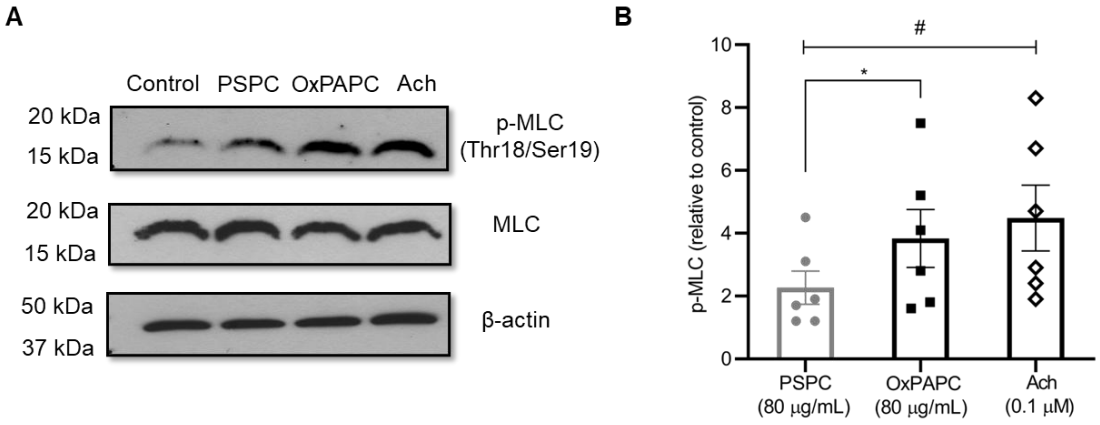

Figure 4.2: OxPAPC induces MLC phosphorylation in HASM cells.
(A) Representative immunoblots of 20 kDa MLC phosphorylation (Thr18/Ser19) (p-MLC), total MLC, and loading control β-actin. **(B)** Scatter dot plot comparing mean±SEM of p-MLC (relative to control) response to PSPC (80 μg/mL), OxPAPC (80 μg/mL) and Ach (0.1μM). The integrated density value first normalized to respective loading control (β-actin) and then calculated as fold change relative to control p-MLC level from at least 3 cell lines (two replicates of each) is shown. The data were analyzed by one-way ANOVA with Dunnett's multiple-comparison test; $^{*,\#}p<0.05$ compared with PSPC control.

4.4.3 Role of Extracellular Ca^{2+} in $[Ca^{2+}]_i$ flux and airway narrowing induced by OxPAPC

To investigate whether extracellular Ca^{2+} is a source for $[Ca^{2+}]_i$ flux in OxPAPC-exposed HASM cells, we compared responses in Ca^{2+}-deficient HBSS (0 mM Ca^{2+}) and Ca^{2+}-replete HBSS (1.26 mM Ca^{2+}). The absence of extracellular Ca^{2+} did not significantly affect the OxPAPC (80 µg/mL)-induced $[Ca^{2+}]_i$ peak from baseline (e.g. 143.0±14.48 nM in 1.26 mM Ca^{2+} buffer *vs* 139.76±25.50 in 0 mM Ca^{2+} buffer) (Figures 4.3A and 4.3B). However, the temporal response of HASM was markedly affected by the absence of extracellular Ca^{2+}, as secondary $[Ca^{2+}]_i$ oscillations were absent (Figure 4.3A and 4.3C). To quantify this effect, using mean curves generated from all cell studies, we performed linear regression analysis to estimate the rate of $[Ca^{2+}]_i$ change over time (slope) in response to OxPAPC (80 µg/mL). Specifically, for Ca^{2+}-replete and Ca^{2+}-deficient conditions we calculated the slope of the $[Ca^{2+}]_i$ response after peak from the time when the curves intersected (~56 seconds after OxPAPC exposure, Figure 4.3C). Consistent with the absence of repeat $[Ca^{2+}]_i$ oscillations, mean $[Ca^{2+}]_i$ decreased markedly in Ca^{2+}-deficient conditions (slope -0.62), whereas $[Ca^{2+}]_i$ remained relatively stable in HASM incubated in Ca^{2+}-replete buffer (slope +0.17) (Figure 4.3D).

To validate a role of extracellular Ca^{2+} in OxPAPC-induced airway narrowing, we used murine TCLS and time-lapse video microscopy to measure changes in airway lumen diameter in response to OxPAPC (80 µg/mL). We did not observe any change in baseline airway lumen area in TCLS in zero-Ca^{2+} HBSS (-1.4% change in lumen area). We confirmed that OxPAPC induces airway closure in Ca^{2+}-containing HBSS, however, this response was abrogated when TCLS were studied in zero-Ca^{2+} HBSS (Figure 4.3E and 4.3F). Negative control PSPC (80 µg/mL) did not induce a distinct reduction in airway lumen in either Ca^{2+}-deficient or Ca^{2+}-replete HBSS (Figure 4.3E). Collectively, these findings indicate that OxPAPC exposure causes peak and prolonged oscillation

of $[Ca^{2+}]_i$ in HASM cells, and that the secondary $[Ca^{2+}]_i$ oscillations appear to be necessary for airway narrowing.

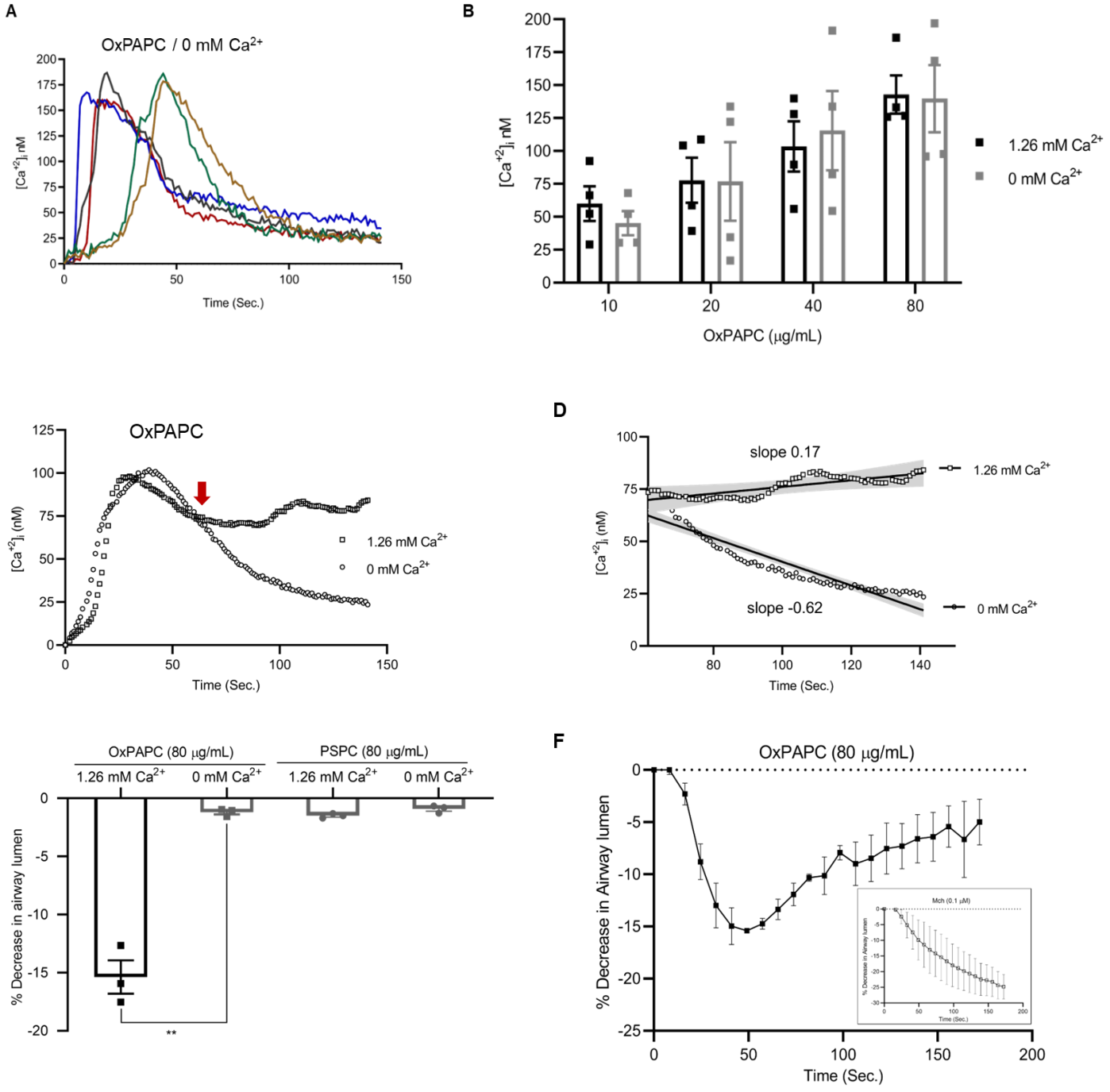

Figure 4.3: OxPAPC mediates extracellular Ca^{2+} dependent secondary $[Ca^{2+}]_i$ oscillation in HASM cells, and airway narrowing in murine TCLS.

Fura-2 AM loaded HASM cells in nominally Ca^{2+} free HBSS buffer (0 mM Ca^{2+}) and $[Ca^{2+}]_i$ change in response to OxPAPC (10-80 µg/mL) was measured up to 3-min. **(A)** Representative temporal tracings showing single transient elevation of $[Ca^{2+}]_i$ in five random HASM cells exposed to OxPAPC (80 µg/mL). **(B)** Scatter dot plot of increase in peak $[Ca^{2+}]_i$ over baseline in response to OxPAPC (10-80 µg/mL) in Ca^{2+}-containing (1.26 mM Ca^{2+}) and 0 mM Ca^{2+} buffer. Each data point represents mean±SEM from at least 30 HASM cells from cultures derived from four different donors. Data analyzed by multiple t tests with Holm-Sidak's multiple comparisons test, no significance ($p>0.05$). **(C)** Each data point represents the average of at least 30 cells (four donors) and shows the $[Ca^{2+}]_i$ in two buffer conditions (1.26 mM Ca^{2+} and 0 mM Ca^{2+}) in response to OxPAPC (80 µg/mL). **(D)** Starting from the time after OxPAPC stimulation (~56 Sec.) where curves intersect after peak $[Ca^{2+}]_i$ (red arrow in Figure 4.3C), nonlinear regression fit with straight-line model was used to estimate rate (slope) of $[Ca^{2+}]_i$ change in different buffer conditions, and compared for statistical significance. The slopes were significantly different ($p<0.001$). **(E)** Scatter dot plot showing percentage decrease from baseline of airway lumen area in murine TCLS in response to OxPAPC (80 µg/mL) or PSPC (80 µg/mL) in 1.26 mM Ca^{2+} and 0 mM Ca^{2+} HBSS buffers. Data represents mean±SEM from at least 18 airways of 3 mice, analyzed by two-tailed t-test, $^{**}p<0.01$. **(F)** Time course of % decrease in airway lumen for murine TCLS. Data represents mean±SEM from at least 18 airways (3 mice) in response to OxPAPC (80 µg/mL). The curve in the insert shows the reference kinetics for % decrease in airway lumen in response to Mch (0.1µM). Legend: 0 mM Ca^{2+} = Ca^{2+} free HBSS buffer; 1.26mM Ca^{2+} = 1.26mM Ca^{2+} HBSS.

4.4.4 TRPA1 channels are required for OxPAPC induced Ca^{2+} influx in HASM cells and airway narrowing in murine TCLS

To identify pathways for OxPAPC-induced Ca^{2+} influx in HASM cells, we used Fura-2 loaded cells in Ca^{2+}-replete HBSS in the presence of Gd^{3+} (500 μM), a non-specific blocker of Ca^{2+}-permeable plasma membrane channels [214](Table 3.1). Gd^{3+} did not affect initial peak in $[Ca^{2+}]_i$ induced by OxPAPC, but sustained, secondary $[Ca^{2+}]_i$ oscillations were abolished (Figures 4.4A and 4.4B). To quantify the effects of Gd^{3+}, we performed linear regression analysis to compare the rate of $[Ca^{2+}]_i$ change over time (slope). In Gd^{3+} treated HASM cells, the decline in OxPAPC-induced $[Ca^{2+}]_i$ (slope -0.77) was similar to that we observed in Ca^{2+}-deficient conditions and markedly different than the response to OxPAPC alone (slope +0.21) that featured repeated $[Ca^{2+}]_i$ increases in individual cells (Figures 4.4C and 4.4D).

On the basis of these findings, we evaluated the role of the nonselective membrane cation channel, transient receptor potential cation channel member A1 (TRPA1), expressed on neuronal and non-neuronal cells in the lungs, including ASM [243]. TRPA1 is a chemosensor for exogenous irritants and endogenous pro-inflammatory mediators, including OxPAPC [165], and its inhibition prevents bronchial contraction evoked by selective TRPA1 agonists [215]. We measured changes in $[Ca^{2+}]_i$ in Fura-2 loaded HASM in the presence and absence of the selective TRPA1 antagonist, HC-030031, using a concentration that significantly inhibits TRPA1 channel activity (50 μM)[216](Table 3.1). TRPA1 antagonism abrogated secondary $[Ca^{2+}]_i$ oscillations induced by OxPAPC without significantly affecting the initial peak increase in $[Ca^{2+}]_i$ (Figure 4.4A and 4.4E). Consistent with this observation, the rate of decline of $[Ca^{2+}]_i$ in HASM cells was accelerated by HC-030031 pretreatment (slope -0.56) compared with cells treated with OxPAPC alone in which mean $[Ca^{2+}]_i$ remained elevated (slope +0.19) (Figures 4.4F and 4.4G). This revealed the requirement of TRPA1 for OxPAPC induced sustained Ca^{2+} influx. To validate this effect, we

measured the effects of TRPA1 inhibition on OxPAPC-induced airway narrowing in murine TCLS and on MLC phosphorylation in HASM cells. Though HC-030031 did not affect baseline lumen area, it did significantly reduce OxPAPC-induced airway narrowing (Figure 4.4H and 4.4I) and MLC phosphorylation (Figure 4.5). Taken together, these results reveal that TRPA1 channels are required for OxPAPC-induced Ca^{2+} influx, and sustained oscillations in $[Ca^{2+}]_i$ and MLC phosphorylation in HASM, as well as bronchial narrowing in response to OxPAPC exposure.

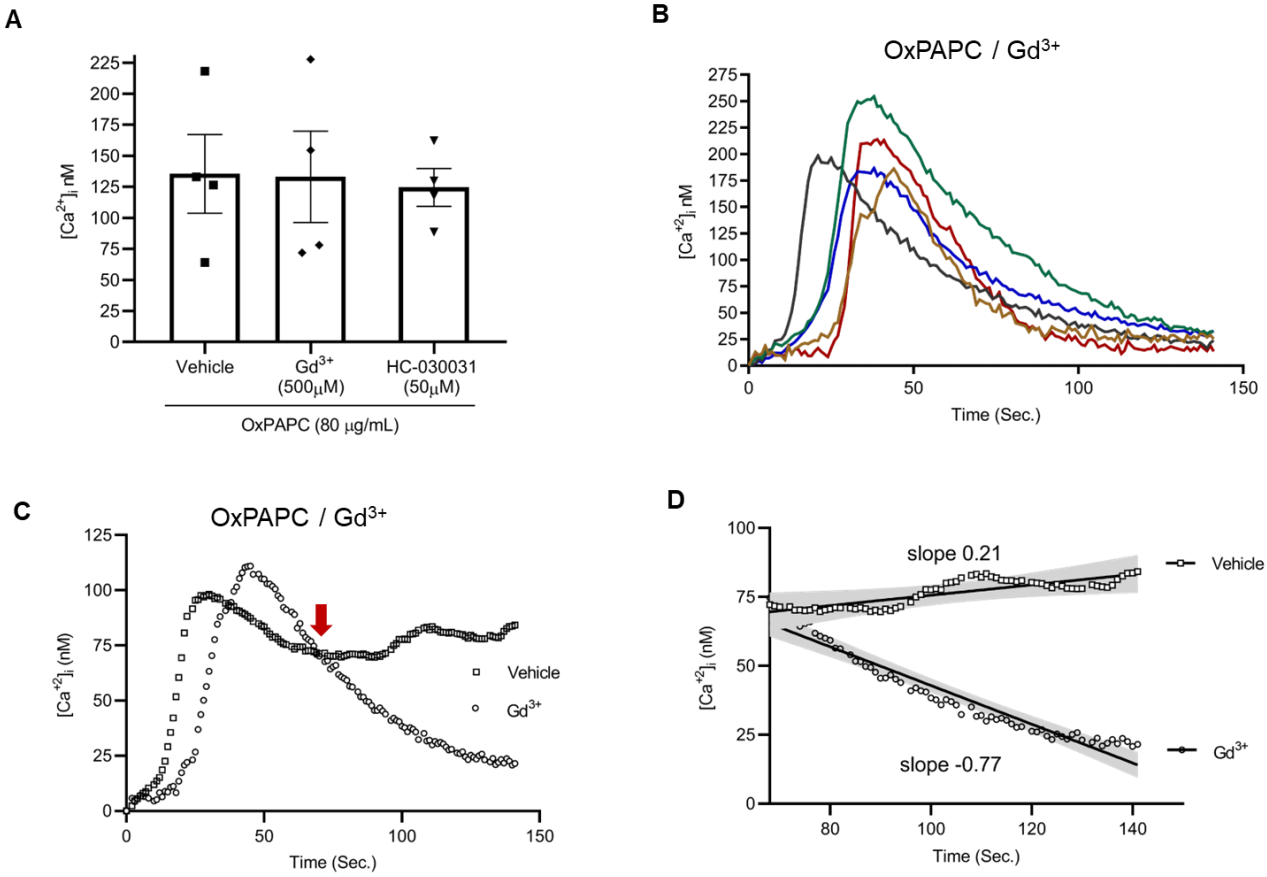

Figure 4.4 ***(Continued)***

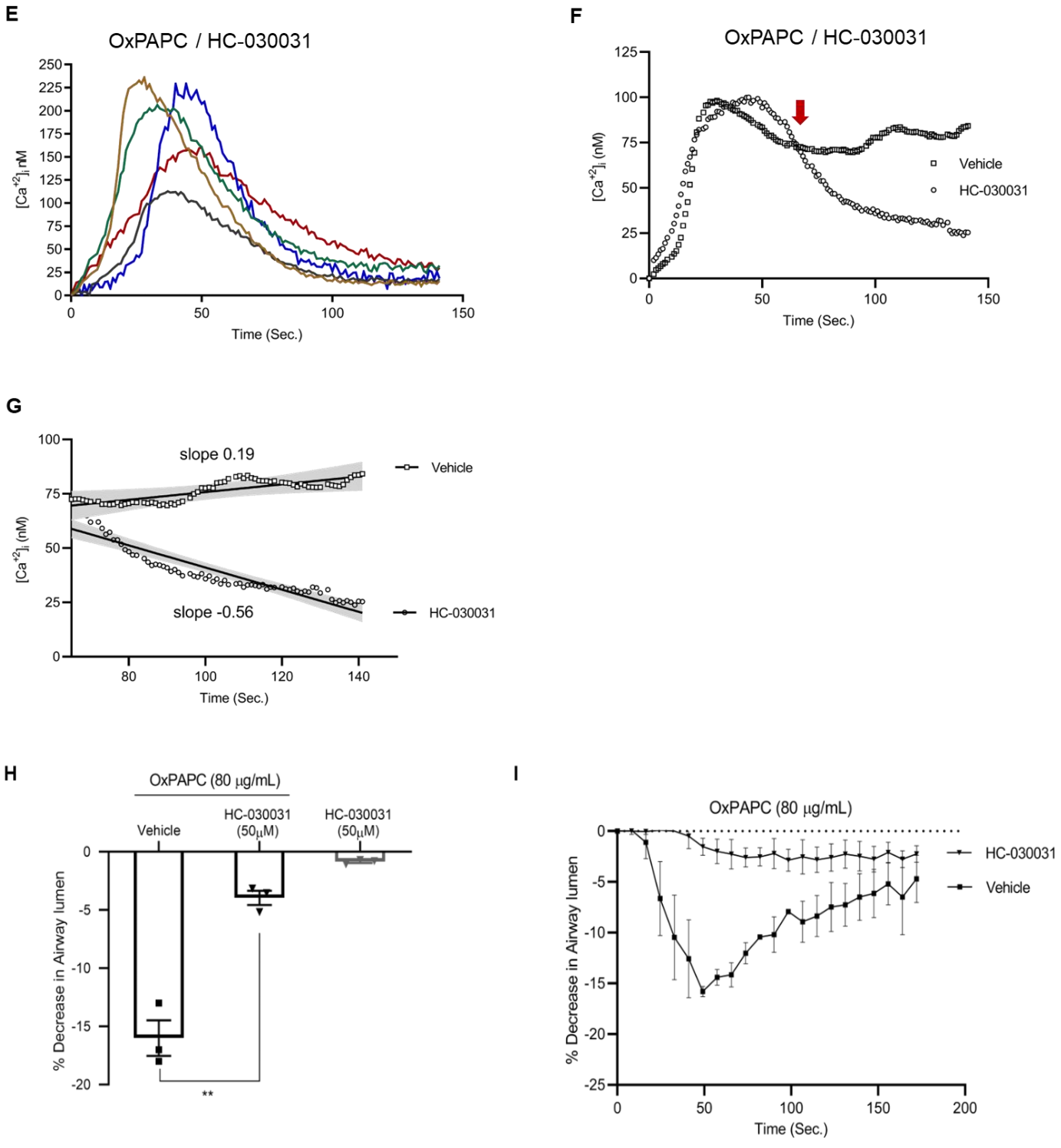

Figure 4.4 ***(Continued)***

Figure 4.4: Plasma membrane TRPA1 mediates Ca^{2+} influx in HASM cells and airway narrowing in murine TCLS induced by OxPAPC.

Fura-2 AM loaded HASM cells were pretreated (15 min) with Gd^{3+} (500 µM)(non-specific Ca^{2+}-channel blocker), HC-030031 (50 µM)(TRPA1 inhibitor), or vehicle, and $[Ca^{2+}]_i$ was recorded for up to 3 minutes in response to OxPAPC (80 µg/mL). **(A)** Scatter dot plot of increase in peak $[Ca^{2+}]_i$ in response to OxPAPC in presence and absence of Gd^{3+} or HC-030031. Data represent mean±SEM from 30 cells measured in cultures from four donors, and analyzed by 1-way ANOVA with Dunnett's multiple-comparison test, no significance ($p>0.05$). **(B)** Representative temporal tracings showing single transient elevation of $[Ca^{2+}]_i$ in response to OxPAPC of five random HASM cells pretreated with Gd^{3+}. **(C)** Each data point represents average $[Ca^{2+}]_i$ in response to OxPAPC of at least 30 cells (four donors) for HASM cells treated with Gd^{3+}. **(D)** Starting from the time after OxPAPC stimulation (~63 sec.) where curves intersect after peak $[Ca^{2+}]_i$ (red arrow in Figure 4.4C), nonlinear regression fit with straight-line model was used to estimate rate (slope) of $[Ca^{2+}]_i$ change in the presence and absence of Gd^{3+}. The slopes were significantly different ($p<0.001$). **(E)** Representative temporal tracings showing single transient elevation of $[Ca^{2+}]_i$ in response to OxPAPC of five random HASM cells pretreated with HC-030031. **(F)** Each data point represents average $[Ca^{2+}]_i$ in response to OxPAPC of at least 30 cells (four donors) for HASM cells treated with HC-030031. **(G)** Starting from the time after OxPAPC stimulation (~60 sec.) where curves intersect after peak $[Ca^{2+}]_i$ (red arrow in Figure 4.4F), nonlinear regression fit with straight-line model was used to estimate rate (slope) of $[Ca^{2+}]_i$ change in the presence and absence of HC-030031. The slopes were significantly different ($p<0.001$). **(H)** Scatter dot plot of percentage decrease in airway lumen over baseline in response to OxPAPC (80 µg/mL) of murine TCLS pretreated with HC-030031 (50 µM). The lack of effect of HC-030031 alone is also shown. Data represents mean±SEM of at least 18 airways from 3 mice and analyzed by two-tailed t-test, $^{**}p<0.01$. **(I)** Time course of % decrease in airway lumen in response to OxPAPC (80 µg/mL) alone (vehicle), and with HC-030031 (50 µM) in murine TCLS. Data represents mean±SEM of at least 18 airways (3 mice).

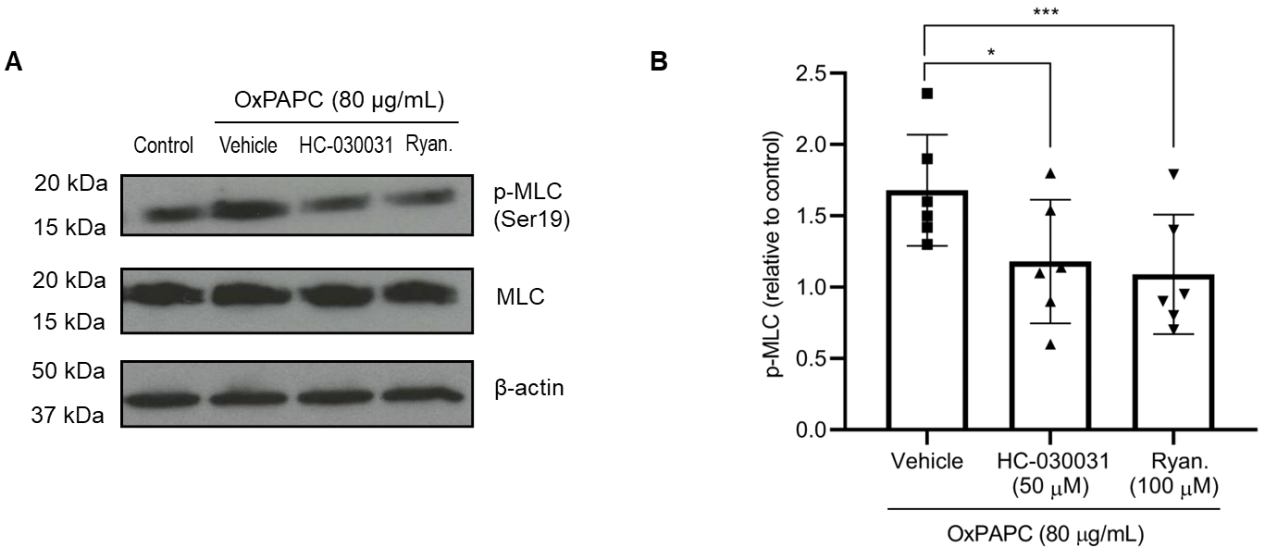

Figure 4.5: OxPAPC-induced MLC phosphorylation requires TRPA1 and ryanodine receptor Ca^{2+} stores in HASM cells.

(A) Representative immunoblots showing 20 kDa MLC phosphorylation (Ser19)(p-MLC), total MLC, and loading control, β-actin in control (untreated) conditions, and in response to OxPAPC (80 μg/mL) alone (vehicle), and with HC-030031 or ryanodine. **(B)** Scatter dot plot comparing mean±SEM of p-MLC (relative to control) in response to OxPAPC (80 μg/mL) alone (vehicle), and with HC-030031 or ryanodine. The integrated density value first normalized to loading control (β-actin) is plotted as fold-change relative to control p-MLC level in experiments from at least 3 cell lines (two replicates of each) is shown. The data were analyzed by two-tailed t-test; $^{*}p<0.05$, $^{***}p<0.001$ compared with control. Legend: Ryan = ryanodine.

4.4.5 Functional expression of TRPA1 in human ASM

To validate a role for TRPA1 in ASM cells, we assessed its expression in cultured HASM cells from four independent donors, using cultured human neurons as a positive control. Immunoblotting revealed TRPA1 protein (expected molecular weight 130 kD) in all HASM cell cultures, and in human neuronal cultures (Figure 4.6A). RT-PCR revealed abundant *TRPA1* mRNA in all HASM cell lines (average cycle threshold value, 20.6), which was confirmed with human neuron cultures (cycle threshold value 29.0) (Figure 4.6B). To confirm the presence of functional TRPA1 in HASM cell cultures, we employed the TRPA1 agonist allyl isothiocyanate (AITC) and measured $[Ca^{2+}]_i$ flux. At low concentrations, AITC induced $[Ca^{2+}]_i$ oscillations (Figure 4.6C) that were reminiscent of the pattern we had observed in response to OxPAPC. At higher concentrations, AITC induced more sustained elevations in $[Ca^{2+}]_i$. We constructed an AITC dose-response curve, which revealed a half-maximal effective concentration of 3.7 µM (Figure 4.6D) in HASM cells.

Immunocytochemistry of HASM cells showed strong labelling of TRPA1 in perinuclear regions, as well as elongated foci along the margins of many cells (Figure 4.6E and 4.6F). We determined the fraction of cells that were labelled for TRPA1 using manual counting of at least 10 cells in four fields for each of the four cell lines we studied and found 73±3.7% labeling frequency. We confirmed TRPA1 antibody labelling using human neuron cultures (Figure 4.6G and 4.6H). Negative controls using a primary antibody omission protocol did not exhibit any background fluorescence for immunocytochemistry or immunohistology of lung tissue (below)(not shown). We next performed TRPA1 immunolabeling in human lung tissue, and we observed TRPA1 staining in ASM, which was colabeled with the mesenchymal cell marker, vimentin (Figure 4.6I-K). We assessed the specificity of TRPA1 labelling in human lung tissues by confirming co-

incident staining of neuronal cells colabeled with the general neuronal marker, tubulin III (Figure 4.6L and 4.6M). Consistent with prior reports [244], we observed co-expression of TRPA1 with some, but not all areas of labeling with the neuronal marker in human airway sections.

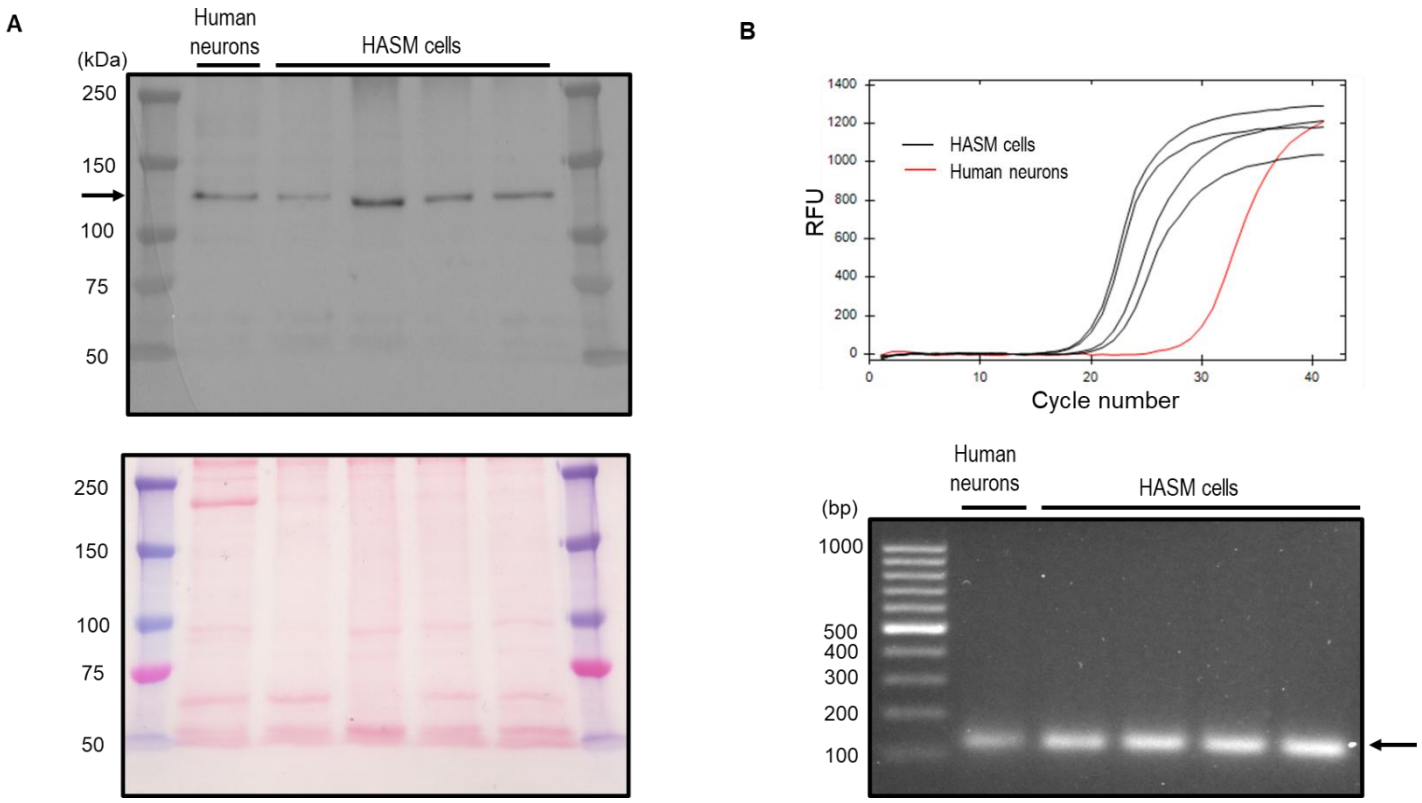

Figure 4.6 ***(Continued)***

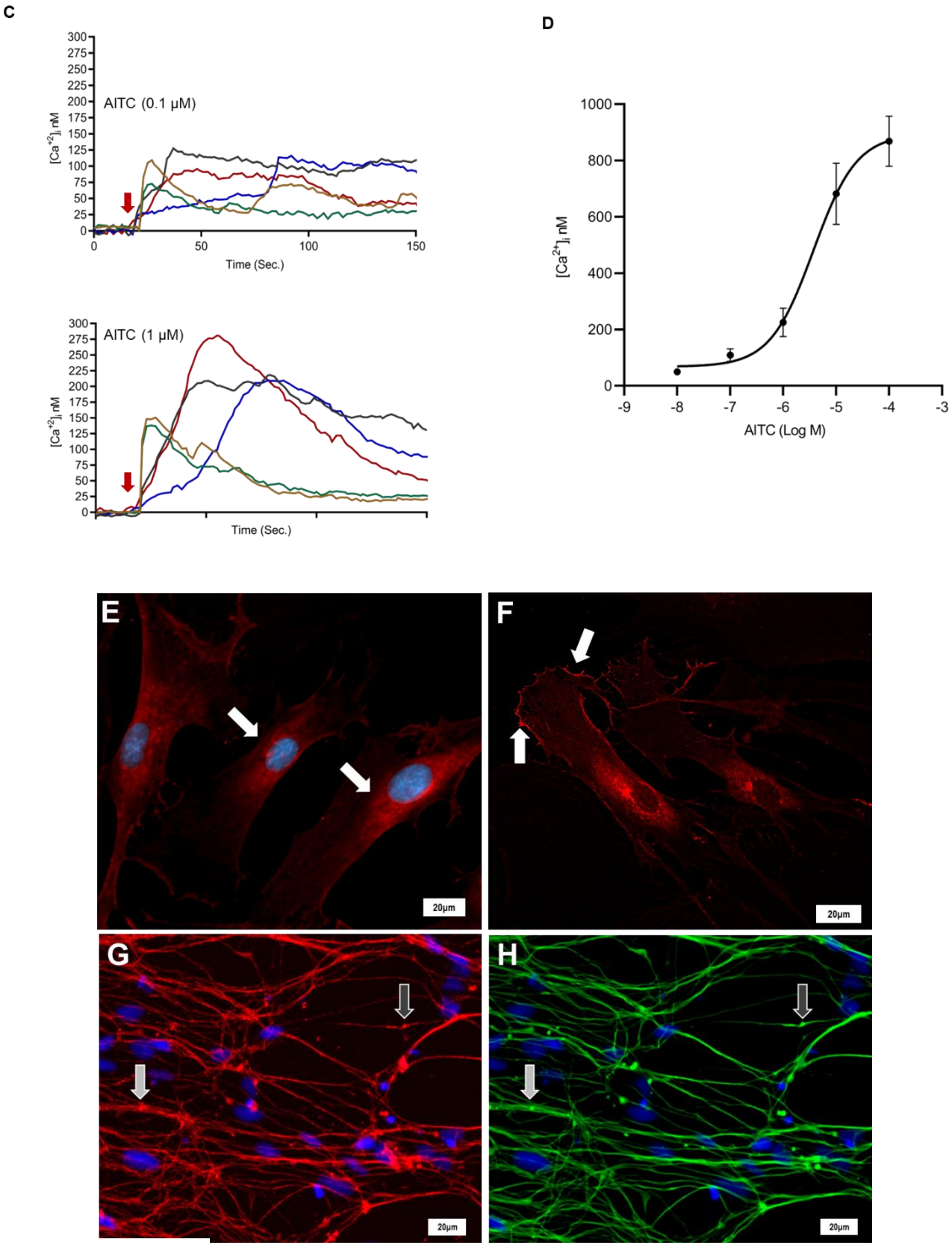

Figure 4.6 ***(Continued)***

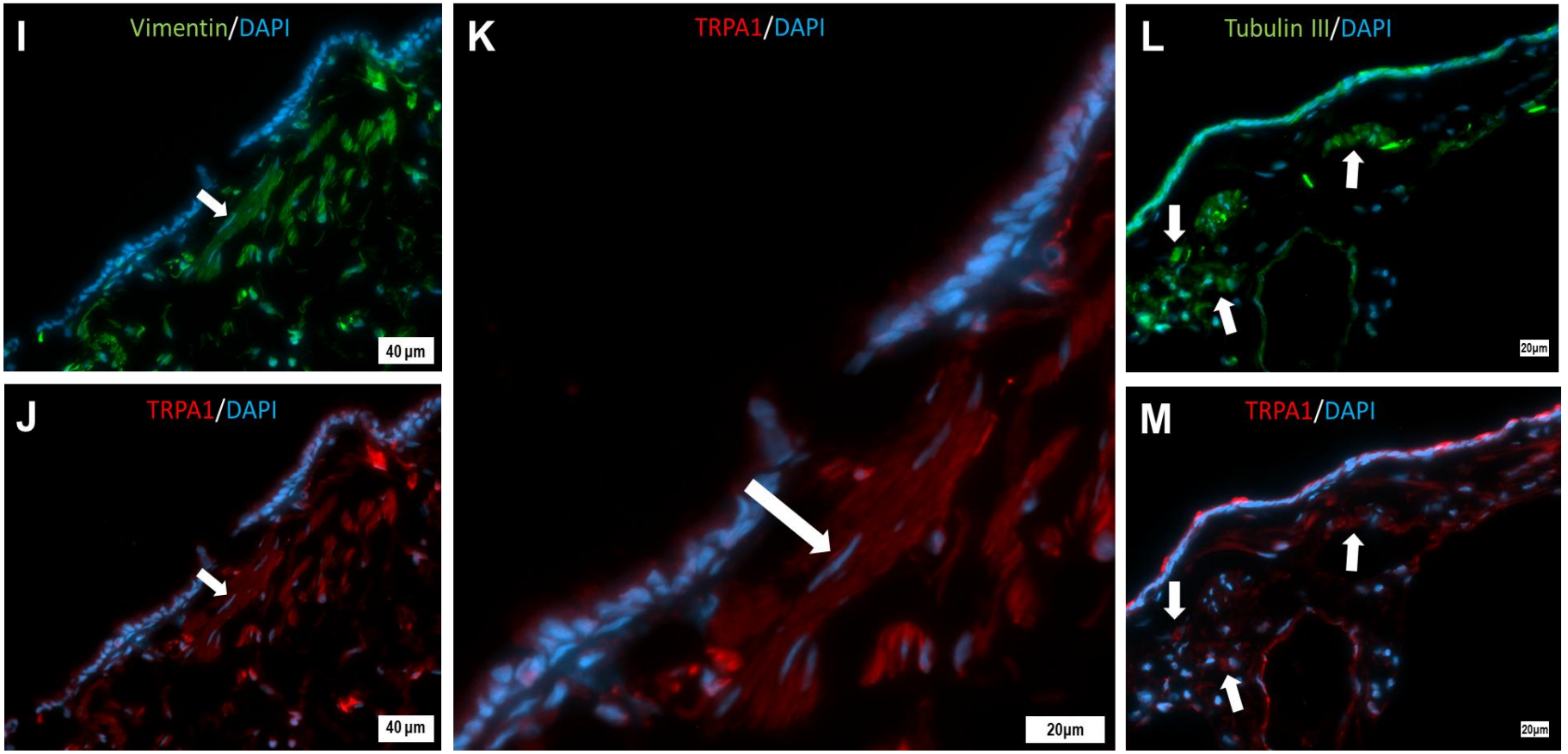

Figure 4.6 ***(Continued)***

Figure 4.6: TRPA1 expression and function in human airway smooth muscle.
(A) Upper panel shows a representative immunoblot for TRPA1 in lysates from four HASM cell cultures, and from a human neuron cell culture (positive control). Arrow indicates a band at the expected molecular weight (130 kDa). The lower panel shows the same blot stained for total protein with Ponceau S to confirm relative protein loading. **(B)** Upper panel shows qRT-PCR amplification curves for TRPA1 in HASM cells. Each black curve represents an independent sample from four HASM cell lines. The red curve represents TRPA1 from a human neuron culture (positive control). The lower panel shows SYBR™-stained agarose gel electrophoresis image of *TRPA1* PCR product gene (band size 116 bp, indicated by arrow). **(C)** Fura-2 AM loaded HASM cells were exposed to AITC (10 nM to 0.1 mM) and $[Ca^{2+}]_i$ was recorded for up to 3 minutes. Representative temporal tracings from four cell lines showing transient Ca^{2+} influx in five different HASM cells exposed to AITC (0.1 µM (upper panel), and 1.0 µM (lower panel)). **(D)** Dose-response curve for AITC-induced change in $[Ca^{2+}]_i$ (EC_{50} of 3.7µM). Each data point represents the mean±SEM $[Ca^{2+}]_i$ for at least 30 HASM cells from four donors. **(E)** Representative epifluorescence and **(F)** confocal immunofluorescence images of TRPA1 (red) labelling (arrows) in cultured HASM cells. Nuclei are stained with DAPI (blue). Images are representative of 4-5 fields in cultures from four independent HASM donors. **(G)** and **(H)**: Representative matching epi-immunofluorescence images of human neuron cell cultures dual labelled for TRPA1 (G, red) and the general neuronal marker, tubulin III (H, green). Colour matched arrows provide common location markers in each panel. Nuclei are stained with DAPI (blue). **(I)** and **(J)**: Representative matching double epi-immunofluorescence images of airways in human lung cryosections showing ASM (I, green, mesenchymal cell marker, vimentin) and, J: TRPA1 (red). Nuclei are stained with DAPI (blue). Arrows identify a common point of reference in images (I and J). Images are representative of sections from 6 different heathy donors. **(K)** Higher magnification of TRPA1 labelling from panel J. Arrow indicates location of an ASM bundle. **(L)** and **(M)**: Representative matching double immuno-epifluorescence images of airways in human lung cryosections showing neuronal elements (green, labelled with general neuron marker, tubulin III) and, M: TRPA1 (red). Nuclei are stained with DAPI (blue). Arrows identify a common point of reference in images (L and M). Images are representative of sections from 6 different heathy donors. Legend: TRPA1 = transient receptor potential ankyrin 1, AITC = allyl isothiocyanate, bp = base pair, RFU = relative fluorescence unit.

4.4.6 OxPAPC induces RyR-dependent $[Ca^{2+}]_i$ flux in HASM cells and airway narrowing in murine TCLS

Because our findings indicate that influx of extracellular Ca^{2+} is not essential for the initial peak in $[Ca^{2+}]_i$ induced in HASM by OxPAPC, we performed additional studies in *Ca^{2+}-deficient* HBSS to mitigate Ca^{2+} influx and define routes of intracellular Ca^{2+}-release. The cell permeable inositol 1,4,5-triphosphate (IP_3) receptor inhibitor, xestospongin C, which blocks release of Ca^{2+} from sarcoplasmic reticulum stores in response to upstream activation of $G_{q\alpha}$ and $G_{12/13}$ coupled receptors, phospholipase C and IP_3 production [217, 218] (Table 3.1), had no effect on OxPAPC -induced peak $[Ca^{2+}]_i$. As expected, xestospongin C did abrogate peak $[Ca^{2+}]_i$ induced by Ach, which binds $G_{q\alpha}$-coupled muscarinic M3 receptors (Figures 4.7A and 4.7B).

We next assessed the individual effects of caffeine and ryanodine, which can inhibit Ca^{2+} release via sarcoplasmic reticulum-associated ryanodine receptors at the concentrations we employed (caffeine, 25 mM; ryanodine, 100 μM)[219-222] (Table 3.1). Caffeine significantly reduced the peak $[Ca^{2+}]_i$ response induced by OxPAPC and Ach in Ca^{2+}-deficient HBSS. Ryanodine also significantly attenuated peak $[Ca^{2+}]_i$ induced by OxPAPC, but had little effect on peak $[Ca^{2+}]_i$ in response to Ach (Figure 4.7A and 4.7B). To identify upstream regulators of RyRs, we used cell permeable 8-Br-cADPR, a competitive inhibitor of cyclic-ADP-ribose (cADPR), which is produced by the CD38 and is needed for RyR activation [222, 245] (Table 3.1). 8-Br-cADPR pretreatment significantly abrogated peak $[Ca^{2+}]_i$ induced by OxPAPC, but it had little effect on peak $[Ca^{2+}]_i$ induced by Ach, which does not typically trigger RyR Ca^{2+} release (Figure 4.7A and 4.7B) [220].

To determine whether OxPAPC induced Ca^{2+} influx via plasma membrane TRPA1 may be dependent on RyR-triggered intracellular Ca^{2+} release, we measured the effect of ryanodine

inhibition on OxPAPC responses in *Ca^{2+}-replete* HBSS (1.26 mM Ca^{2+}) (Figure 4.7C). As expected, this prevented induction of a rapid peak $[Ca^{2+}]_i$, however ryanodine was without effect on TRPA1-dependent oscillations in $[Ca^{2+}]_i$ and the concomitant gradual rise in $[Ca^{2+}]_i$ (slope +0.57) (Figure 4.7D). This confirms that TRPA1-dependent Ca^{2+} influx and secondary oscillations are not dependent on ryanodine-sensitive intracellular Ca^{2+} release. As a negative control, we confirmed that OxPAPC caused no influx of Ca^{2+} (slope +0.09) in HASM cells in Ca^{2+}-deficient HBSS in the presence of ryanodine.

To validate our findings, we assessed the effects of caffeine and ryanodine pre-exposure on OxPAPC-induced bronchial narrowing in murine TCLS. Consistent with Ca^{2+} flux data in HASM cells, caffeine was sufficient to prevent both OxPAPC- and Mch-induced airway narrowing, whereas ryanodine significantly attenuated lumen closure in response to OxPAPC, but not Mch (Figure 4.7E - 4.7G). To decipher direct effects on ASM, we also assessed MLC phosphorylation in HASM cells and observed that ryanodine was sufficient to significantly reduce OxPAPC-induced MLC phosphorylation, a marker of myocyte contraction (Figure 4.5A and 4.5B).

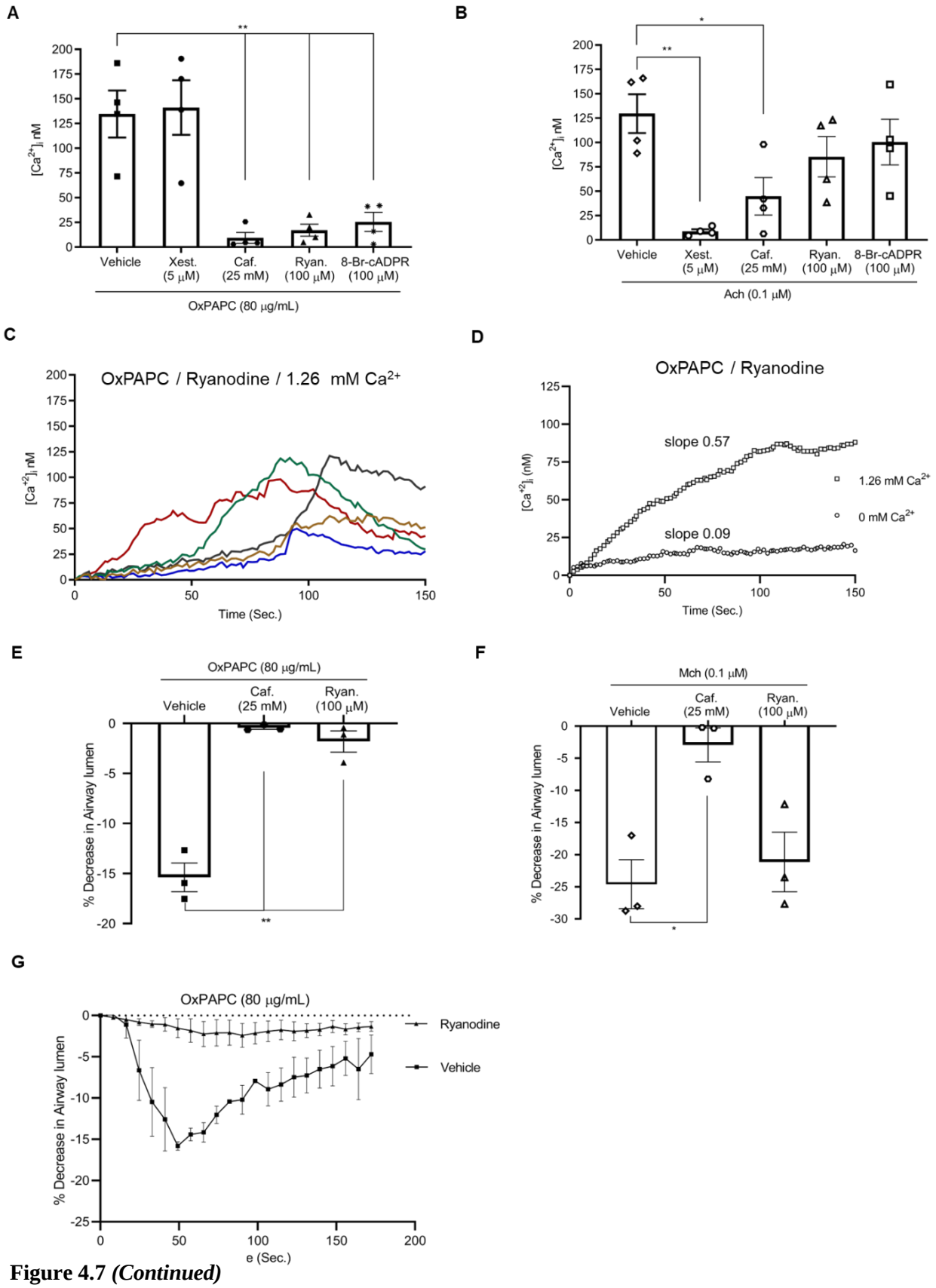

Figure 4.7 ***(Continued)***

Figure 4.7: Ryanodine receptor is required for peak $[Ca^{2+}]_i$ flux in HASM cells and airway narrowing in murine TCLS induced by OxPAPC.

Fura-2 AM loaded HASM cells were pretreated with xestospongin C (5 μM, 30 min)(IP3 receptor inhibitor), caffeine (25 mM, 10 min) or ryanodine (100 μM, 10 min)(ryanodine receptor inhibitors), 8-Br-cADPR (100 μM, 15 min)(cADPR inhibitor). $[Ca^{2+}]_i$ flux was recorded in response to OxPAPC (80 μg/mL) or acetylcholine (Ach)(0.1 μM, positive control) for up to 3 minutes. **(A)** and **(B)** Scatter dot plots for increase in peak $[Ca^{2+}]_i$ for cultures in Ca^{2+} free HBSS buffer (0 mM Ca^{2+}) in response to OxPAPC (A) or Ach (0.1 μM) (B) in the presence and absence of xestospongin C (Xest), caffeine (Caf), ryanodine (Ryan), or 8-Br-cADPR. Data represent mean±SEM of at least 30 cells from four donors (7-10 cells per cell line), and are analyzed by one-way ANOVA with Dunnett's multiple-comparison test; $^{*}p<0.05$, $^{**}p<0.01$ (compared with vehicle control). **(C)** Representative temporal tracings of five random HASM cells showing oscillation of $[Ca^{2+}]_i$ for cultures in Ca^{2+}-replete HBSS (1.26 mM Ca^{2+}) and pretreated with ryanodine (100 μM) in response to OxPAPC (80 μg/mL). **(D)** Data from experiments in C, representing temporal change in $[Ca^{2+}]_i$ in response to OxPAPC for cultures in Ca^{2+}-replete HBSS (1.26 mM Ca^{2+}) or Ca^{2+}-deficient HBSS (0 mM Ca^{2+}) and pretreated with ryanodine. Data is mean±SEM of at least 30 cells from four donors. Nonlinear regression fit with straight-line model was used to estimate rate (slope) of $[Ca^{2+}]_i$ change in response to OxPAPC. The slope was significantly different between 1.26 mM Ca^{2+} and 0 mM Ca^{2+} conditions ($p<0.001$). **(E)** and **(F)** Scatter dot plots for the percent decrease in airway lumen over baseline in TCLS in response to OxPAPC (80 μg/mL) (E) or methacholine (Mch)(0.1 μM) (F) in the presence and absence of caffeine, ryanodine and for vehicle control are shown. Data represent mean±SEM for at least 18 airways from 3 mice, and are analyzed by Dunnett's multiple-comparison test; $^{*}p<0.05$, $^{**}p<0.01$ (compared with vehicle control). **(G)** The temporal decrease in closure of airways in TCLS is shown. Each data point represents the mean±SEM of at least 18 airways (3 mice) in response to OxPAPC alone (80 μg/mL)(vehicle) and in TCLS pretreated with ryanodine (100 μM). Legend: Ach = acetylcholine, Xest = xestospongin C, Caf = caffeine, Ryan = ryanodine, Mch = methacholine, 0 mM Ca^{2+} = Ca^{2+} free HBSS buffer; 1.26mM Ca^{2+} = 1.26mM Ca^{2+} HBSS.

4.5 Discussion

Our study reveals that acute exposure of OxPAPC induces elevation of $[Ca^{2+}]_i$ in HASM cells that leads to contraction. Our novel observations identify two Ca^{2+} pathways: one involving activation of TRPA1 channels on the plasma membrane, and another involving CD38-regulated RyR release of Ca^{2+} from sarcoplasmic reticulum stores. These pathways coordinate physiologically relevant airway narrowing in murine TCLS and MLC phosphorylation in ASM, as confirmed with selective inhibitors of TRPA1 and of cADPR, a product of the ecto-enzyme CD38 that is associated with ASM hypercontractility [245, 246]. Our findings suggest that OxPAPC exposure correlates with increased TRPA1 activity, and directly or indirectly affects intracellular targets, such as CD38 and RyR, and promote airway narrowing. Identifying a role for TRPA1 extends our understanding of OxPC in asthma pathobiology, as our prior work did not confirm other cell membrane receptor-mediated pathways, though we did rule out candidates such as platelet activating factor receptor, scavenger receptor CD36, EP1/EP2 receptors, and toll like receptors 2 and 4 [176].

1-palmitoyl-2-arachidonoyl-sn-glycerol-3-phosphatidylcholine (PAPC), which is abundant in cell membranes, membranous organelles and lipoproteins is susceptible to oxidation of its polyunsaturated C:20 arachidonic chain, which can be fragmented or structurally reorganized to generate a mixture of bioactive OxPC, termed “OxPAPC” [231]. The accumulation of OxPAPC contributes to progression of chronic and acute conditions, such as atherosclerosis, sepsis, acute lung injury, and pain [141, 156, 165, 227, 231]. We showed that this also includes asthma, as airway OxPAPC abundance and profile are associated with clinical measures of AHR, and promotes release of interleukin IL-6, IL-8 and GM-CSF from ASM cells [176]. We confirm here that OxPAPC induces airway narrowing in murine TCLS preparation. These observations are consistent with multifunctional capabilities of ASM cells to support contraction, airway

remodeling and inflammation [247, 248]. Confirmation of a direct effect of OxPAPC on ASM cells to trigger contraction, and the mechanistic underpinnings for such a response, was lacking prior to our present study. This new finding represents one element of OxPC-associated asthma pathobiology, because it also promotes the release of inflammatory mediators by airway cells [176], disrupt airway epithelial wound healing [178], and can form oxidation specific epitopes on lung and immune cells [137].

An increase in $[Ca^{2+}]_i$, regulated by receptors and ion channels present in the plasma membrane and the sarcoplasmic reticulum, is a critical trigger for ASM cell contraction [249]. This leads to calmodulin-mediated activation of MLC kinase, and phosphorylation of the 20 kDa regulatory MLC to activate actomyosin crossbridge cycling, and force development [250]. In this study, we demonstrate that OxPAPC exposure rapidly induces TRPA1- and RyR-dependent MLC phosphorylation, revealing that airway narrowing in TCLS caused by OxPAPC most likely results from direct effects on ASM cells. We further substantiated a direct effect of OxPAPC on ASM cells by recording the rapid and sustained increase in $[Ca^{2+}]_i$ in cultured HASM cells. This is consistent with studies in endothelial cells [235] in which rapid and reversible intracellular Ca^{2+} flux was evident in the face of OxPAPC challenge. On this basis, our work focused on identifying pathways for Ca^{2+} flux in HASM cells, including potential cell surface and intracellular OxPAPC receptors and targets. This focus was buttressed by our observations that the elevation of $[Ca^{2+}]_i$ in response to OxPAPC includes a rapid, transient peak, followed by a sustained plateau characterized by slow oscillations that persist for at least three minutes. Our experiments using zero Ca^{2+} buffer and gadolinium (Gd^{3+}), a lanthanide ion that non-specifically blocks Ca^{2+}-permeable plasma membrane channels, revealed that extracellular stores are essential for sustained secondary $[Ca^{2+}]_i$ oscillations, but they are not required for the rapid rise in $[Ca^{2+}]_i$ caused by

OxPAPC. This effect is of physiological importance, as we show that OxPAPC-induced airway narrowing is abolished in the absence of an extracellular Ca^{2+} pool. Collectively, our findings suggest that OxPAPC regulates temporally resolved pathways for Ca^{2+} flux and ASM contraction, and these may involve different cell surface and intracellular receptors or protein targets.

Our prior work did not identify a surface receptor that mediates OxPAPC-induced cytokine release in HASM, despite published evidence that OxPAPC interacts with toll-like receptors, scavenger receptors, and receptors for platelet-activating factor and prostaglandins [251, 252]. However, because OxPAPC-induced secondary Ca^{2+} oscillations were abolished in Ca^{2+}-deficient extracellular media and by Gd^{3+}, our data indicates that plasma membrane protein channels are involved. Oxidized derivatives of PAPC, specifically 1-palmitoyl-2-(5-oxovaleroyl)-sn-glycero-3-phosphocholine (POVPC) and 1-palmitoyl-2-glutaroyl-sn-glycero-3-phosphocholine (PGPC), stimulate Ca^{2+} permeable TRP (Transient Receptor Potential) channels in vascular smooth muscle cells [253]. Liu and colleagues [165] showed OxPAPC to be an agonist for TRPA1, but not other TRP channels, as it interacts with unique N-terminal cysteine and lysine residues of TRPA1 to elicit dose-dependent Ca^{2+} influx in HEK293 cells and mouse sensory neurons. This is of particular interest to our work, as TRPA1 is expressed by ASM, the TRPA1 agonist, AITC, triggers Ca^{2+} influx in HASM cells, and pre-clinical studies have identified TRPA1 as a pharmacological target for treatment of allergic inflammatory conditions [215, 254, 255]. Using immunoblotting, RT-PCR and immunofluorescence, we confirm the expression of TRPA1 by cultured HASM cells and in ASM tissue of human lung cryosections, and by measuring changes in intracellular Ca^{2+}, we report a strong concentration-response effect for the TRPA1 agonist AITC, to confirm TRPA1 function in HASM cells. A new small molecule inhibitor of TRPA1, GDC-0334, abrogates allergic airway inflammation and airway contraction in multiple pre-clinical models of asthma, and is

being tested in Phase I human trials [215]. Based on these reports, we also assessed the effects of HC-030031, a selective inhibitor of TRPA1, and found that it prevented both secondary oscillations in $[Ca^{2+}]_i$ and the phosphorylation of 20 kDa MLC induced by OxPAPC in HASM cells. The relevance of these effects is evident from our finding that TRPA1 inhibition prevents OxPAPC-induced airway narrowing in murine TCLS. Thus, we have identified a pathway in which OxPAPC exposure leads to TRPA1 activation in HASM cells, and this induces Ca^{2+} influx that is required for contraction and airway narrowing.

To explore the intracellular sources for Ca^{2+} flux in response to OxPAPC, we conducted studies using inhibitors of IP_3 and RyRs. To mitigate contributions of Ca^{2+} influx induced by OxPAPC, all studies were completed in zero-Ca^{2+} buffer. IP_3 and RyRs on the sarcoplasmic reticulum modulate $[Ca^{2+}]_i$ in response to contractile stimuli [249]. Our studies show that IP_3 receptor inhibition is without consequence to changes in intracellular Ca^{2+} induced by OxPAPC. Thus, OxPAPC does not elicit Gq-coupled receptor mediated IP_3 generation and downstream Ca^{2+} release from the sarcoplasmic reticulum. Conversely, pharmacologic inhibition RyR [219, 220, 222] completely blocked acute peak rise in $[Ca^{2+}]_i$ induced by OxPAPC. To understand how OxPAPC promotes RyR opening, we investigated an upstream activator, cADPR, a product of the ectoenzyme CD38, which in smooth muscle can directly bind and activate RyR, block the RyR inhibitory accessory protein 12.6-kDa FK506-binding protein (FKBP12.6), or induces calmodulin kinase II-mediated RyR phosphorylation and activation [222, 245]. Using cell permeable 8-Br-cADPR to compete with cADPR, we observed the abrogation of OxPAPC-induced increase in $[Ca^{2+}]_i$. This confirms that OxPAPC promotes cADPR-mediated RyR activation to induce acute peak $[Ca^{2+}]_i$ by releasing a specific cation pool from the sarcoplasmic reticulum. Notably, we also completed studies with HASM cells in Ca^{2+}-replete buffer, and observed that RyR inhibition did

not prevent oscillations of intracellular Ca^{2+} that are characteristic of TRPA1 opening after OxPAPC exposure. This strongly suggests that TRPA1 activity is not dependent on mobilization of intracellular Ca^{2+} pools via RyRs.

Airway narrowing underpins asthma exacerbations, and we reported that accumulation of OxPC associates with asthma clinical symptoms [176]. Here we confirmed that OxPAPC directly induces airway narrowing in murine lung slices. This is consistent with reports that oxidized phospholipids increase tone in isolated arteries [256, 257], bovine smooth muscle cells [258], and potentiates agonist-induced constrictor responses [259]. On the basis of our observations concerning the pools of Ca^{2+} induced by OxPAPC in cultured HASM cells, we investigated whether these pathways were sufficient to modulate airway narrowing in murine TCLS preparations [227, 260]. Airway narrowing induced by OxPAPC was abrogated when studies were conducted in zero-Ca^{2+} extracellular conditions. Furthermore, HC-030031 (TRPA1 antagonist) significantly reduced OxPAPC induced airway narrowing, confirming a direct role for TRPA1 in OxPAPC-induced bronchial constriction. In addition, we revealed that Ca^{2+} released via RyRs is required for airway constriction, because RyR inhibition significantly reduced OxPAPC-induced phosphorylation of 20 kDa MLC in HASM cells and airway narrowing in TCLS. Because inhibition of either RyR or TRPA1 channel-mediated Ca^{2+} flux is sufficient to prevent airway constrictor responses to OxPAPC, coordinated effects of these pools appears to be necessary to activate ASM contraction. Our work has uncovered OxPAPC as a novel regulator of ASM contraction and thus could contribute to AHR, a hallmark feature of asthma, in some individuals. Our work also provides rationale and need for additional studies that provide a more comprehensive role of OxPAPC in the context of asthma pathophysiology. This includes more fulsome understanding of how OxPAPC exposure leads to activation of TRPA1, whether OxPAPC might activate CD38 leading

to cADPR production and RyR opening, and the precise pharmacomechanical coupling mechanisms that determine a need for both TRPA1 and RyR Ca^{2+} pools to elicit contraction. The specific bioactive constituents of OxPAPC that elicit changes in $[Ca^{2+}]_i$ and contraction of ASM cells still need to be identified. Because OxPAPC also induces cytokine release by HASM cells [176], it will be essential to understand how this may compound bronchoconstrictor responses. In conclusion, our studies provide the first evidence that OxPAPC, which accumulate in the lungs upon allergen exposure in mice and human, can trigger airway contraction through specific Ca^{2+} release pathways in ASM cells, a new understanding that contributes to fuller understanding of airway pathophysiology.

Chapter 5: Oxidized Phosphatidylcholines Induce Protein Kinase C-Dependent Inhibition of β_2-Adrenergic Receptor Responses in Airway Smooth Muscle Cells

Jignesh Vaghasiya[1,2], Anurag Sikarwar[2], Azadeh Dalvand[1,2], Sujata Basu[1,2], Alaina Bagan[2], Nathan Varghese[2], Angela A Duaqui[2], Dheerendra Pandey[1,2], Sparshita Mishra[2], Amir Ravandi[1,3,4], Christopher D Pascoe[1,2] & Andrew J Halayko[1,2,4] on behalf of the Canadian Respiratory Research Network

[1]Dept of Physiology and Pathophysiology, University of Manitoba, Winnipeg, MB, Canada. [2]Biology of Breathing Group, Children's Research Hospital of Manitoba, Winnipeg, MB, Canada. [3]Institute of Cardiovascular Sciences, St. Boniface Hospital Albrechtsen Research Centre, Winnipeg, Manitoba, Canada. [4]Dept of Internal Medicine, Max Rady College of Medicine, University of Manitoba, Winnipeg, MB, Canada.

This research work is to be submitted for publication in *American Journal of Respiratory Cell and Molecular Biology*

Author Contributions:
Jignesh Vaghasiya: Study design, execution, data plan & analysis, and manuscript writing
Anurag Sikarwar: Assisted with tracheal rings experiments
Sujata Basu: Performed *in vivo* lung function test
Azadeh Dalvand, Alaina Bagan, Nathan Varghese, Angela A Duaqui, Dheerendra Pandey & Sparshita Mishra: Assisted with experimental procedures (mentored and trained by Jignesh)
Nathan Varghese, Aamir Ravandi, and Christopher Pascoe: Reviewed manuscript
Andrew Halayko: Conceived the entire project, its design, data plan, edited and approval of final manuscript.

5.1 Abstract:

β_2 adrenergic receptor (β_2AR) agonists are frontline bronchodilator therapies for asthma. Many patients exhibit refractoriness, but understanding of mechanisms for β_2AR insensitivity is incomplete. We discovered that oxidized phosphatidylcholines (OxPC) accumulate in the human lungs, correlate with airway hyperresponsiveness, and induce contraction and cytokine synthesis in HASM cells. Here, we test whether OxPC impair bronchodilator responses to β_2AR agonists, and identify mechanism(s) that underpin β_2AR insensitivity. Using tracheal rings from BALB/c mice we assayed the effects of oxidized 1-palmitoyl-2-arachidonoyl-sn-glycero-3-phosphocholine (OxPAPC) on β_2AR agonist (isoproterenol (Iso))-induced relaxation of methacholine (MCh) contracted airways. OxPAPC pre-exposure significantly attenuated Iso-induced airway relaxation, as evident by a 4.3-fold increase in Iso EC_{50} and 12.2% reduction in maximum relaxation. OxPAPC did not affect relaxation induced by the adenylate cyclase (AC) activator, forskolin. OxPAPC pre-treatment significantly inhibited Iso-induced bronchodilation in murine thin cut lung slice (TCLS) preparations. Intranasal OxPAPC pre-challenge of BALB/c mice inhibited inhaled albuterol-mediated suppression of MCh-induced respiratory resistance. In cultured HASM cells, OxPAPC dose-dependently inhibited Iso- (but not forskolin)-induced phosphorylation of the Protein Kinase A substrate VASP by up to 53%. A live cell cADDis assay for intracellular cAMP confirmed that OxPAPC dose-dependently reduced Iso-elicited cAMP generation up to 50%. OxPAPC pre-exposure did not reduce the abundance of cell surface HA-tagged human β_2AR in HEK-293 cells. However, pharmacologic inhibition of Protein Kinase C was sufficient to prevent the suppressive effects of OxPAPC on both Iso-induced relaxation of murine tracheal rings, and cAMP signaling in cultured HASM cells. In summary, OxPAPC impairs β_2AR agonist induced bronchodilation by suppressing β_2AR-mediated cAMP signaling via PKC-dependent effects

upstream of AC in ASM cells. These observations reveal a new mechanism for bronchodilator insensitivity.

5.2 Background

Long and short-acting β_2 adrenergic receptor (β_2AR) agonists are mainstay reliever therapies for asthma [91, 92, 261]. They principally trigger relaxation of ASM to reverse acute bronchospasm and airway obstruction. β_2AR are Gs-coupled, thus agonists induce effector adenylate cyclase (AC), which generates intracellular cAMP that activates downstream Protein Kinase A (PKA)- and Exchange Protein Activated by cAMP (EPAC)-mediated pathways [78, 92, 262, 263]. A significant fraction of asthmatics are not fully responsive to β_2AR agonist therapy [114], and they exhibit higher risk for asthma exacerbations that can further worsen bronchodilator responses [115, 119]. Bronchodilator insensitivity is associated with β_2AR gene polymorphisms [117, 118], and receptor desensitization is linked to environmental exposures to allergens and air pollution [116], and prolonged β_2AR agonists use. However, the myriad of inductive mechanisms for β_2AR insensitivity still need to be fully defined.

Oxidative stress develops in the lung with exposure to inhaled allergen, environmental toxicants, particulates and microbes and is a fundamental element of persistent inflammation in chronic lung disease [129-131]. In asthma, oxidative stress correlates with disease severity and diminished pharmaco-therapeutic efficacy [264-266]. Our recent review [137] highlights evidence for oxidation specific epitopes, which form from the end products of phospholipid oxidation, as effectors of chronic disease pathobiology. These include oxidized phosphatidylcholines (OxPC) generated via oxidation of polyunsaturated fatty acid tails of the phospholipid [141, 251]. Multiple studies link OxPC with lung disease pathophysiology [141, 166, 168, 170, 176]. We reported that OxPC accumulate in the airways in association with airway dysfunction in human asthmatics after

bronchial allergen challenge [176]. OxPC exposure induces airway epithelial cell metabolic and mitochondrial dysfunction [178], promotes release of IL-6, IL-8, and GM-CSF by cultured human ASM cells [176], and initiates airway narrowing by directly triggering ASM contraction [177]. OxPC have emerged as mediators of oxidative stress in the airways and allergic asthma pathophysiology, but their potential role as factors that link oxidative stress-associated suppression of bronchodilator responses is unknown.

In the current study, we investigate the effects of OxPC exposure on the response of β_2AR agonists, including airway dilation and β_2AR mediated signaling in ASM cells, and test for evidence of β_2AR insensitivity and the molecular mechanism(s) that may underpin these effects. We used cultured HASM cells to investigate OxPC effects on β_2AR function and signaling, murine tracheal rings and thin cut lung slices (TCLS) for *ex vivo* analysis of β_2AR mediated bronchial relaxation, and adult BALB/c mice for an *in vivo* assay of bronchodilator responses to inhaled albuterol. Collectively these studies reveal that OxPC exposure associates with Protein Kinase C-dependent suppression of β_2AR mediated cAMP generation and airway reopening, and loss of β_2AR agonist efficacy in preventing methacholine-induced increase in respiratory resistance. These observations suggest a significant effector role for OxPC in β_2AR dysfunction and bronchodilator insensitivity associated with allergic asthma.

5.3 Materials and methods

5.3.1 Dose-response relaxation study in mouse tracheal ring

Female BALB/c mice (6-8 wk-old) were euthanized by pentobarbital sodium (135 mg/kg i.p.), then trachea was isolated and placed in a dissecting dish containing ice-cold Krebs-Henseleit bicarbonate buffer (K-H buffer) (composition in mM: 118 NaCl, 23.5 $NaCO_3$, 4.69 KCl, 1.18 KH_2PO_4, 1.00 $MgCl_2$, 2.50 $CaCl_2$ and 5.55 dextrose). Trachea were cut into ~2mm long rings, and the epithelium denuded using surgical thread [267]. Randomly assigned tracheal rings were incubated for 24 hrs in serum-free DMEM (1% Penecillin/Strptomycin, 37°C, 5% CO_2) (control), or in DMEM spiked with PSPC (80 µg/mL) or OxPAPC (40-80 µg/mL). For some studies, rings were pre-incubated with the PKC inhibitor GF109203X (10µM, 2 hrs) prior to co-incubation with DMEM alone, of DMEM spiked with PSPC or OxPAPC (80 µg/mL).

After incubation, tracheal rings were mounted in individual chambers of a micro-myograph (Danish Myo Technology, Aarhus, Denmark) in K-H buffer (37ºC) bubbled with 95% O_2/5% CO_2 for measurement of isometric force. Rings were stretched to ~0.6 mN for 45 minutes, then stimulated thrice at 20 minute intervals with K-H buffer containing 66 mM KCl to determine maximum contractile force. Thereafter, rings were stably pre-contracted with 1 µM Mch (which corresponds to approximately the EC_{50}). When plateau force was attained, cumulative dose response studies were performed to assess airway relaxation for isoproterenol (10^{-11}M to 10^{-5}M Iso) or forskolin (10^{-9}M to 10^{-5}M). For all experiments, a final K-H buffer-66 mM KCl contraction was induced to confirm no loss of tissue viability over the course of the study.

5.3.2 Dose-response relaxation study in murine thin-cut lung slice (TCLS)

Randomly selected murine TCLS were incubated with either control (media), PSPC (80 µg/mL) or OxPAPC (80 µg/mL) in DMEM-media supplemented with 1% P/S (37°C and 5% CO_2) for 24 hrs. After incubation individual TCLS were mounted in a custom perfusion chamber perfused with HBSS (room temperature) by gravity feed from a multi-tube manifold controlled by a solenoid valve system. Baseline airway size was recorded, then perfusate was switched to Mch (0.3 µM) for 3 minutes to achieve stable, submaximal airway narrowing (~30 % airway closure). Thereafter, the perfusate was switched to HBSS containing Mch (0.3 µM) and increasing concentrations of Iso (10^{-9}M to 10^{-5}M). Airway lumen size was video-recorded for 3 minutes at each Iso concentration. Airway re-opening was measured and normalized as a % of the Mch-induced airway pre-constricted lumen at baseline.

5.3.3 In vivo lung function test in mice to assess broncho-relaxant response

The female BALB/c mice (7-9 wks old) were treated with OxPAPC (10 µg/ g body weight) or saline for two days via i.n. instillation under isoflurane anesthesia. Then 1 hr after the second treatment, mice were anesthetized with sodium pentobarbital (90 mg/kg, i.p) and tracheotomy was performed with a catheter. Each mouse was then connected to a flexiVent small animal ventilator (SCIREQ Inc., Montreal, QC, Canada) and subjected to respiratory mechanics measurements using a forced oscillation technique as mentioned in [268, 269]. The change in total respiratory resistance (Rrs) was measured sequentially at baseline, with broncho-constrictor agent methacholine (Mch, 25 mg/mL), and followed by Mch (25 mg/mL) containing different albuterol concentrations (0.3, 1, or 3 mg/mL). In the present study, albuterol a short-acting β_2AR agonist, was used as a broncho-relaxant agent to prevent bronchoconstriction (increase in Rrs) induced by Mch. Each challenge was delivered over 10 sec using an inline nebulizer at the beginning of the

respective measurements. The respiratory system resistance (Rrs) was measured for a total of 12 measurements after each challenge using flexiVent SnapShot-150 protocol. As a time matched control, some animals only received serial challenge with MCh to account for any change in successive individual broncho-constrictor responses. The broncho-relaxation effect of albuterol was measured as the prevention of the MCh-induced increase in Rrs (denoted in Figure 5.1F as % inhibition of peak Rrs from the concurrent Mch response).

5.3.4 cAMP assay in HASM cells

Real-time intracellular cAMP in HASM cells was performed using the cAMP difference detector in situ (cADDis) sensor (product # D0200G, Montana Molecular, Bozeman, MT). In black-wall, clear-flat-bottom, 96-well plates (Sarstedt, Numbrecht, Germany), 10,000 cells/well were seeded in growth media (DMEM containing 5% FBS and 1% P/S), then cells were incubated with 0.25 µM trichostatin-A and a BacMam vector for the green-down cADDis sensor for 48 hours. Cultures were maintained 6-8 hrs in fresh growth media, before switching to serum free DMEM supplemented with 1% ITS spiked with OxPAPC (10-80 µg/mL) or 1% ITS media only (vehicle) for 24 hrs.

For the cAMP assay, media was replaced with PBS and after a short incubation at room temperature cell fluorescence was read with a BioTek Cytation5 plate reader (Agilent, Santa Clara, CA, USA) (excitation and emission wavelengths of 485 nm and 528 nm, respectively). Baseline fluorescence was monitored for 5 minutes, then cells were stimulated with Iso (1 nM) and fluorescence changes were measured at 30 second intervals for 30 min.

5.3.5 VASP shift assay for HASM cells

Cyclic AMP activates protein kinase A (PKA), which phosphorylates VASP (vasodilator-stimulated phosphoprotein), an endogenous protein substrate in HASM cells [270]. We used an immunoblot assay to measure changes in VASP phosphorylation (p-VASP) in response to the β_2AR agonist, Iso. Confluent HASM cell cultures were incubated in serum-free conditions (48 hrs), then media was replaced with HBSS/0.1% BSA for 30 minutes (37°C) before addition of Iso (10^{-10}M -10^{-5}M). After 7 minutes (37°C), cells were washed with ice-cold HBSS, then protein lysates prepared in Laemmli Loading Buffer (containing β-mercaptoethanol), and stored at −20°C. For gel electrophoresis, samples were warmed to room temperature, centrifuged (2000 RPM, 5 mins), and the supernatants were incubated at 95°C (5 min). Thereafter, 25µL of each sample was loaded on 8% SDS-PAGE gels for electrophoresis (100V constant, ~1.5 h, and 80V for the last 30 minutes), and "wet" transfer to nitrocellulose membranes. Membranes were blocked (3% BSA in TBS-T (Tris-buffered saline containing 0.1% Tween 20)), then incubated with mouse monoclonal anti-VASP (1:1000) in TBS-T/1% BSA overnight (4ºC). After incubation with secondary antibody (1:5000 goat anti-mouse IgG-peroxidase, 1 hr, room temperature) we used Enhanced Chemiluminescence Amersham™ ECL™ detection reagents with a ChemiDoc™ Imaging System (Bio-Rad, Hercules, CA, USA). Protein bands were quantified as integrated density value by spot densitometry. VASP phosphorylation in response to cAMP stimulant was calculated as percentage phosphorylated VASP (p-VASP) to total VASP.

For studies with OxPAPC pre-exposure cultures were incubated in serum-free media, or media spiked with PSPC (80 µg/mL) or OxPAPC (5-80 µg/mL) for 24 hrs. Thereafter cells were stimulated with Iso (1 nM)(EC_{50} equivalent for VASP shift assay) or forskolin (1 µM). For experiments using selective inhibitors, cultures were pre-treated for 2hrs (before adding OxPC)

with either PKC inhibitor, GF109203X (10μM)(Tocris, Toronto, ON, Canada) or cyclooxygenase-2 inhibitor, indomethacin (10μM)(Sigma-Aldrich, Saint Louis, MO, USA). Inhibitors remained in media for the duration of subsequent OxPAPC (80 μg/mL) exposure. For some studies we used the PKC activator, 12-O-tetradecanoylphorbol-13-acetate (TPA)(0.1-10 μm, 1hr), added to serum-starved HASM cultures.

5.3.6 β_2AR internalization assay

We adopted protocols described by Nayak et al [271] to measure β_2AR internalization. Human embryonic kidney 293 (HEK293) cells that stably express NH_2-terminal HA-tagged-human β_2-adrenoceptor (HA-β_2AR) were grown to confluence in DMEM supplemented with 10% FBS, 1% P/S and 500 μg/mL G418, then transferred to 24-well plates (1.5×10^5 cells per well) pre-coated with 0.1% poly-D-lysine and cultured overnight. Cultures were then treated with OxPAPC (10-80 μg/mL), or vehicle for 24 hrs in DMEM, 1% P/S, and 1% ITS. Cells were fixed on ice (10% formalin-buffered saline, 10 min), and after washing with TBS (pH 7.5), incubated in blocking buffer (TBS, 1% BSA, 45mins, RT). Cell surface HA-β_2AR was detected by incubating fixed cells with horseradish peroxidase-conjugated chicken polyclonal anti-HA-tag (1 μg/mL, 1h, RT)(Abcam, Cambridge, UK). After multiple washes with TBS, 150 μL of 1-Step™ Slow TMB-ELISA, 3,3′,5,5′-tetramethylbenzidine substrate solution (Thermo Scientific, Rockford, IL, USA) was added to each well for 5 minutes. The developing solution was transferred to 96-well plates containing 50 μL 2N H_2SO_4 to stop the colorimetric reaction. We measured 450 nm absorbance with an Epoch BioTek Plate Reader with Gen5 software (Agilent, Santa Clara, CA, USA).

5.3.7 Immunoblotting for PKC phosphorylation in HASM cells

The cultured HASM cells were treated with OxPAPC (80 μg/mL) for different time points (1-24 hrs) or with PKC activator TPA (0.2 μM for 1 hr) as positive control. After treatment, cells were

washed with ice-cold PBS and lysed with ice-cold RIPA buffer. Lysates were sonicated, centrifuged, and supernatant protein concentration was quantified. 10 μg of total protein was run on 8% gel, blotted onto nitrocellulose, and probed with p-PKC (1:1500) and β-actin (1:20000) antibodies.

5.3.8 Statistical analysis

For relaxation dose-response studies, at least 5-6 tracheal rings from 5-6 mice were studied, and for TCLS experiments we measured at least 15 airways from at least 3 mice. Data were analyzed by nonlinear-curve-fit (variable slope- four parameters) for comparison between groups. For *in vivo* lung function testing, we performed experiments in 5 animals per group, and data were analyzed by two-way RM ANOVA with Sidak's multiple comparisons test. HASM cell culture experiments were performed with 5 cell lines derived from 5 independent donors. Unless otherwise specified, statistical significance was determined by t-test or one-way ANOVA with Dunnets's or Tukey's multiple-comparison tests using GraphPad Prism version 10.1.1 (San Diego, CA, USA). Data are shown as mean ± SE unless otherwise specified. $P<0.05$ was considered significant.

5.4 Results

5.4.1. OxPAPC impairs β_2AR agonist-induced relaxation in murine tracheal rings

We assessed effects of OxPAPC (80 µg/mL) pre-exposure on airway relaxation in epithelium-denuded murine tracheal rings that had been pre-contracted with Mch. We observed a significant increase in isoproterenol (Iso) EC_{50} (17.8 nM Iso *vs* 3.3 nM Iso for controls), and a significant decrease in maximum tracheal relaxation (62.5% for OxPAPC-treated *vs* 71.2% for controls)(Figure 5.1A). These data demonstrate that OxPAPC (80 µg/mL) diminished Iso relaxation potency by 4.4 times, and efficacy was reduced by 12%. In contrast, compared to vehicle-exposed (control) tracheal rings, pre-exposure to neither 40 µg/mL OxPAPC nor the oxidation resistant lipid PSPC (negative control, 80 µg/mL) were sufficient to affect Iso-induced relaxation.

To understand how OxPAPC may affect β_2AR downstream signaling, we assessed tracheal relaxation induced by forskolin, a direct activator of adenylate cyclase (AC). The forskolin dose-response relationship was unaffected by OxPAPC pre-exposure, with a forskolin relaxation EC_{50} of 0.7 µM and 0.9 µM in control and OxPAPC-treated tracheal rings, respectively (Figure 5.1B). Similarly, pre-exposure with PSPC (negative control) did not significantly affect the forskolin relaxation EC_{50} (0.7 µM). OxPAPC pre-treatment also did not affect maximum relaxation induced by forskolin (Figure 5.1B). These findings suggest that OxPAPC may interfere with agonist-induced β_2AR response upstream of AC, as forskolin-induced relaxation is unaffected by OxPAPC.

A

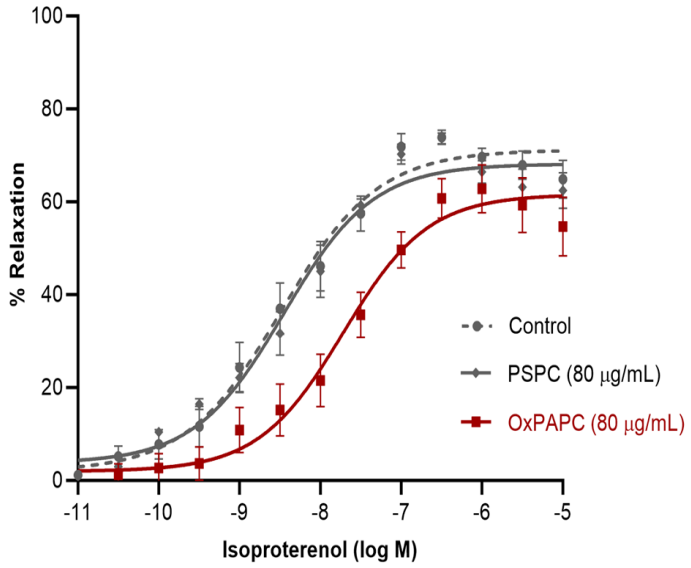

Treatment Group	Isoproterenol EC_{50} (Mean ± SEM)	% Maximum relaxation (Mean ± SEM)
Control	3.3 ± 0.11 nM	71.2 ± 2.3%
PSPC (80 µg/mL)	3.5 ± 0.10 nM	68.2 ± 1.8%
OxPAPC (40 µg/mL)	4.1 ± 0.10 nM	74.4 ± 1.5%
OxPAPC (80 µg/mL)	17.8 ± 0.13 nM***	62.5 ± 2.8%**

B

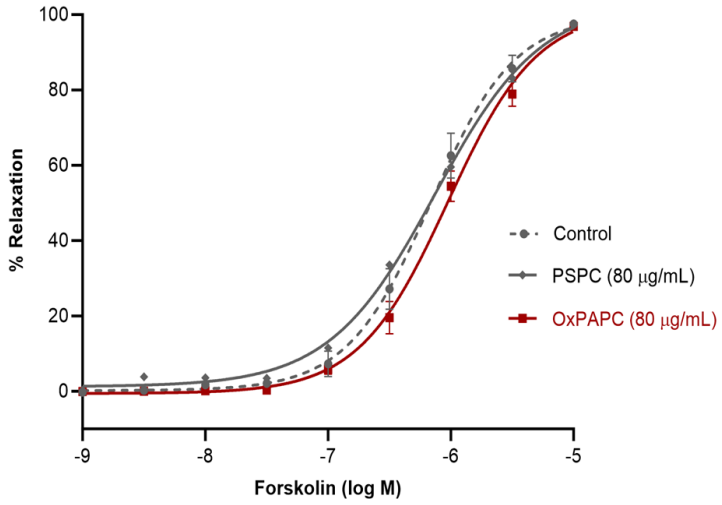

Treatment Group	Forskolin EC_{50} (Mean ± SEM)	% Maximum relaxation (Mean ± SEM)
Control	0.7 ± 0.05 µM	99.8 ± 3.9 %
PSPC (80 µg/mL)	0.7 ± 0.09 µM	101.7 ± 6.7 %
OxPAPC (40 µg/mL)	0.6 ± 0.02 µM	98.6 ± 1.7 %
OxPAPC (80 µg/mL)	0.9 ± 0.04 µM	100.2 ± 3.8 %

Figure 5.1 ***(Continued)***

C

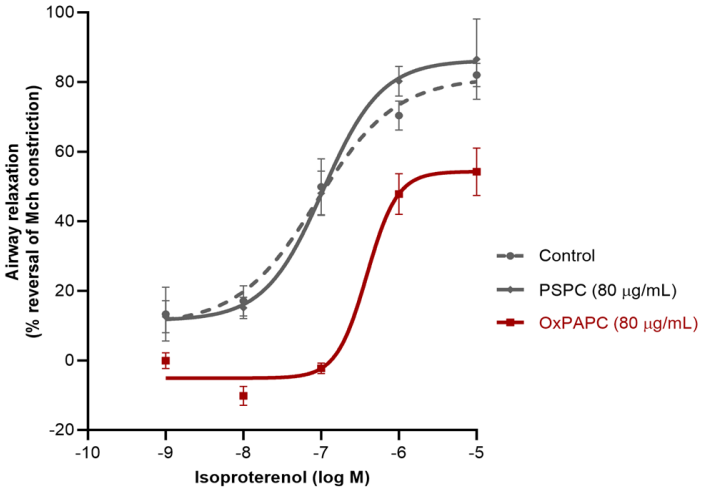

Treatment Group	Isoproterenol EC_{50} (Mean ± SEM)	% Maximum relaxation (Mean ± SEM)
Control	0.09 ± 0.22 μM	81.3 ± 7.1
PSPC (80 μg/mL)	0.11 ± 0.16 μM	86.3 ± 6.7
OxPAPC (80 μg/mL)	0.39 ± 0.22 μM***	54.3 ± 4.8***

D

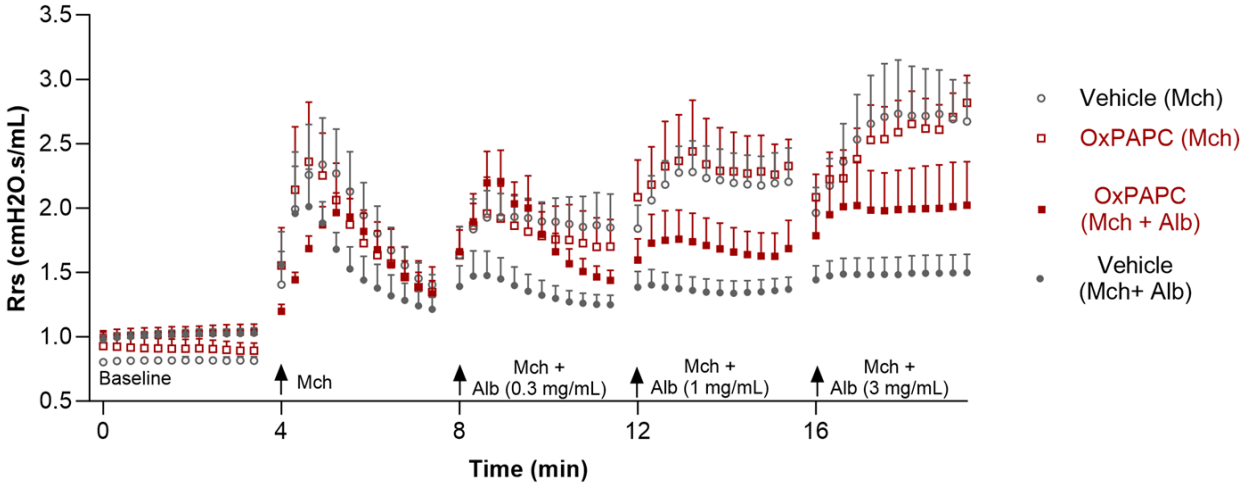

E

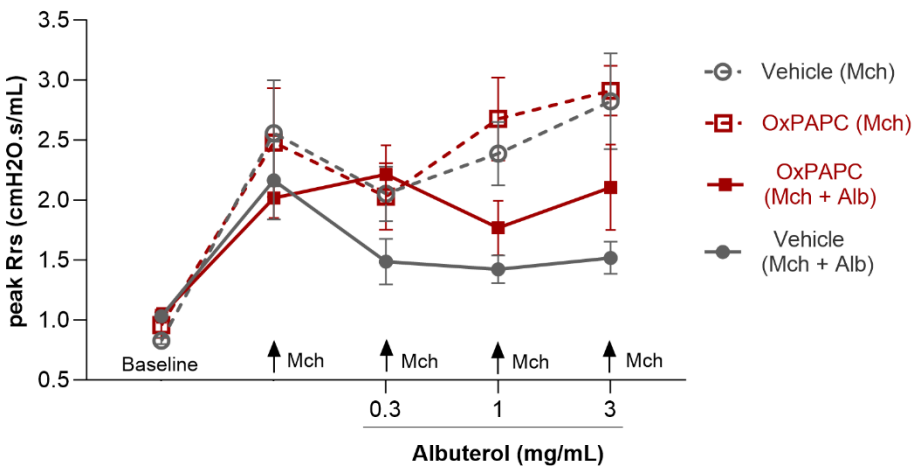

Figure 5.1 ***(Continued)***

F

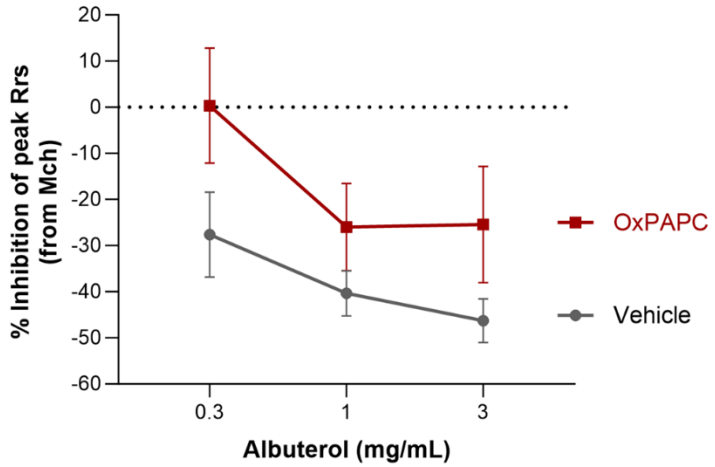

Figure 5.1. OxPAPC reduces β2AR agonist effects in murine tracheal rings, TCLS study, and *in vivo* lung function assessment.

(A and B) Epithelium-denuded murine tracheal rings (~2 mm long) were incubated with OxPAPC (40-80 µg/mL), PSPC (80 µg/mL), or control (media) for 24 hours (37^0C) and then isometric force was measured. Pre-constricted rings with Mch (1 µM) were used to study relaxation dose-response with the β2AR agonist, isoproterenol (Iso) (A) or the AC enzyme activator, forskolin (B). Data were analyzed by nonlinear-curve-fit (variable slope- four parameters) and compared for significant difference between treatment groups. Each data point represents mean ± SEM from at least 5-6 tracheal rings (5-6 BALB/c female mice). **(C)** Murine TCLS (average diameter of ~250 µm) were incubated with OxPAPC (80 µg/mL), PSPC (80 µg/mL), or control (media) for 24 hours (370C) and then subjected to submaximal pre-contractile state (~30 % airway closure) with Mch (0.3 µM) to study relaxation with Iso. The airway re-opening effect of Iso was denoted as % reversal from Mch-induced airway pre-constriction. Data were analyzed by nonlinear-curve-fit (variable slope- four parameters). Each data point represents mean ± SEM from at least 15 airways from three BALB/c female mice**. (D-F)** Mice were treated with OxPAPC (10 µg/ g body weight) or vehicle (saline) via intranasal instillation for two days. The respiratory system resistance (Rrs) was measured at baseline, with broncho-contractile agent Mch (25 mg/mL) and then with Mch (25 mg/mL) containing broncho-relaxant agent albuterol (0.3, 1 or 3 mg/mL). Concurrent controls for vehicle and OxPAPC were also maintained except albuterol challenge. Arrows in (D) represents each challenge followed by 12 measurements. Broncho-protective effect of albuterol is denoted as % inhibition of peak Rrs from concurrent Mch response (F). Data represent mean ± SEM from five mice/group and were analyzed by multiple t-test, one-way or two-way RM ANOVA followed by Sidak's multiple comparison test. **p<0.01, ***p<0.001 compared to control. Legend: Mch= methacholine, Alb= albuterol

5.4.2. OxPAPC diminishes β_2AR agonist-induced airway re-opening in murine TCLS study

Using TCLS we assessed the impact of OxPAPC pre-exposure on bronchial re-opening. The Iso-induced reversal in lumen area of Mch pre-contracted airways was measured in TCLS that had been cultured in the presence and absence of OxPAPC (80 µg/mL) or PSPC (an oxidation-resistant OxPC) (Figure 5.1C). Iso induced a maximum airway relaxation of ~80 % in control and PSPC pre-exposed TCLS, and had comparable Iso EC_{50} values of 0.09 µM and 0.11 µM, respectively. Conversely, OxPAPC pre-treatment significantly decreased both the sensitivity to Iso (EC_{50} increased to 0.39 µM), and significantly reduced the maximum relaxation response (Figure 5.1C). These data demonstrate that OxPAPC pre-exposure reduced β_2AR agonist potency by 3.2-times and efficacy by ~33%, and this correlates with a significant impairment of relaxation of intrapulmonary airways.

5.4.3. OxPAPC reduces broncho-protective effects of a β_2AR agonist in vivo

We modified a novel approach to measure *in vivo* bronchodilator responsiveness in adult mice [272], using the forced oscillation technique to test the ability of inhaled albuterol to prevent methacholine-induced respiratory resistance (Rrs)[268, 273]. Each animal was subjected to four serial challenge with Mch challenges (25 mg/mL) in concert with increasing concentrations of albuterol (0, 0.3 mg/mL (0.03% w/v), 1 mg/mL (0.1% w/v), and 3 mg/mL (0.3% w/v)). Rrs was measured 12 times for 4 minutes after each MCh/albuterol challenge (Figure 5.1D). The albuterol concentrations we used were elected to overlap the standard clinical formulation (~0.083 %w/v). Mch induced a significant increase in peak Rrs that was serially reproducible, and was not different between the four sequential challenges (Repeated Measures One-Way ANOVA, $p>0.30$ for all comparisons). Co-delivery of albuterol significantly prevented Mch-induced peak Rrs by 28-46%

in a concentration dependent manner, and was statistically significant for both 1 and 3 mg/mL albuterol (T-test, $p<0.05$)(Figures 5.1E and 5.1F).

To determine whether OxPAPC modifies the broncho-protective effects of albuterol, mice were pre-treated with intra-nasal OxPAPC (10 µg/g body weight) for two days prior to measuring Rrs. OxPAPC pre-treatment had no effect on the peak Rrs response to the sequential Mch challenge (Repeated Measures One-Way ANOVA, $p>0.99$) (Figure 5.1E). However, we consistently observed that OxPAPC pre-treatment reduced the albuterol inhibition of Mch-induced peak Rrs (Figures 5.1E and 5.1F). Most strikingly, the broncho-protective effect of low concentration albuterol (0.3 mg/mL) was virtually abrogated by OxPAPC exposure, and the inhibitory effects of 1 mg/mL and 3 mg/mL albuterol were reduced by 36-45%, albeit not achieving statistical significance (ie. for albuterol 0.3, 1 and 3 mg/mL, $p=0.300$, 0.533 and 0.451, respectively). These data demonstrate that *in vivo* OxPAPC exposure is sufficient to reduce broncho-protective effects of inhaled albuterol, which could increase need for more frequent use and increased dosing of β_2AR bronchodilators to control airway hyperreactivity.

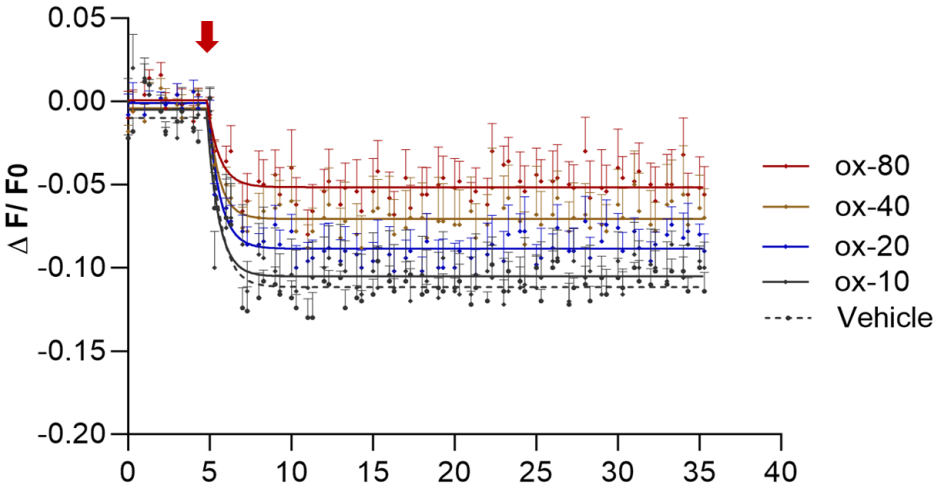

cAMP (k*steady state)		
Treatment	**Mean**	**SEM**
vehicle	0.141	0.001
OxPAPC (10 µg/mL)	0.141	0.005
OxPAPC (20 µg/mL)	**0.118****	**0.002**
OxPAPC (40 µg/mL)	**0.098*****	**0.005**
OxPAPC (80 µg/mL)	**0.071*****	**0.005**

Figure 5.2. OxPAPC decreases β_2AR agonist induced real-time cAMP signaling in HASM cells. Real-time intracellular cAMP response in live HASM cells was measured using a green down cADDis sensor. After sensor transduction, cells were pre-treated with OxPAPC (10-80 µg/mL) or vehicle (media) for 24 hrs, and cAMP signaling in response to Iso (1 nM) was measured by change in cell fluorescence using a plate reader. Fluorescence kinetics from 5 independent cell lines (in triplicate for each) (left) plotted for non-linear curve fit using [pharmechanics]-baseline then fall to steady state time course. cAMP product was calculated as fluorescent decay rate multiplied by the steady-state change in fluorescence (k*plateau). Data were analyzed by one-way ANOVA with Dunnets's multiple-comparison tests. **p<0.01, ***p< 0.001 vs control. Legend: ox = OxPAPC

5.4.4. OxPAPC decreases β_2AR agonist induced cAMP production in HASM cells

As β_2AR mediated cAMP triggers signaling pathway for airway smooth muscle relaxation, we measured effects of OxPAPC exposure on real-time cAMP generation in HASM cells using a cADDis sensor live cell bioassay [274, 275]. Iso (1 nM) rapidly induced cAMP generation (0.141± 0.001, as a product of k*steady state). OxPAPC pre-treatment dose-dependently decreased Iso-induced cAMP generation by 16-50% between 20 µg/mL and 80 µg/mL compared to the vehicle control (Figure 5.2).

Intracellular cAMP activates protein kinase A (PKA) to promote ASM relaxation, thus we also assessed OxPAPC effects on Iso-induced PKA activation by tracking phosphorylation of the PKA target substrate, vasodilator-stimulated phosphoprotein (VASP). Using a VASP shift immunoblotting assay, we demonstrated that Iso (10^{-10}M to 10^{-5}M) induced VASP phosphorylation (p-VASP) with an EC_{50} of 0.42 nM (Figure 5.3A). Consistently, OxPAPC pre-exposure dose-dependently reduced 1nM Iso-induced % p-VASP, with a significant reduction of ~25% using 40 µg/mL (47.5 % p-VASP) and ~53% with 80 µg/mL (29.8 % p-VASP) compared to vehicle control (63.4% p-VASP), and pre-treatment with the oxidation-resistant lipid PSPC (80 µg/mL) (68% p-VASP) (Figure 5.3B). To determine whether OxPAPC was affecting cAMP generation downstream of β_2AR, similar to our approach using tracheal rings (Figure 5.1A), we assessed the response to the adenylate cyclase activator, forskolin, in HASMs. In OxPAPC pretreated cultures (80 µg/mL), forskolin (1 µM) induced 53% p-VASP, and this was similar to that induced in vehicle control conditions (52.6%) or PSPC pre-treated cultures (53.8%) (Figure 5.3C).

Collectively, these findings show that OxPAPC pre-exposure diminishes β_2AR agonist induced cAMP production and PKA activation via an mechanism that is upstream of AC in HASM cells.

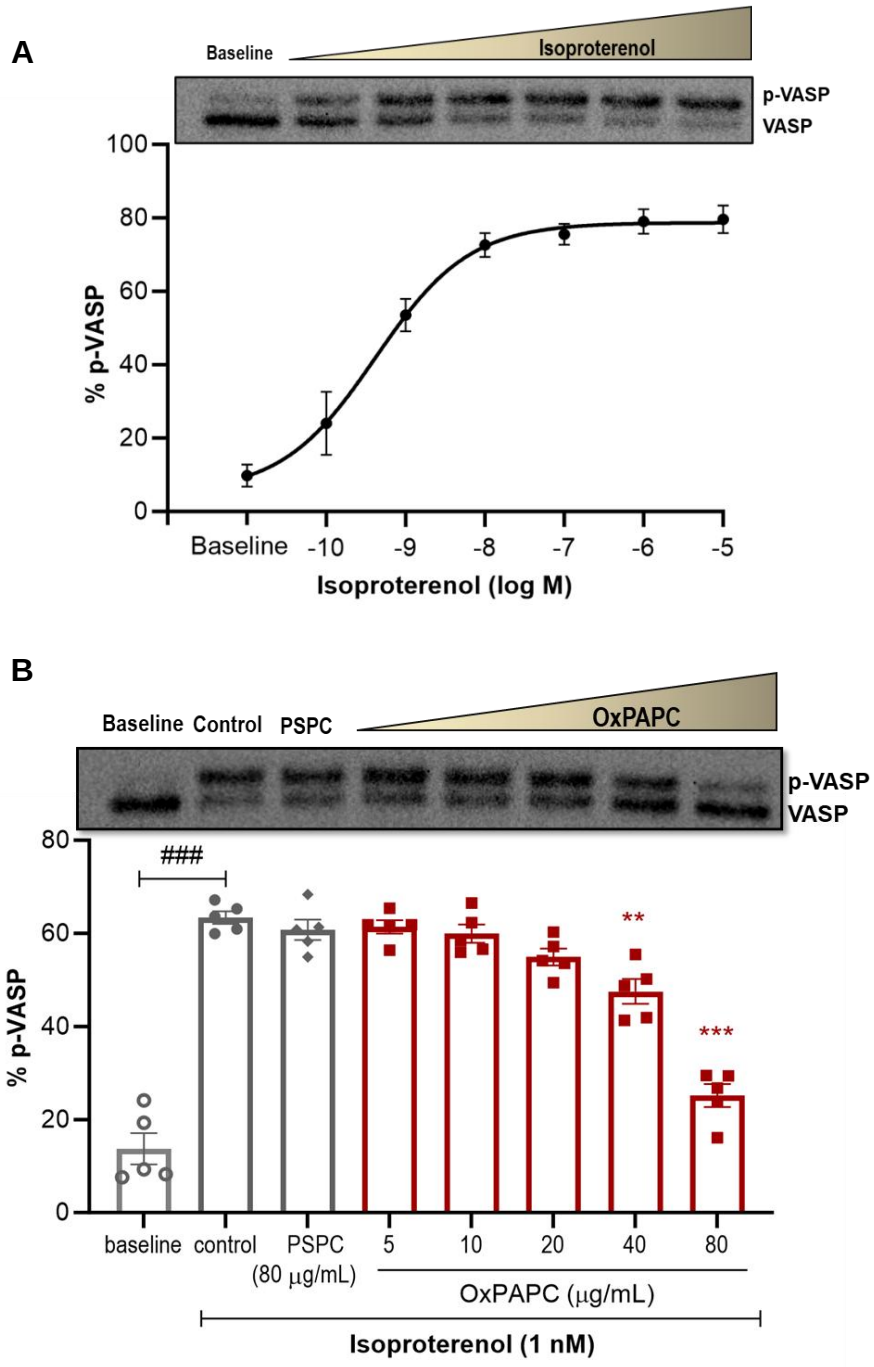

Figure 5.3 ***(Continued)***

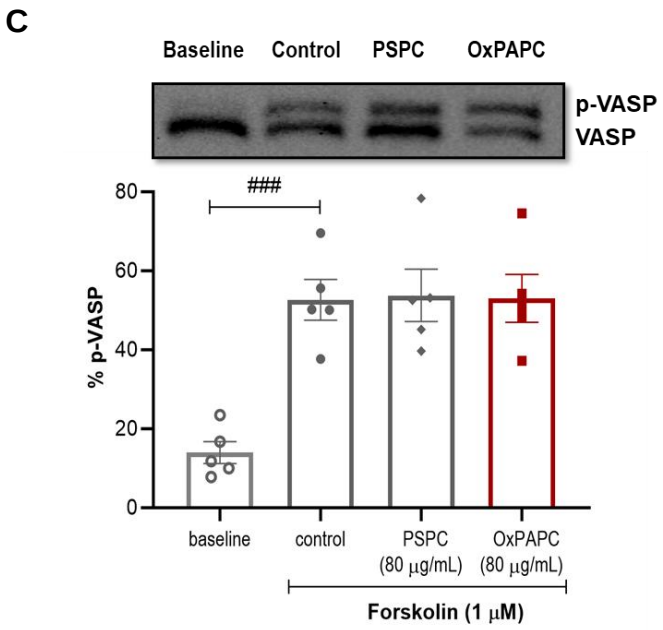

Figure 5.3. OxPAPC decreases cAMP-dependent PKA signaling (VASP phosphorylation) in response to β_2AR agonist in HASM cells.

(A) 48-hrs serum starved HASM cells were treated with Iso from 10-10M to 10-5M for 7 minutes (37°C) and then lysed for immunoblotting to measure p-VASP formation. A representative immunoblot (top) shows the p-VASP band shifted up from the VASP band by Iso treatment. Iso dose-dependently increased %p-VASP formation with half-maximum response (EC50) of 0.42 nM. Densitometry analysis of p-VASP and VASP band was performed to calculate percentage (% p-VASP) as a fraction of the total (VASP + p-VASP) for each condition. Data were analyzed by nonlinear-curve-fit (variable slope- four parameters) to establish Iso EC50. Each data point represents mean ± SEM from 5 HASM cell lines (Independent donor). **(B & C)** 24 hrs serum starved HASM cells were treated with either control (media), PSPC (80 μg/mL), or OxPAPC (5-80 μg/mL) in 1% ITS media for 24 hrs and then VASP shift assay performed with Iso (1 nM) in (B) or forskolin (1 μM) in (C). Representative immunoblots (top) show VASP and p-VASP bands with different treatment conditions, and densitometry was performed to calculate % p-VASP. The scatter dot plot compares %p-VASP between different treatments, with each data point representing mean ± SEM from 5 different HASM cell lines. Data were analyzed by one-way ANOVA with Tukey's multiple-comparison tests. **p<0.01, ***p< 0.001 vs control; ###p<0.001 vs baseline.

5.4.5. OxPAPC does not affect cell surface abundance of β_2AR receptors

We used HEK293 cells that stably express functional HA-tagged β_2AR to perform on-cell immune-absorption assays to monitor baseline cell surface receptor distribution [271]. Pre-exposure with OxPAPC (10-80 µg/mL) was without effect on the abundance of cell surface β_2AR in comparison to that measured in vehicle control conditions (Figure 5.4).

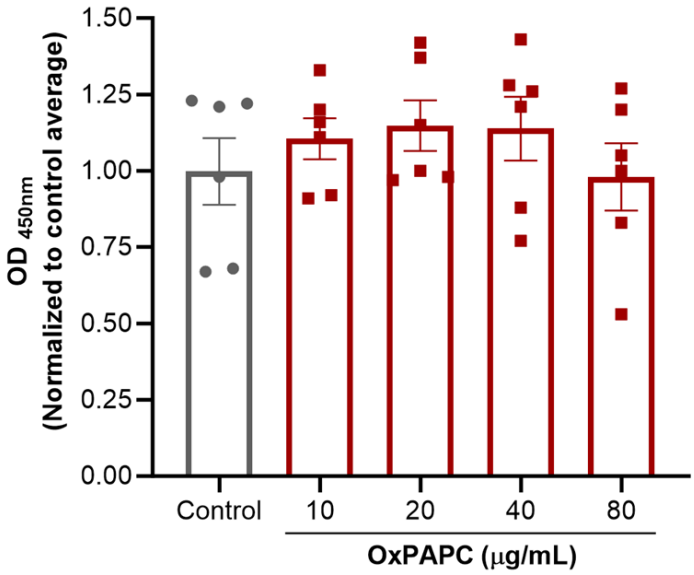

Figure 5.4. OxPAPC does not affect cell surface abundance of β_2AR receptors.
HA-tagged β_2AR expressing HEK-293 cells were treated with OxPAPC (10-80 µg/mL) or control for 24 hrs. Surface β_2AR abundance was measured using colorimetry (OD at 450 nM) assay after incubation with HRP-conjugated anti-HA IgG. The scatter bar plot represents mean±SEM from five independent experiments (each in triplicate) and analyzed by one-way ANOVA.

5.4.6. OxPAPC induces PKC-dependent β_2AR desensitization

Our previous work using kinome array technology revealed that OxPAPC exposure causes the sustained phosphorylation (activation) of protein kinase C (PKC) in HASM cells [176]. Moreover, PKC activation was concomitant with and required for expression of COX_2 and oxylipins in HASM cells. Notably , multiple reports indicate that PKC [276, 277], or COX_2 via PGE2 induction [278] can contribute to β_2AR desensitization, therefore we used selective pharmacological inhibitors to test whether PKC activity or COX_2 induction by OxPAPC may be involved in the inhibition of β_2AR signaling. The PKC inhibitor (GF-109203X) was without effect on Iso-induced p-VASP (58.5%) in control conditions (Figure 5.5A). As expected OxPAPC pre-exposure limited Iso-induced p-VASP to only 17%. However, PKC inhibition with GF-109203X was sufficient to prevent this effect, re-enabling the Iso-induced PKA response (43.3 % p-VASP). This represents a 64.4% abrogation of the inhibitory effect of OxPAPC on β_2AR signaling. In contrast, we found that co-treatment of OxPAPC-exposed HASMs with the COX_2 inhibitor, indomethacin, was without effect, and did not restore response to 1 nM Iso stimulation, as p-VASP only attained a level of 13.5%, which is similar to that in OxPAPC exposed HASM cells (17%).

To validate the role of PKC in mediating OxPAPC-induced β_2AR dysfunction, we performed additional studies to confirm PKC activation, the sufficiency of PKC activation to inhibit β_2AR signaling, and that OxPAPC effects on airway relaxation in intact airways requires PKC activity. We first used immunoblotting to measure pan-Ser660-phospho-PKC in HASM cells exposed to OxPAPC (80 µg/mL, 1 hr) and detected a significant (~200%) increase in phospho-PKC over baseline levels. This level of activation was comparable to that achieved using the PKC activator, TPA (Figure 5.5B). Notably, prolonged OxPAPC exposure for up to 24 hrs induced sustained PKC phosphorylation above baseline. We next tested whether PKC activation alone is sufficient to

diminish β_2AR mediated responses, using the VASP shift assay to monitor the effect of PKC activation (TPA, 0.1-10 µM, 1 hr) on Iso-induced p-VASP formation (Figure 5.5C). PKC activation with TPA was sufficient to decrease Iso induced p-VASP formation (40.2 % p-VASP at 10µM TPA) by up to ~26% compared to that of concurrent control (54% p-VASP). Finally, to test for the requirement of PKC activity in OxPAPC impairment of Iso-induced relaxation of isolated murine tracheal rings, using design similar to studies in Figure 5.1A, we performed an Iso dose-response relaxation study and compared responses in the presence and absence of OxPAPC pre-treatment. Similar to observations with the VASP shift assay (Figure 5.5A), PKC inhibition prevented the inhibitory effects of OxPAPC on Iso relaxation (Figure 5.6). Iso EC_{50} for OxPAPC pre-exposed rings (17.8 nM) was significantly higher than for control conditions (3.3 nM, Figure 6 includes this control curve from Figure 5.1A for reference). However, GF-109203X rescued the Iso EC_{50} (7.4 nM) in OxPAPC pre-treated tracheal rings, achieving a level similar to that for control preparations treated with GF-109203X (Iso EC_{50} 7.5 nM). Notably, maximum Iso-induced relaxation was maintained with PKC inhibition in OxPAPC-pre-treated tracheal specimens. (Figure 5.6). Collectively, these findings demonstrate that PKC activity is required for OxPAPC-induced suppression of β_2AR mediated PKA activation in ASM cells, and relaxation of murine tracheal rings.

A

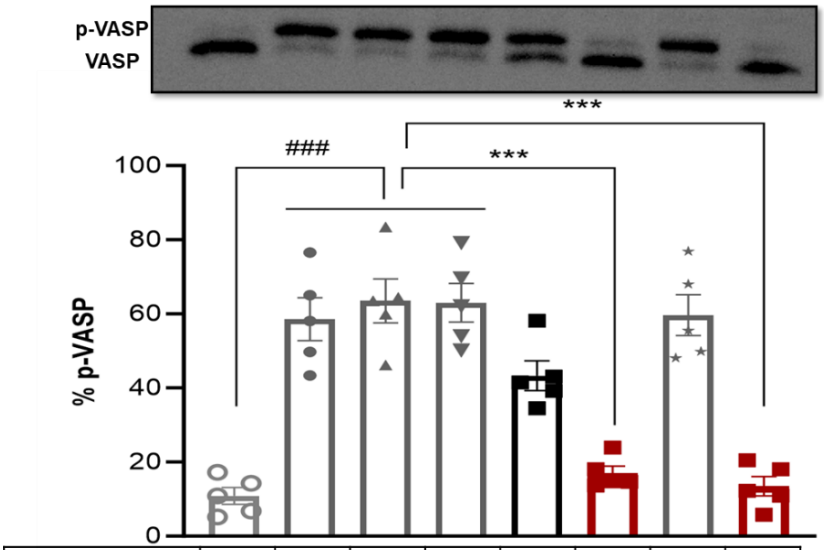

Baseline	+							
Isoproterenol (1 nM)		+	+	+	+	+	+	+
Vehicle			+					
GF-109203X (10 µM)				+	+			
Indomethacin (10 µM)							+	+
OxPAPC (80 µg/mL)					+	+		+

B

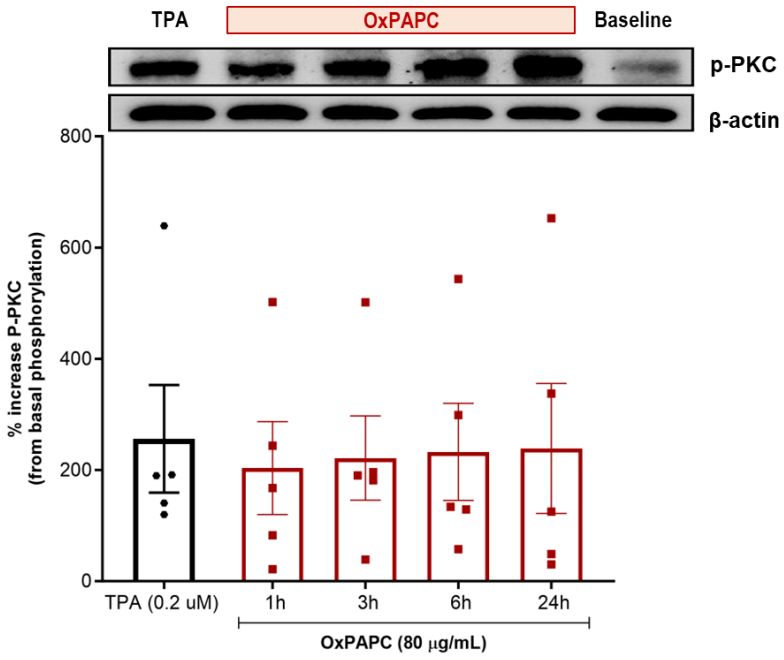

Figure 5.5 ***(Continued)***

C

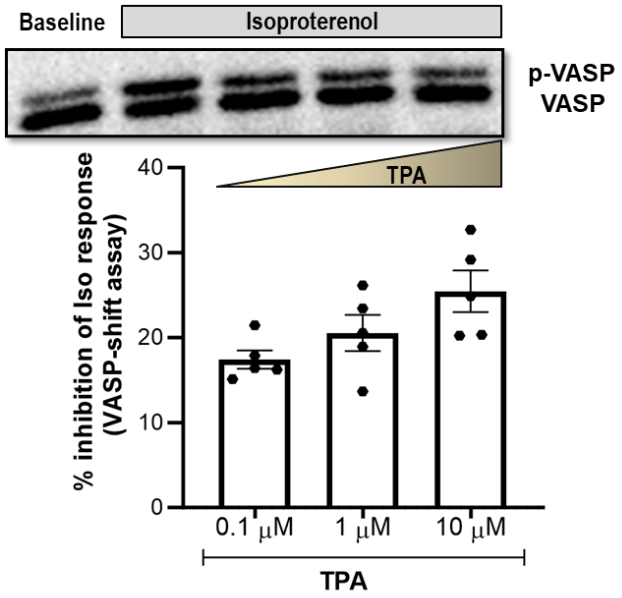

Figure 5.5. PKC activity is required for OxPAPC-induced inhibition of cAMP-dependent PKA signaling (VASP phosphorylation) in HASM cells.

(A) 24-hrs serum starved HASM cells were incubated with either PKC-inhibitor (GF109203X) or COX_2 inhibitor (Indomethacin) in the presence of OxPAPC (80 μg/mL). Representative immunoblots (top) show p-VASP and VASP bands with respective treatments as mentioned in the table (bottom). Integrated density of p-VASP and VASP bands were used to calculate % p-VASP and the scatter bar plot represents mean±SEM from five HASM cell lines.*** P<0.001 vs controls. Data were analyzed by one-way ANOVA with Tukey's multiple-comparison tests. ***p< 0.001 vs controls;$^{###}$p<0.001 vs baseline. **(B)** Representative immunoblots (top) of PKC phosphorylation (Ser660) and loading control β-actin is shown for treatment with OxPAPC or TPA. Scatter dot plot comparing mean±SEM of % increased PKC phosphorylation over baseline in response to OxPAPC (80 μg/mL) and TPA (0.2 μM, 1 hr). The integrated density value was first normalized to the respective loading control (β-actin) and then calculated as the percentage increased from baseline from five independent cell lines. **(C)** 24-hrs serum starved HASM cells were stimulated with TPA (0.1-10 μM) for 1 hr and then VASP shift assay was performed with Iso 1nM. Representative immunoblot (top) shows phosphorylated VASP (p-VASP) and VASP bands, and densitometry was performed to calculate % p-VASP. The scatter bar plot represents the % reduction (mean±SEM) of Iso response by TPA from five HASM cell lines.

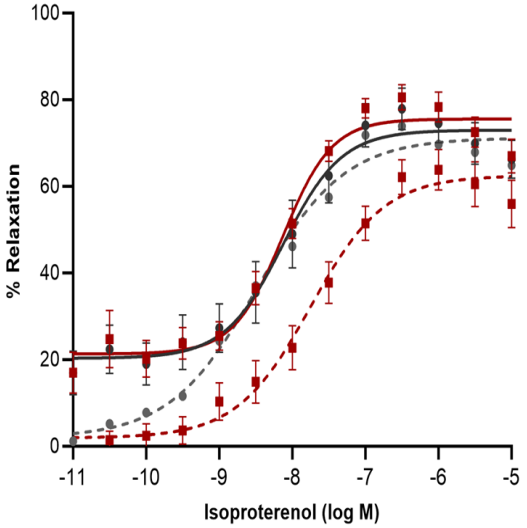

Treatment group	Isoproterenol EC_{50} (Mean ± SEM)	% Maximum relaxation (Mean ± SEM)
Control	3.3 ± 0.11 nM	71.2 ± 2.3%
OxPAPC (80 µg/mL)	**17.8 ± 0.13 nM*****	**62.5 ± 2.8%****
GF-109203X (10 µM) + Vehicle	7.5 ± 0.14 nM	73.0 ± 2.8%
GF-109203X (10 µM) + OxPAPC (80 µg/mL)	7.4 ± 0.09 nM	75.6 ± 1.9%

Figure 5.6. OxPAPC-induced impairment of murine tracheal ring relaxation requires PKC activity. Epithelium-denuded murine tracheal rings were pre-incubated with GF-109203X (10 µM) for 2 hrs (37^0C) then with OxPAPC (80 µg/mL) for 24 hours in the presence of inhibitor. Relaxation dose-response was performed with Iso. Data were analyzed by nonlinear-curve-fit (variable slope- four parameters). This graph also shows control curves from Figure 5.1A for reference. Each data point represents mean±SEM from 6 tracheal rings (6 BALB/c female mice).

5.5 Discussion

This is the very first study that shows that OxPC promote β_2AR dysfunction by uncoupling β_2AR from downstream signaling pathways in HASM cells, thus impairing bronchorelaxation. The compromised β_2-agonists effectiveness in a significant number of asthmatics is a major hurdle to front-line reliever therapy, however mechanism(a) are not well-known. Recently, our group [176] discovered that aeroallergen challenge is associated with the accumulation of a unique profile of OxPC, which participate in several key features of asthma pathophysiology including airway hyperresponsiveness, airway contraction, and inflammation. None of the currently available standard asthma therapies directly mitigate these oxidative stress mediators in the lungs and they engage in complex signaling pathways, therefore we sought to investigate the impact of OxPC on β_2AR desensitization. By using murine tracheal rings and TCLS *ex vivo,* mouse lung function testing *in vivo,* and cultured HASM cells, this study shows that OxPC attenuate broncho-relaxant action of β_2AR agonists on the airways. This study provides further research potential that OxPC accumulation in airways is one of the factors responsible for clinically well-known bronchodilator insensitivity in chronic obstructive lung diseases such as asthma.

In the relaxation dose-response study using epithelium-denuded tracheal rings, we demonstrated that OxPAPC exposure is associated with inhibition of β_2AR function as revealed by lower potency and efficacy to β_2AR agonist Iso. While forskolin effects via direct activation of the AC, without involving the upstream (β_2AR-$G_{\alpha s}$) signaling pathway, remains unaffected by OxPAPC treatment in this study. This intriguing observation demonstrates that OxPAPC potentially uncouple β_2AR from its downstream effector AC. This *ex vivo* relaxation impairment effect was also confirmed in smaller airways using murine TCLS, in which we showed consistently lowered potency and efficacy of Iso, revealing β_2AR dysfunction by OxPAPC in both central and smaller airways.

To translate these observations into preclinical study, next we used a small animal lung function test to measure bronchodilator response against Mch-induced increase in respiratory resistance. Here we used short acting β_2AR agonist, albuterol, as a relaxant agent because it is most commonly prescribed bronchodilator in clinics. Consistently, we found that intranasal OxPAPC challenge lowers albuterol effect of preventing Mch-induced increase in respiratory resistance. This reflects that direct intranasal challenge with OxPAPC can inhibit bronchoprotective action of β_2AR agonist in mice, complementing our *ex vivo* findings.

To get further mechanistic insights, we employed cultured HASM cells to understand the intracellular effect of OxPAPC in ASM cells, as these are the key structural cells involved in changing the diameter of the airway [250]. Intracellular cAMP signaling in response to relaxant agents is a key cellular event involved in ASM relaxation. Therefore, we assessed cAMP signaling in HASM cells by performing a VASP shift assay. We first validated the VASP shift assay in cell lines that are used for this study by performing a dose-response study with Iso, which is proven to be a sensitive assay to detect total cAMP signaling by means of PKA-induced VASP phosphorylation [279, 280]. Additionally, we also used cAMP sensor cADDis transduced HASM cells to measure real-time cAMP signaling [281]. In both assays, OxPAPC treatment significantly diminishes real-time cAMP signaling (measured by cADDis assay) and specifically cAMP-PKA signaling (assessed by VASP shift assay) elicited by β_2AR agonist Iso. These findings confirm that OxPAPC treatment reduces cAMP signaling in HASM cells that is paralleled with noted impairment of airway relaxation. Next, using HEK293 cells overexpressing surface β_2AR, this study confirmed that OxPAPC exposure neither affect cell surface β_2AR levels nor internalize receptors.

Our recent study [176] shows that PKC activation is sustained by OxPAPC exposure that perpetuates pro-inflammatory cytokines and COX_2 induction in HASM cells. Having established both PKC and COX_2 as important signaling hub for OxPAPC in ASM pathophysiology, we further performed mechanistic studies to investigate the role of these signaling pathways in mediating OxPC effects on β_2AR function. It is also known that both PKC activity [276, 277] and COX_2-induced PGE2 signaling [278] are well known to cause β_2AR desensitization. Interestingly, we found that small molecular PKC inhibitor prevented inhibitory action of OxPAPC in both cAMP assay with HASM cells and relaxation study with tracheal rings. This shows that PKC activity is required for OxPAPC-mediated β_2AR function impairment. However, COX_2 inhibitor did not affect OxPAPC impact on β_2AR function. Most importantly, PKC-induced β_2AR desensitization noted in this study is consistent with an earlier investigation by Boterman and group [276, 277], in which they showed that PKC activation causes inhibition of Iso relaxation while forskolin response remains unaffected in bovine tracheal smooth muscle. This consistently confirm the inhibitory role of PKC on β_2AR responsiveness. Additionally, our work confirms that OxPAPC can sustain PKC activation in HASM cells and TPA, direct PKC activation, can also diminish β_2AR signaling. The earlier mechanistic study [282] performed in lymphocytes showed that PKC activation causes β_2AR uncoupling from the downstream signaling pathways without involving receptor downregulation from the cell surface. This mechanism correlates to the findings in the current study that OxPAPC-induced PKC activity participates in β_2AR uncoupling from downstream signaling pathways without impacting cell surface β_2AR level. Additionally, PKC also inhibits dopamine receptor function that results in diminishing cAMP signaling in neuronal cells [283], revealing inhibitory effect on dopamine receptor as well. Of note, higher PKC activity was previously observed in lymphocytes isolated from asthma patients donors that correlates with

disease severity [284]. This implies that PKC activity is a potential signaling hub in asthma pathophysiology and that may contribute to bronchodilator insensitivity. In ASM cells, COX_2-induced PGE2 in an autocrine fashion is reported to cause β_2AR desensitization [278], and in our previous study [176] we reported that OxPAPC causes COX_2 induction which further perpetuates the release of oxylipins replete with prostaglandins, leukotrienes and epoxyeicosatrienoic acid derivatives in an autocrine fashion. However, we did not notice the involvement OxPC-COX_2 signaling axis in β_2AR inhibition in this study.

In summary, our work has discovered that OxPAPC attenuates the bronchodilator's ability to relax airways and uncovers a related mechanistic understanding. This provides a need for future studies to gain a fulsome understanding of receptor or non-receptor mediated PKC activation by OxPAPC, and which specific PKC isoforms are involved to understand the comprehensive role of OxPAPC in the context of bronchodilator insensitivity. This also includes obtaining further mechanistic insights into how PKC inhibits β_2AR function and which specific bioactive constituents of OxPAPC are involved that would help in designing therapy to mitigate OxPC impact on bronchodilator efficacy. In summary, this detailed study provide the first evidence that OxPC can cause β_2AR dysfunction via PKC activity and thus impair bronchorelaxation. Our work in this study also suggests a mechanism for oxidative stress mediators-induced β_2AR desensitization in obstructive lung diseases like asthma.

Chapter 6: Neutralizing Oxidized Phosphatidylcholine Reduces Airway Inflammation and Hyperreactivity in a Murine Model of Allergic Asthma

Jignesh Vaghasiya[1,2], Aruni Jha[1,2], Sujata Basu[1,2], Alaina Bagan[2], Siwon K. Jengsuksavat[2], Amir Ravandi[1,3,4], Christopher D. Pascoe[1,2] & Andrew J. Halayko[1,2,4] on behalf of the Canadian Respiratory Research Network

[1]Department of Physiology and Pathophysiology, University of Manitoba, Winnipeg, MB, Canada. [2]Biology of Breathing Group, Children's Research Hospital of Manitoba, Winnipeg, MB, Canada. [3]Institute of Cardiovascular Sciences, St. Boniface Hospital Albrechtsen Research Centre, Winnipeg, Manitoba, Canada. [4]Department of Internal Medicine, Max Rady College of Medicine, University of Manitoba, Winnipeg, MB, Canada.

This research work is published in Biology.

Author Contributions:
Jignesh Vaghasiya: Study design, execution, data analysis, and manuscript writing
Aruni Jha: Study execution
Sujata Basu: Performed mice lung function test
Alaina Bagan: Assisted with flowcytometry under my supervision
Siwon Jengsuksavat: Assisted with MSD assay under my supervision
Amir Ravandi: Procured E06 mAb and manuscript review
Christopher Pascoe: Study execution and manuscript review
Andrew Halayko: Conceived the project and its design, data plan, and edited manuscript

6.1 Abstract

Oxidative stress is associated with asthma pathobiology. We reported that oxidized phosphatidylcholines (OxPC) are mediators of oxidative stress, and accumulate in the lung in response to allergen challenge. The current study begins to unravel mechanisms for OxPC accumulation in the lung, providing the first insights about how OxPC underpin allergic airway pathophysiology, and preclinical testing of selective neutralization of OxPC in a murine model of allergic asthma. We hypothesized that intranasal delivery of E06, a natural IgM antibody that neutralizes the biological activity of OxPC, can ameliorate allergen-induced airway inflammation and airway hyperresponsiveness. Adult BALB/c mice were intranasally (i.n.) challenged with HDM (25 μg/mouse, 2 weeks). Some animals also received E06 monoclonal antibody (mAb)(10 μg) i.n. 1 hr before each HDM challenge. HDM challenge reduced mRNA for anti-oxidant genes (*SOD1, SOD2, HO-1 and NFE2L2*) in the lung by several orders of magnitude ($p<0.05$). Concomitantly, total immune cell number in BALF increased significantly ($p<0.001$). E06 mAb treatment prevented allergen-induced BALF immune cell number by 43% ($p<0.01$). This included a significant blockade of eosinophils (by 48%, $p<0.001$), neutrophils (by 80%, $p<0.001$), macrophages (by 80%, $p<0.05$), and CD4 (by 30%, $p<0.05$) and CD8 (by 42%, $p<0.01$) lymphocytes. E06 effects correlated with a significant reduction in TNF (by 64%, $p<0.001$) and IL-1β (by 75%, $p<0.05$), and a trend to diminish accumulation of other cytokines (e.g. IL-4, -10, and -33, and IFN-γ). E06 mAb treatment also inhibited HDM exposure-induced increases in total respiratory resistance and small airway resistance by 24% and 26%, respectively. In conclusion, prophylactic treatment with an OxPC-neutralizing antibody significantly limits allergen-induced airway inflammation and airway hyperresponsiveness, suggesting that OxPC are important mediators of oxidative stress-associated allergic lung pathophysiology.

6.2 Background

Asthma is a chronic lung disease characterized by lung inflammation, AHR and remodeling [1]. Front line therapy for asthma includes inhaled corticosteroids and β_2-adrenergic receptor agonists as controller and reliever medications to limit airway inflammation and dilate bronchial airways, respectively [92, 262, 285, 286]. Many asthmatics are refractory to therapy and have uncontrolled symptoms [11, 108, 228, 287], which suggests the presence of underlying persistent airway pathobiology. A feature of treatment-refractory asthma is sustained oxidative stress in the lung, which develops in response to inhaled environmental pollutants, which is a feature of steroid refractory asthma pathobiology [122, 288, 289]. This is associated with the accumulation of inflammation-induced reactive oxygen species (ROS), due in part to impairment of endogenous antioxidant systems and effective redox balance [121, 290-294]. ROS accumulation is not directly inhibited by inhaled corticosteroids or beta-adrenergic receptor agonists used for standard asthma control. ROS modify protein and lipid molecules, generating new bioactive forms that contribute to the chronicity of inflammation and pathophysiology. Notably, systemic treatment with exogenous anti-oxidant therapeutics has not been effective [209], perhaps due to a need to more specifically target oxidized biomolecules in the lung. Our recent findings shows that a panel of oxidized phosphatidylcholines (OxPC) accumulate in the lungs of human asthmatics after allergen challenge, and correlate with clinical indices of airway dysfunction [177, 178].

Oxidative stress modifies phospholipids - including phosphatidylcholine in cell membranes, lipoproteins and extracellular fluids of the lung - by targeting double bonds in fatty acyl chains to generate numerous fragmented and/or structurally modified forms [127]. OxPC promote pathophysiology of atherosclerosis [233], pain-inducing inflammation [164], acute lung injury [166, 168], and neurodegenerative diseases [295]. Recent evidence indicates that OxPC can trigger

a number of biological responses that are fundamental to asthma pathophysiology. In human subjects, segmental bronchial challenge with allergens induces the accumulation of panels of OxPC that associate with AHR and the severity of the late asthmatic response [176, 296]. *In vitro* studies with airway epithelial cells demonstrate that OxPC promote ROS production, suppress metabolic function of mitochondria, and inhibit wound closure [178]. OxPC also promote the pro-inflammatory function of human airway smooth muscle cells, inducing the release of IL-6, IL-8 and GM-CSF, and the production of oxylipins, including leukotrienes, prostaglandins and isoprostanes [176]. Moreover, OxPC directly induce both ASM contraction, in part by activating TRPA1, and bronchospasm in murine TCLS preparations [177, 178]. Mechanism for OxPC-induced TRPA1 activation is not known yet, however, recent study reveals requirement of cysteine and lysine residue on N-terminal of channel protein for OxPC agonistic activity [165]. Nonetheless, the specific contributions of OxPC to asthma pathophysiology *in vivo*, including airway inflammation and AHR, has not been deciphered in human asthma or in animal models of allergic asthma.

E06 is a murine monoclonal IgM antibody (E06 mAb) that selectively reacts with phosphocholine of oxidized phospholipids, including OxPC [193-195]. It was developed by Dr. JL Witztum using apolipoprotein E knock-out mice [193]. Studies *in vitro* and *in vivo* demonstrate that E06 mAb inhibits pro-inflammatory effects of OxPC in macrophages [166], reduces infarct size caused by OxPC in porcine model of reperfusion injury and protects from OxPC-induced cardiomyocyte death [297], and inhibits OxPC contributions to inflammatory hyperalgesia [164, 206]. Additionally, transgenic mice ($Ldlr^{-/-}$-E06-scFv-Tg) that express high plasma levels of the E06 single chain variable fragment (E06-scFv) are resistant to atherosclerosis [162] and myocardial ischemic-reperfusion injury [297]. Notably, in these animals E06-scFv is also present in the lung,

and imparts protection against hyperoxia-induced lung injury [204]. Taken together, these reports indicate that neutralizing the biological activities of OxPC has potential for therapeutic benefit, but this potential has not yet been evaluated in an animal model of allergic asthma.

To our knowledge the current study is the first to assess the specific contribution of OxPC in allergen-induced airway inflammation and AHR in a murine model of asthma. We test the hypothesis that neutralization of OxPC in the lung using intranasal delivery of E06 mAb is sufficient to prevent from allergen-induced airway inflammation and AHR in mice. This approach is unique as it directly tests whether OxPC may be an important component of persistent inflammation that is refractory to mainstay asthma therapies, and a previously unknown element of severe asthma pathophysiology.

6.3 Materials and methods

6.3.1 Murine model of allergic asthma and E06 mAb treatment

As detailed previously, 8-10 weeks BALB/c mice were subjected to repeated intranasal HDM, five days sequential days each week for two weeks [269, 298]. For this purpose, individual mice were anesthetized with isoflurane (Forane, Baxter, USA), then administered 25 µg HDM (in 35 µL saline) by intranasal instillation (i.n). HDM dose (with 3278 EU/mg of protein) was selected based on our prior studies and it is well-tolerated without other adverse health effects on mice [298, 299]. Age-matched allergen naïve animals received intranasal saline (35 µL). For treatment with E06 mAb, animals were administered antibody i.n. (10 µg in 35 µL saline) 60 minutes before each HDM challenge, and control animal received saline alone.

6.3.2 Real Time-PCR for antioxidant genes

RNA was extracted from the left lung using the Qiagen RNeasy Kit spin columns. Purity and RNA concentration was measured using Nanodrop 2000 (Thermo Fisher Scientific, Waltham, MA USA). cDNA was generated from 1µg of total RNA using the BioRad iScript cDNA Synthesis Kit. Real time-PCR (RT-PCR) was performed using BioRad SsoAdvanced Universal SYBR Green Supermix and BioRad CFX96 Touch Real Time-PCR system. 18S RNA was used as a housekeeping gene for analysis. Primers for *SOD1, SOD2, HO-1* (Heme oxygenase 1), and *NFE2L2* (Nuclear factor erythroid 2-related factor 2) were designed and purchased from IDT Technologies (San Diego, CA, USA) (Table 6.1). Data was analyzed using ddCT calculation, with the averaged control CT values being used as the reference sample, where a value of $\log_2 0$ refers to no change from the reference control.

Table 6.1. Primer sequence for RT-PCR

Gene	Forward	Reverse
SOD1	ACAATGGTGGTCCATGAGAAA (Sense)	GTTTACTGCGCAATCCCAATC (AntiSense)
SOD2	GCAAGGAACAACAGGCCTTA (Sense)	CCCAGTTGATTACATTCCAAATAGC (AntiSense)
HO-1	CTAGCCTGGTGCAAGATACTG (Sense)	CAACAGGAAGCTGAGAGTGAG (AntiSense)
NFE2L2 (NRF2)	CCATTCCCGAATTACAGTGTCT (Sense)	AGCGAGGAGATCGATGAGTAA (AntiSense)

Legend: *SOD1* – Superoxide dismutase 1, *SOD2* – Superoxide dismutase 2, *HO-1* – Heme oxygenase 1, *NFE2L2* - Nuclear factor erythroid 2-related factor 2 or NRF2.

6.3.3 Lung function assessment

Forty-eight hours after final HDM challenge each mouse was anesthetized (sodium pentobarbital, 90 mg/kg, i.p), and underwent tracheostomy with a 20-gauge polyethylene catheter. The tracheal cannula was connected to a flexiVent FX small animal ventilator (SCIREQ Inc., Montreal, QC, Canada) and mice were ventilated (150 breaths/min, tidal volume of 10 mL/kg, and a PEEP of 3 cmH_2O). Measurement of airway resistance and lung stiffness was performed at baseline and following inhalation of serial challenge with increasing concentrations of nebulized methacholine (Mch) (35 μL, 0-50 mg/mL Mch, 10 sec delivery) [269, 273]. To assess lung function we interrupted mechanical ventilation with a volume perturbation signal using the preset flexiVent Prime-3 protocol, enabling measurement of mechanical impedance (Zrs). By fitting Zrs to the constant phase model flexiVent software calculated peripheral tissue damping (G), and tissue elastance or stiffness (H) [268, 272]. This setup also allowed us to measure total respiratory system resistance (Rrs) using flexiVent SnapShot-150 protocol simultaneously. Each parameter was calculated as an average of 12 measurement performed after each Mch challenge.

6.3.4 Bronchoalveolar Lavage Fluid (BALF) Collection

After lung function assessment, BALF was collected using 2× 1 mL ice-cold sterile saline. BALF was centrifuged (1100 RPM × 10 min, 4^{o}C). The supernatant was removed and stored (-80°C) for subsequent multi-plex cytokine analysis, or was used for OxPC extraction and analysis (below). The cell pellet was used for subsequent differential immunophenotype analysis (see below).

6.3.5 OxPC quantification in BALF

OxPC were extracted from BALF supernatant using the Folch method, then quantified using ultra-high performance liquid chromatography-tandem mass spectrometry (LC-MS/MS) as we have detailed [299].

6.3.6 Flow cytometry immunophenotyping of inflammatory cells in BALF

BALF cell pellets were re-suspended in 1 mL ice-cold PBS / 0.1 mM EDTA and total leukocyte number was counted (10 µL cell suspension in a hemocytometer for manual cell number counting). Cell counts were averaged to calculate a total number of cells and normalized per total BALF volume (represented as nos. of cells × 10^4/ml of BALF).

For cell immunophenotyping the re-suspended cell pellet was centrifuged (5 min, 1200 rpm, 4°C), and the resulting pellet re-suspended in 1 mL FACS buffer (PBS, 0.5% BSA), then for 10 minutes (on ice) in 100 µL FC blocker (anti-CD16/CD32, 1 µL in 100 µL FACS buffer). After washing with 1 mL FACS buffer, cells were re-suspended in the granulocyte or lymphocyte fluorescent antibody cocktails (30 min, 0.5 µL of each antibody in 20 µL FACS buffer)(Table 3.2). After washing cells in FACS buffer they were slowly re-suspended in 2% paraformaldehyde (400µL, on ice, 15 min), washed again in FACS buffer, and re-suspended in FACS buffer (500 µL) for storage (4°C, dark) until analysis using an Attune® NxT acoustic focusing cytometer (Life Technologies Holdings Pte Ltd, Singapore). For multi-color flow cytometry, instrument compensation was

established using spleen $CD4^+$ cells labelled individually with each antibody (Table 3.2). Murine spleen cells were isolated from allergen naïve animals with fine tissue grinding and erythrocyte lysis prior to labelling with individual antibodies as noted above (Table 3.2). After completing instrument compensation, BALF cells labelled with granulocyte and lymphocyte antibody panels were acquired by cytometer and analyzed using FlowJo (Version 10.8.1) software, with the gating strategies outlined in Figure 6.1 for cell surface markers (Table 6.2). The absolute number for each cell type was calculated by converting percentage distribution into absolute number (nos. of cells $\times 10^4$/mL of BALF) using respective total cell counts.

Table 6.2. Cell surface markers for identification of granulocytes or lymphocytes.

Panel	Cell types	Cell surface markers
Granulocytes	Eosinophils (Eos)	$CD11c^{low}$ Siglec-F^+
	Neutrophils (Neu)	$CD11c^{low}$ Siglec-F^- $CD11b^{high}$ Ly-$6G^+$
	Alveolar Macrophages (AM)	$CD11c^{high}$ Siglec-F^+ $CD11b^{int}$ $F4/80^+$
	Interstitial Macrophages (IM)	$CD11c^{low}$ Siglec-F^- $CD11b^{high}$ $F4/80^+$
Lymphocytes	B cells	$B220^+$
	CD3 cells	$CD3^+$
	CD4 cells	$CD3^+$ $CD4^+$
	CD8 cells	$CD3^+$ $CD8^+$

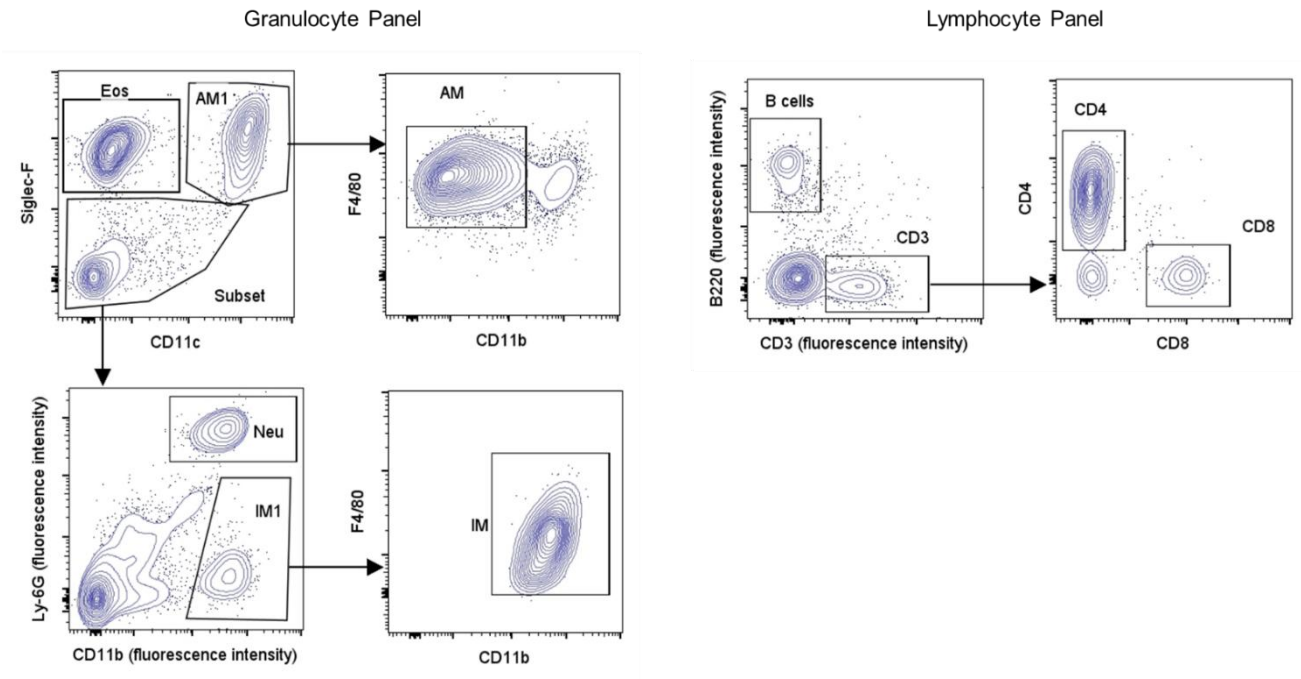

Figure 6.1. Flow cytometry gating strategy for identification of inflammatory cell populations in BALF. Differential leukocytes in BALF was identified using flow cytometry with the gating strategy depicted above for granulocyte (left) and lymphocyte (right) identification. Hierarchical gating of non-debris and single cells was followed by differential leukocytes identification based on multiple cell surface markers as mentioned in Table 6.2. Legend: Eos: Eosinophils, Neu: Neutrophils, AM: Alveolar Macrophages, IM: Interstitial Macrophages.

6.3.7 BALF cytokines analysis

Cytokines and chemokines in BALF supernatant were profiled using V-PLEX Mouse Cytokine 19-Plex Kit from Meso Scale Discovery (Maryland; USA) following manufacturer's instructions. The panel included the following targets: interleukin (IL) -1β, -2, -4, -5, -6, -9, -10, -12p70, -15, -17A/F, -27p28/IL-30 and -33, and IFN-γ, IP-10, KC/GRO, MCP-1, MIP-1α, MIP-2 and TNF.

6.3.8 Statistical analysis

Each treatment group consisted of five animals for the positive control HDM challenge protocol and four animals were included in the E06 treatment group. Depending on the experimental design, data were analyzed as described in the text using t-test, one-way or two-way ANOVA with Dunnets's post-hoc test using GraphPad Prism version 8.4.3 (San Diego, CA, USA). Data are shown as mean±SEM unless otherwise specified. $P<0.05$ was considered statistically significant.

6.4 Results

6.4.1 HDM challenge induces lung inflammation and inhibits expression of anti-oxidant genes

Repeated HDM challenge increased in BALF inflammatory cell number by 17-fold compared to saline challenged (allergen-naïve) animals ($41.8\pm7.5x10^4$ cells/mL vs $2.2\pm0.7x10^4$ cells/mL, respectively; $p<0.001$) (Figure 6.2A). This was associated with a profound increase in eosinophils ($p<0.001$), and multi-fold and significant accumulation of neutrophils ($p<0.01$), alveolar macrophages ($p<0.05$), and interstitial macrophages ($p<0.001$) (Figure 6.2A). HDM challenge also caused a significant increase in B-cells ($p<0.01$), CD4+ and CD8+ cells ($p<0.001$) (Figure 6.2A). Of note, HDM challenge caused a predominant increase in CD4+ over CD8+ cells, with the CD4+/CD8+ cells ratio increasing from 3.0 in control group to 11.6 in HDM group. Recent work shows that both CD4+ and CD8+ cells play a central role in HDM-induced allergic asthma in mice [300]. We observed a concomitant decrease ($p<0.05$) in lung mRNA abundance for the anti-oxidant genes, *SOD1, SOD2, HO-1,* and *NFE2L2* (Figure 6.2B). This confirms that HDM challenge induces both marked allergic lung inflammation and loss of anti-oxidant gene mRNA that is consistent with redox imbalance that can underpin oxidative stress.

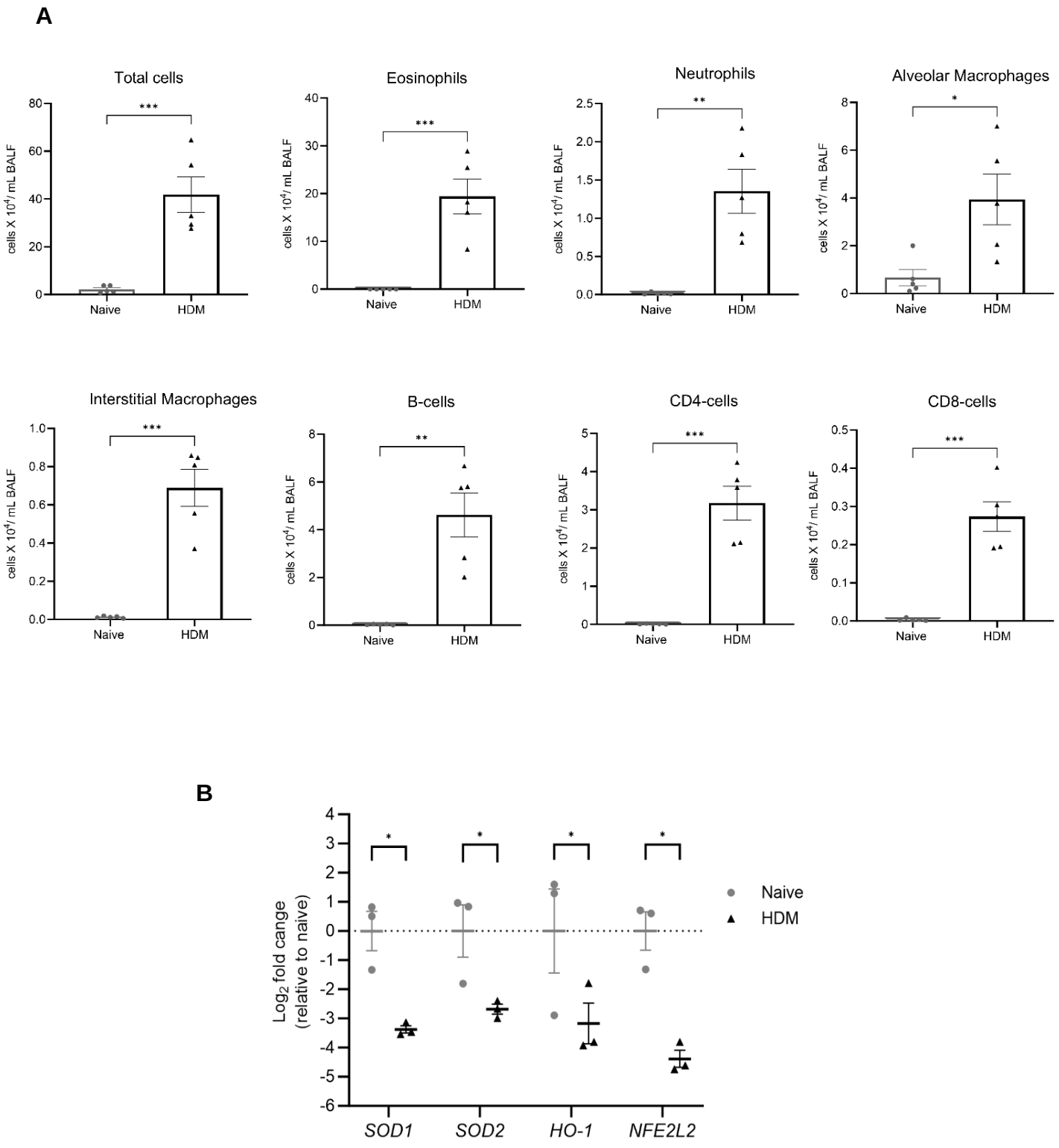

Figure 6.2 ***(Continued)***

Figure 6.2. HDM challenge causes inflammatory cells infiltration and redox imbalance in mice lungs. BALF inflammatory cells and lung antioxidant genes were assessed at 48 hrs after the final HDM challenge. **(A)** Total BALF cells were manually counted and normalized to initial BALF volume. Differential leukocytes was identified using flow cytometry. Scatter dot plots compare mean±SEM of total cells and absolute leukocyte counts from five animals per group and were analyzed by two-tailed t-test, *$p<0.05$, **$p<0.01$, and ***$p<0.001$ HDM vs. naïve. **(B)** Scatter dot plot shows relative Log2 fold change of antioxidant genes in murine lung tissue from three random animals per group. Data represent mean±SEM and analyzed by pairwise t-test with Holm-Sidak's multiple comparisons test, *$p<0.05$ HDM vs. naïve. *SOD1*: Superoxide dismutase 1, *SOD2*: Superoxide dismutase 2, *HO-1*: Heme oxygenase 1, *NFE2L2*: Nuclear factor erythroid 2-related factor 2, HDM: House dust mite.

6.4.2 HDM challenge induces OxPC formation in the lung

LC-MS/MS analysis detected 33 different OxPC moieties in BALF samples collected from all mice. The total basal concentration of OxPC was 71.1 ± 17.2 ng/mL in allergen naïve animals, but this increased more than 200% in HDM challenged animals (229.3 ± 33.5 ng/mL of BALF; $p<0.01$ vs. naïve)(Figure 6.3A). Agglomerative hierarchical clustering analysis of individual OxPC species in individual BALF samples revealed a distinct increase in the clustered abundance of OxPC in BALF from allergen-naïve and HDM-challenged mice (Figure 6.3B).

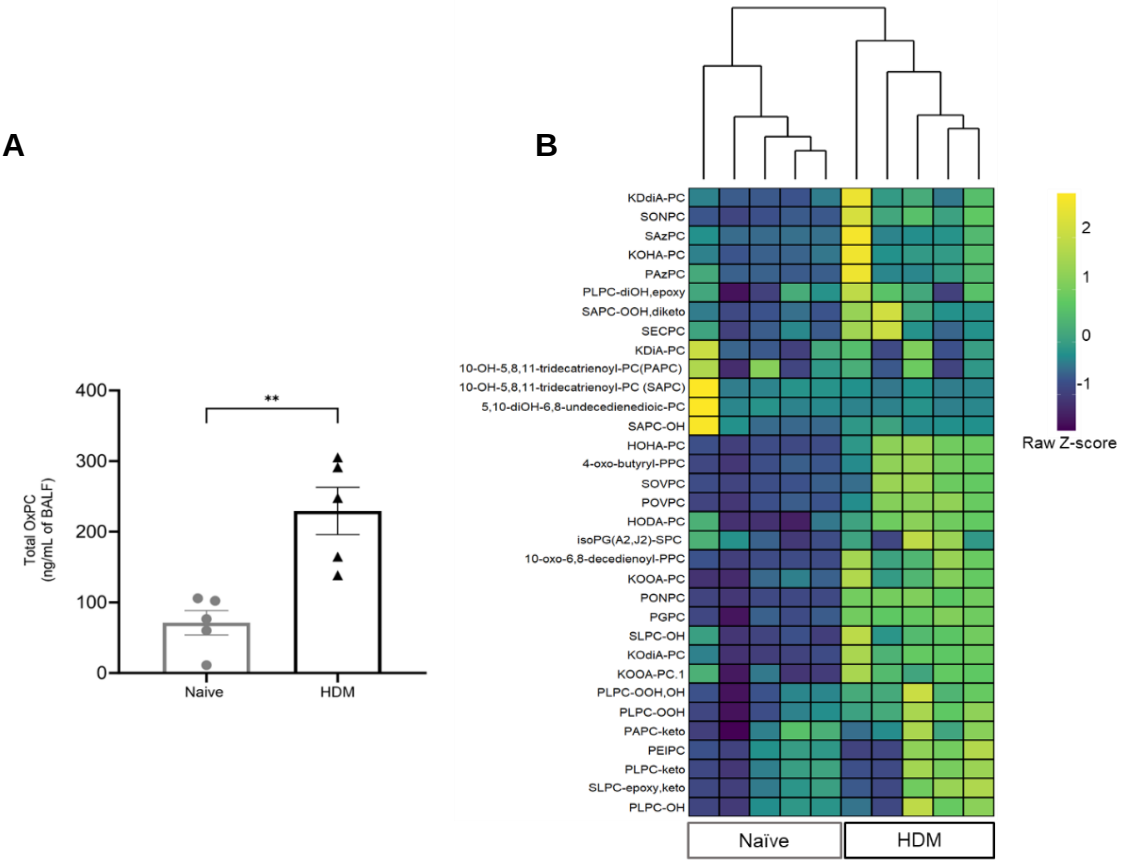

Figure 6.3. HDM challenge increases OxPC formation in the mice lungs.
BALF OxPC were measured by LC-MS/MS at 48 hrs after the final HDM challenge. **(A)** The measured OxPC levels were normalized to the initial BALF volume and total OxPC is presented as mean±SEM from 5 animals per group. The data were analyzed by two-tailed t-test;**$p<0.01$ HDM vs. naïve. **(B)** The heatmap compares individual OxPC moieties detected in BALF from naïve and HDM-challenged mice. The heatmap color is based on the row Z-score (color key). Agglomerative hierarchical clustering (as shown in the top dendrogram – the vertical length of the dendrogram is proportional to the dissimilarities between the groups or individual animals) shows that HDM challenged group is tightly clustered and completely different from the allergen naïve group based on the individual OxPC moieties level.

6.4.3 E06 mAb treatment reduces HDM-induced infiltration of lung inflammatory cells

E06 mAb treatment significantly reduced HDM-induced total BALF cell counts by 43% ($p<0.01$, E06-HDM vs. saline-HDM) (Figure 6.4B). Differential cell analysis showed that the effect of E06 mAb treatment was associated with a ~80% suppression in accumulation of both neutrophils ($p<0.001$, E06-HDM vs. saline-HDM) and alveolar macrophages ($p<0.01$, E06-HDM vs. saline-HDM) (Figure 6.4C), which was reflected in a significant decrease in the percentage of each cell type ($p<0.01$ for Neu and $p<0.05$ for AM, comparing E06-HDM vs. saline-HDM) (Figure 6.4E). E06 treatment was also associated with significantly lower (48%) BALF eosinophil counts ($p<0.01$, E06-HDM vs. saline-HDM) and a trend for fewer interstitial macrophages (33% lower; $p=0.196$, E06-HDM vs. saline-HDM) (Figure 6.4C). Similarly, E06 treatment inhibited HDM-induced infiltration of CD4+ and CD8+ lymphocytes by 30% ($p<0.05$, E06-HDM vs. saline-HDM), and 42% ($p<0.01$, E06-HDM vs. saline-HDM), respectively (Figure 6.4D). B-cells accumulation appeared to decrease by 36%, but this did not reach statistical significance ($p=0.278$, E06-HDM vs. saline-HDM)(Figure 6.4D). The percentage distribution of eosinophils, interstitial macrophages, B cells, CD4+ and CD8+ cells in BALF was unchanged by E06 treatment (Figure 6.4E).

A

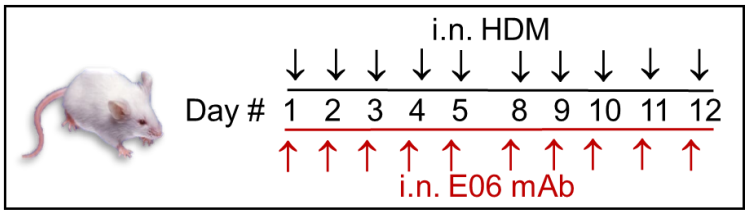

Figure 6.4 ***(Continued)***

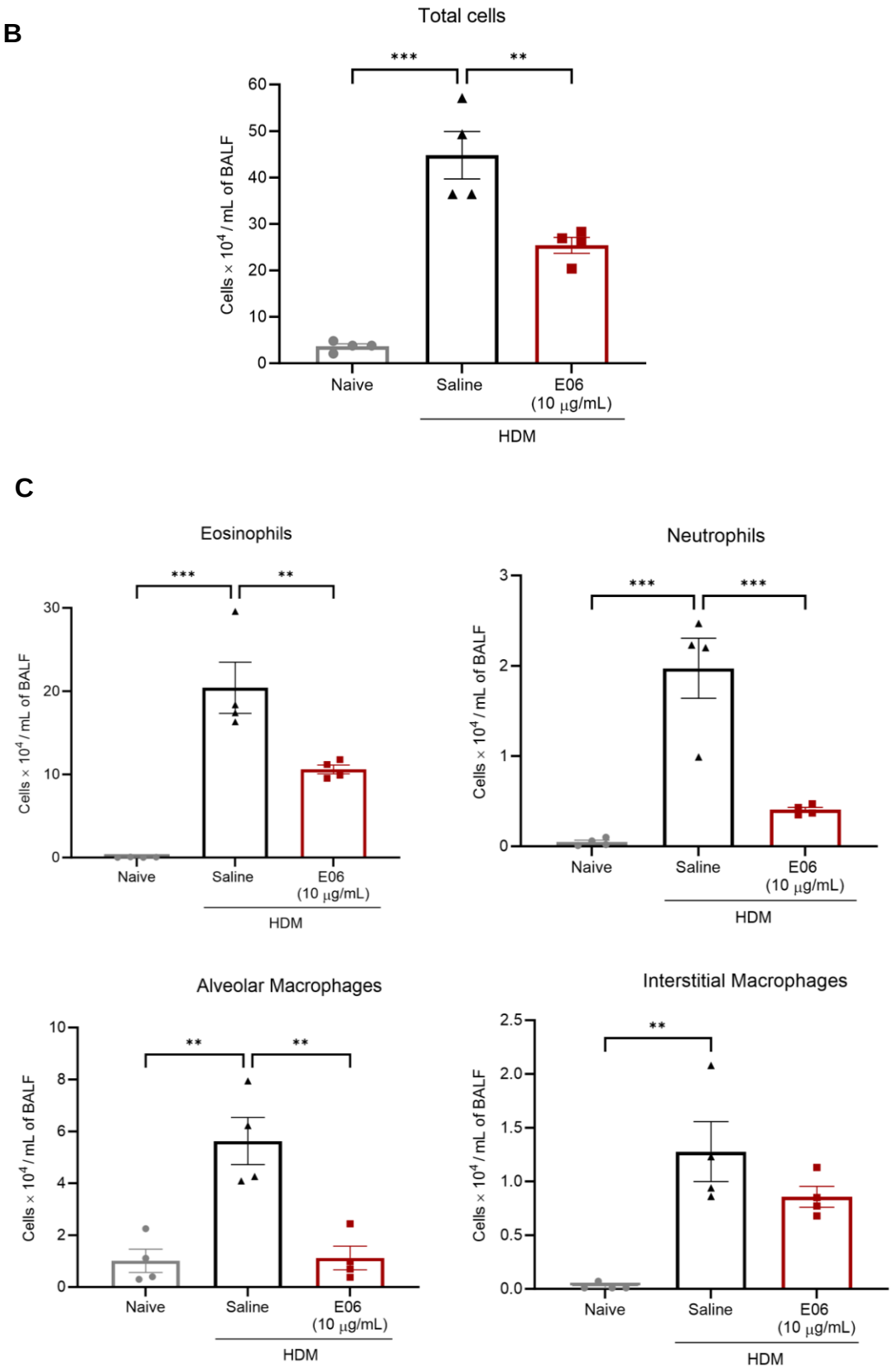

Figure 6.4 ***(Continued)***

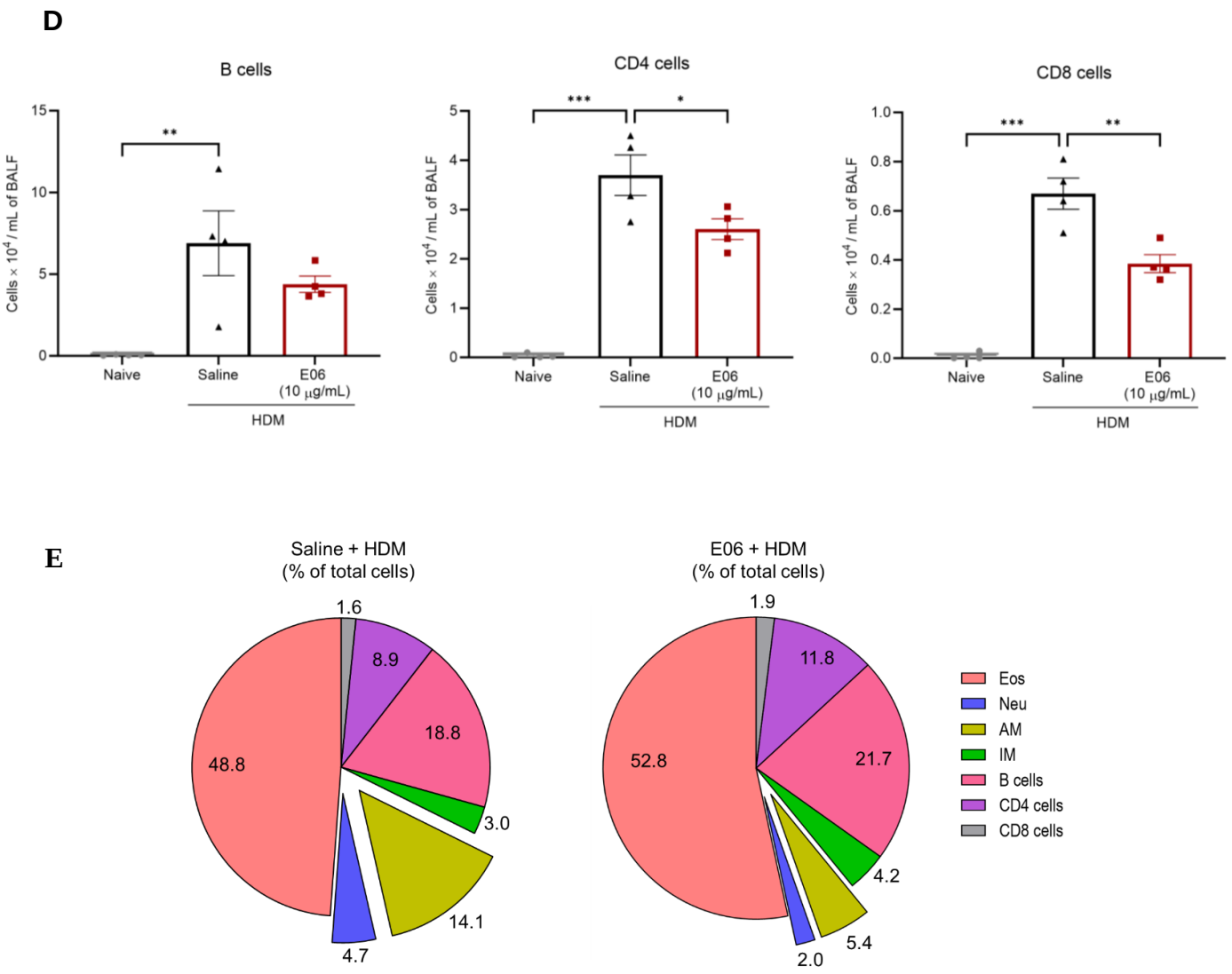

Figure 6.4: E06 mAb treatment reduces HDM-induced inflammatory cells infiltration in airway of mice.

(A) A schematic shows treatment design for E06 mAB and HDM. Black arrows represent HDM (25 μg/day i.n.) challenge and red arrows represent treatment with i.n. E06 mAB (10 μg/day). On each treatment day, E06 treatment occurred 60 minutes before HDM challenge. BALF inflammatory cells were assessed 48 hrs after the last treatment day using flow cytometry. **(B-D)** Scatter dot plots compare (mean±SEM) absolute cell counts (total cells and individual leukocytes) between treatment groups (n=4 mice) and analyzed by one-way ANOVA with Dunnett's multiple comparisons test, *p<0.05, **p<0.01, and ***p<0.001 vs. saline + HDM group. **(E)** Pie charts compare relative percentage distribution of leukocytes (as a percentage of total cells) between treatment groups. Exploded sections in chart (Neu and AM) represents significance difference between treatment groups (**p<0.01 for Neu, *p<0.05 for AM) by paired two-tailed t-test. The number in the chart represents the average percentage from 4 animals per group. Legend: HDM: House Dust mite, i.n.: intra nasal, Eos: Eosinophils, Neu: Neutrophils, AM: Alveolar Macrophages, IM: Interstitial Macrophages.

6.4.4 Impact of E06 mAb treatment on HDM-induced BALF cytokines and chemokines

Mesoscale multi-plex analysis confirmed that allergen challenge led to a significant increase in a number of asthma-associated cytokines and chemokines in BALF (Figure 6.5). The levels of IL-9, -12p70, and -27p28 were below detection limits across all groups (data are not shown), and though IL-2 and MCP-1 were not consistently detected in BALF from allergen-naïve animals, they were elevated and detected in BALF from HDM challenged mice.

E06 mAb treatment did result a 64% inhibition of HDM-induced TNF (2.43±0.25 pg/mL in E06-HDM group vs. 6.84±0.99 pg/mL in saline-HDM group; $p<0.001$) and 75% suppression of IL-1β accumulation (2.45±0.52 pg/mL in E06-HDM vs. 9.89±3.33 pg/mL in saline-HDM; $p<0.05$) (Figure 6.5). E06 mAb treatment was also sufficient for a trend to inhibit the accumulation of HDM-induced IL-33 (37% decrease, $p=0.586$, E06-HDM vs. saline-HDM), IFN-γ (45% decrease, $p=0.201$), IL-4 (73% decrease, $p=0.191$), and IL-10 (54% decrease, $p=0.282$). E06 mAb treatment was not sufficient to affect the accumulation of IL-2, -5, -6, -17A, or KC/GRO, MIP-1α, MIP-2, MCP-1 and IP-10 in HDM-challenge mice (Figure 6.5).

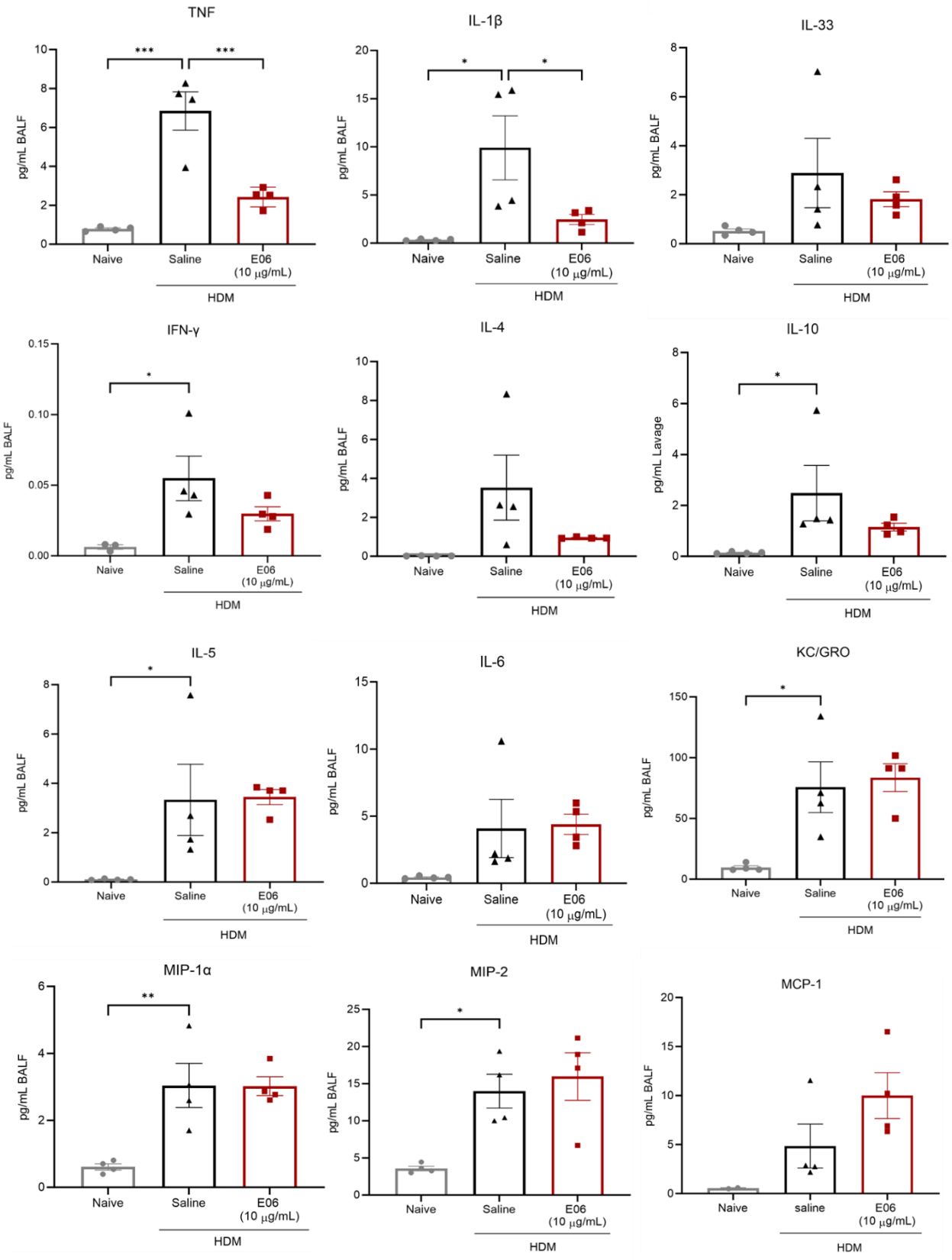

Figure 6.5 ***(Continued)***

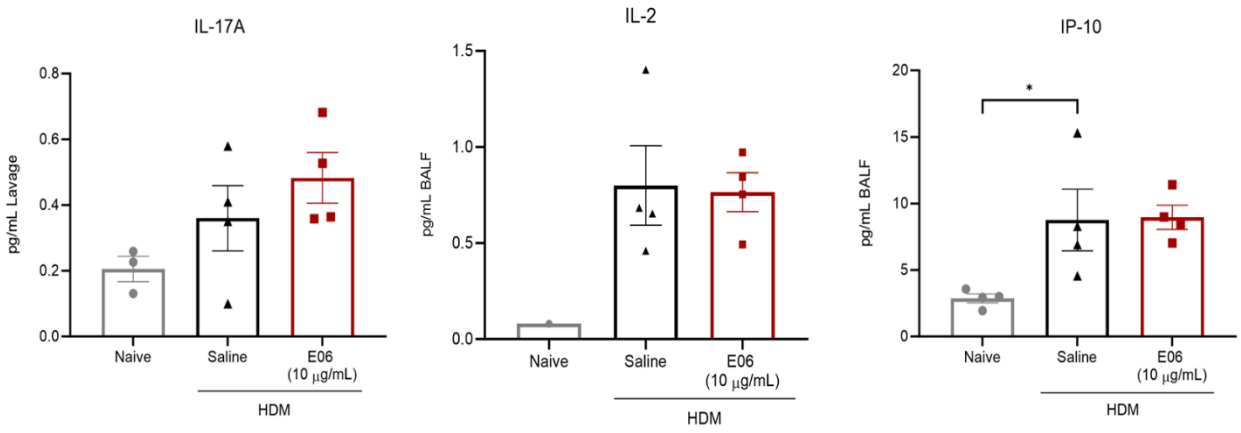

Figure 6.5: Impact of intranasal E06 mAb treatment on HDM-induced pro-inflammatory cytokines abundance in airway of mice.

BALF cytokines abundance was assessed 48 hrs after the last treatment. For all data, cytokine level is normalized to initial BALF volume and presented as mean±SEM from 4 animals per group. Data were analyzed by one-way ANOVA with Dunnett's multiple comparisons test, *$p<0.05$, **$p<0.01$, and ***$p<0.001$ vs. saline + HDM group.

6.4.5 Impact of E06 mAb treatment on HDM-induced lung airway hyperreactivity

Consistent with the induction of airway inflammation by repeated challenge with HDM, we also observed allergen-induced increase in total respiratory resistance (Rrs) ($p>0.05$ at 25 mg/mL Mch and $p<0.01$ at 50 mg/mL Mch, comparing saline-HDM vs naive), small airway resistance (tissue damping (G)) ($p>0.05$ at 25 mg/mL Mch and $p<0.05$ at 50 mg/mL Mch, comparing saline-HDM vs naive), and lung elastance (H) ($p>0.05$ at 25 mg/mL Mch and $p<0.01$ at 50 mg/mL Mch, comparing saline-HDM vs naive) in response to Mch exposure, compared to allergen-naïve animals (Figure 6.6). In allergen-challenged animals, E06 mAb decreased Rrs and G by 24% and 26%, respectively (Figure 6.6), revealing a protective trend against allergen-induced airway hyperreactivity ($p=0.156$ for Rrs and $p=0.241$ for G at 50 mg/mL Mch, comparing E06-HDM vs saline-HDM). Interestingly, despite these trends, E06 mAb treatment was seemingly without effect on the increased lung elastance (H) induced by repeated HDM challenge.

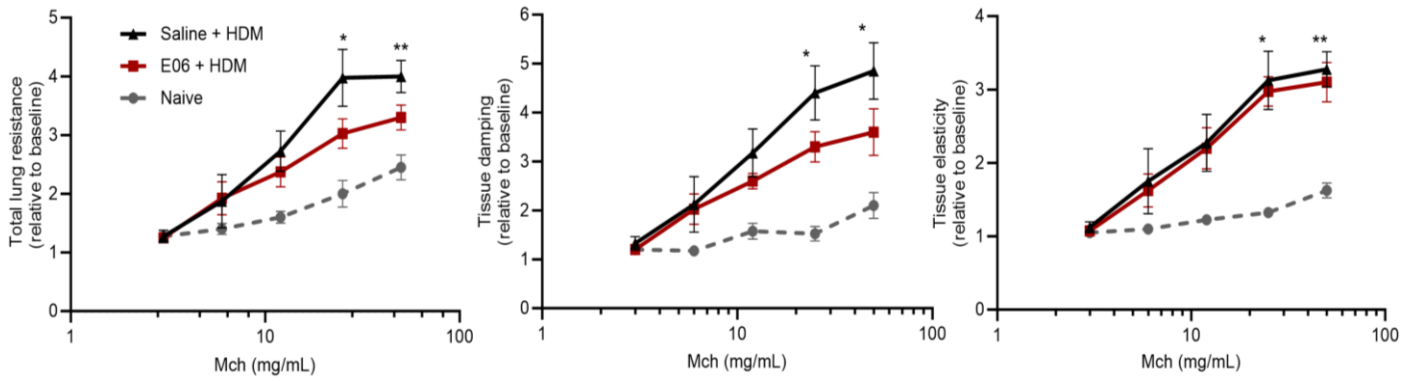

Figure 6.6: Impact of E06 treatment on HDM-induced airway hyperreactivity in mice.
Mouse lung function was assessed 48 hrs after treatment using a flexiVent small animal ventilator in response to sequential challenge with saline and Mch (3-50 mg/mL). Lung function data [total respiratory resistance (Rrs), tissue damping (G), and tissue elastance (H)] were normalized using respective baseline lung function for each mouse. Data represent mean±SEM from 4 animals per group and analyzed by two-way ANOVA with Dunnett's multiple comparisons test, *$p<0.05$ and **$p<0.01$ vs. naïve controls. Legend: Mch = methacholine.

6.5 Discussion

This study shows some of the first experimental evidence that the biological activities of OxPC contribute to airway inflammation and airway hyperreactivity in a murine model of allergic asthma. We used repeated i.n. HDM challenge to induce substantial airway inflammation and hyperreactivity [269], and in so doing, we revealed that this also includes a loss of expression of anti-oxidant genes and the accumulation of the oxidative stress biomarkers, OxPC, in the lungs. As OxPC accumulation in murine lung parallels our prior observations in human asthmatics [176], we investigated whether OxPC directly contribute to allergic inflammation and lung pathophysiology. We used a pre-clinical prevention design, treating allergen-challenged mice intranasally with an antibody that neutralizes the biological properties of OxPC [193]. We report that the monoclonal natural IgM antibody, E06 mAb, is sufficient to limit allergen-induced allergic airway inflammation and hyperreactivity.

Allergen-induced airway inflammation and AHR in humans [301, 302] and mice [269, 303] is marked by an influx of inflammatory cells, including eosinophils, neutrophils, and CD4+ lymphocytes that are regulated by, and contribute to the release of Th1 and Th2 cytokines [20, 303]. The murine model of intranasal HDM-challenge in our studies exhibits these features. We also demonstrate that allergen challenge mitigates the expression of important anti-oxidant genes – *SOD1, SOD2, HO-1,* and *NFE2L2* – indicating a disruption of endogenous redox homeostasis in the lung. Impaired antioxidant capacity is associated with asthma, for example, SOD activity in lung cells is inversely associated with disease severity, inflammation and airway hyperreactivity [304, 305]. Reactive molecular species such as ROS directly activate structural and immune cells to promote inflammation, but they also modify and bio-activate endogenous molecules, including phospholipids such as phosphatidylcholine, which further accentuate oxidative pathobiology [127,

306]. OxPC generation and deposition is an end-result of oxidative stress, thus they are recognized markers of persistent oxidative biology in neurodegenerative disease [295, 306, 307] and myocardial injury [156, 161]. This is also true for chronic lung disease, as we reported that OxPC accumulate in BALF from atopic human asthmatics after lung allergen challenge, and they are persistently elevated in BALF individuals who exhibit AHR [176]. Lipidomic profiling of BALF from HDM-challenge mice in the current study is, to our knowledge, the first to reveal that OxPC accumulation in the lung is a predominant feature of pre-clinical murine models of allergic asthma.

OxPC contribute to inflammation, cytotoxicity and oxidative stress through multiple mechanisms, thus have potential to be significant contributors to asthma pathobiology. They can act as damage-associated molecular patterns, activating toll-like receptors on immune cells and endothelial cells [127, 232]. They cause endothelial dysfunction, impairing nitric oxide signaling and promoting vascular permeability, properties that have been exploited to generate murine models of acute lung injury [166]. Moreover, OxPC can act as irritants that activate TRPA1, leading to calcium influx and contraction of airway smooth muscle, airway narrowing as well as neurogenic pain [165, 177]. Oxidative damage and cell membrane disruption by OxPC promote neuronal cell death pathways [207, 306, 308]. Inflammation and pro-inflammatory cytokine and chemokine production induced by OxPC is associated with NF-κB activation and complex kinase networks [166, 176, 309]. We reported that OxPC activates protein kinase C in human airway smooth muscle cells, and this is associated with cyclooxygenase-2 expression and oxylipin production [176]. Moreover, OxPC promote ROS generation, and inhibit mitochondrial metabolism and wound healing capacity in lung epithelial cells [178]. Lipid uptake, synthesis, and storage in macrophages and adipocytes is modulated by OxPC, thereby promoting lipid accumulation, foam cell formation in atherosclerotic plaques, and foamy macrophage formation in response to cigarette smoke exposure [170]. Our

new observations that neutralizing the biological activity of OxPC in the lungs of allergen challenged mice is associated with a mitigation of inflammation and lung pathophysiology are consistent with a central role for OxPC in asthma pathobiology. In addition to OxPC, other lipid peroxidation end-products such as MDA and 4-HNE are an important OSEs that also contribute to asthma pathobiology and severity [137, 310].

Commercially available E06 mAb is used for diagnostic applications to selectively detect E06-reactive OxPC in various inflammatory diseases [156, 166, 307, 311, 312]. E06 selectively binds to the phosphocholine headgroup of oxidized phospholipids and it does not interact with unoxidized phosphocholine [193, 195]. The therapeutic potential of E06 lies in its capacity to neutralize OxPC bioactivity, and there are multiple recent reports of therapeutic properties, including anti-inflammatory, -atherogenic, and -nociceptive effects, as well as promoting inflammation resolution. Examples include, decreased infarct size with intracoronary E06 in a porcine model of ischemia/reperfusion injury [158], increased macrophage uptake of oxidized lipids and lower lung inflammatory markers with intranasal E06 in cigarette smoke-exposed mice [170], and reduced OxPC-induced pain inflammation and hypersensitivity with local E06 application [164, 206]. Transgenic mice that express high levels of the single-chain variable fragment of E06 (E06-scFv, a functional E06 component responsible for binding to OxPC) in plasma are resistant to OxPC-induced inflammatory signaling in atherosclerosis, aortic stenosis, and hepatic steatosis [162]. Notably, in these mice E06-scFv is expressed in the lung, and the animals are refractory to hyperoxia-induced oxidative stress and lung inflammation [204]. Based on these prior studies, we chose to investigate effects of lung-delivered E06 mAb (at a dose that is similar to prior reports) over the course of repeated allergen challenge.

A unique observation of our work is that the inflammation-reducing effects of E06 mAb treatment is principally associated with a reduction in neutrophils and alveolar macrophages. This is consistent with known effects of OxPC on neutrophil and macrophage mediated inflammation in the lung [166, 313, 314]. OxPC effects on allergen-induced airway neutrophil and macrophage number is also consistent with the reduced levels of several pro-inflammatory cytokines in BALF, including IL-1β (produced by alveolar macrophages and airway epithelium) and Th1-cytokines (TNF and IFN-γ) [27]. We noted a declining trend of E06 mAb treatment on lung eosinophil, CD4 and CD8 lymphocyte accumulation, and this was paralleled by trends (but not statistically significant) for reduced Th2-defining (IL-4) and epithelium-derived cytokines (IL-33) [27]. IL-33 is an important marker of severe and steroid-refractory asthma [315, 316]. Our previous reports [316, 317] showed that both Th1-cytokines (TNF and IFN-γ) synergistically increases IL-33 expression and steroid fails to inhibit these effects. Interestingly in this study, E06-induced reduction of both TNF and IFN-γ correlates with a trend for IL-33 reduction suggesting unique effects of OxPC in asthma pathophysiology. Of note, IL-10, an anti-inflammatory Th2 signal that increases following HDM challenge [269, 318, 319], also shows a trend to decrease with E06 mAb treatment, an observation that may reflect the declining BALF lymphocyte counts. Overall, E06 mAb treatment shows a general inflammation suppressive effect. An important limitation of our study is that we used a predicted effective dose of E06 mAb based on prior studies with mouse models of other inflammatory diseases. As we did not have sufficient capacity to perform an extensive screen to determine an optimized dose and inhaled delivery modality, our study does not likely demonstrate the full therapeutic potential for lung-delivered E06 mAb.

Our study also assessed the impact of E06 mAb treatment of allergic inflammation associated lung dysfunction. Repeated HDM challenge results in significantly increased reactivity to Mch, as

revealed by measurement of total respiratory resistance and "tissue damping", which includes a significant component related to small airway restriction and lung stiffness. E06 mAb treatment resulted in >20% improvement in both total lung resistance and tissue damping compared to HDM challenged mice. Though not statistically significant, this is a potentially significant clinical effect, however, due to limitations in availability of the E06 mAb we were not able to perform a full dose-response study that would have enabled treatment optimization. An interesting observation is that tissue damping may be improved by E06 mAb, suggesting the potential for correcting surfactant dysfunction that may have been induced by HDM challenge [320]. As phosphatidylcholine is a major component of surfactant, this observation suggests that OxPC formation may compromise surfactant function and contribute to lung dysfunction in murine models. To address this possibility, future studies that incorporate advanced surfactometry are warranted, as this will also reveal whether any therapeutic potential of E06 mAb is associated with protective effects on lung surfactant.

Our ability to fully assess the potential magnitude that E06 therapy might hold for allergic airway pathophysiology is limited by the fact that we did not include a comparison group treated with clinically relevant doses of inhaled corticosteroids. A recent study by Lewis et al [321] reported that 3 mg/kg fluticasone propionate was not sufficient to abrogate inflammation and AHR in mice challenged with mixed allergens. Notably, they observed a 20% reduction in maximum methacholine-induced respiratory resistance, which is equal to or less than the effects of intranasal E06 in our work. They also reported a <50% decrease in CD4+ cells, which mimics the effects of E06 we report here. Interestingly they also observed that inhaled corticosteroid was without effect on the change in expression of anti-oxidant genes [321]. This suggests that oxidative stress leading to formation of OxPC may have been a feature of their allergen challenged animals, even with

corticosteroid treatment. This warrants a future study of co-treatment with corticosteroids and E06, as there appears to be potential for additive or synergistic effects. As E06 does not interact with other OSEs (MDA, 4-HNE), therefore additional effects of anti-oxidants with E06 may enhance their therapeutic benefit.

The most significant limitation of the current study relates to lack of optimization of the dose of E06 mAb we used for repetitive intranasal delivery. We used a single dose (10 µg) in a limited number of animals. E06-scFv TG mice exhibit plasma and lung E06 expression between 20-30 µg/mL [162, 204]. Testing the full therapeutic potential of exogenously delivered E06 at this concentration range is cost prohibitive. Our observations suggest that future studies are needed using E06-scFv TG mice to understand more specific requirement of OxPC in murine model of allergic asthma. E06-scFv TG mice show significantly reduced infiltration of inflammatory cells in aortas in an atherosclerosis study [162]. Thus, studying HDM effects during sustained lung expression of E06 will provide fulsome understanding of the role of OxPC in allergen-induced airway inflammation and AHR. In future, a cost-effective strategy to develop E06 as therapy would be to assess therapeutic benefit of intranasal E06-scFv synthetic peptide that specifically blocks OxPC bioactivity [162].

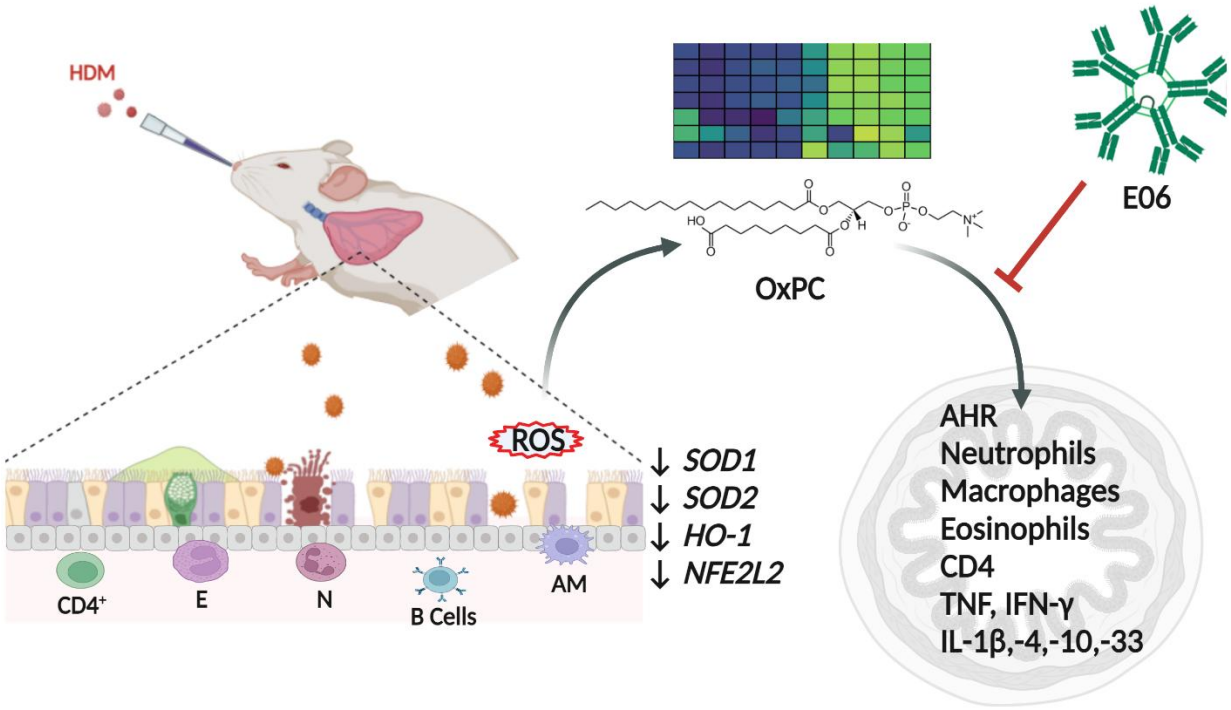

Figure 6.7: Schematic overview for role of OxPC in asthma pathobiology.
Intranasal HDM-challenge in mice causes influx of various inflammatory cells (e.g., eosinophils, neutrophils, alveolar macrophages, and CD4+ and B-lymphocytes) in the airways. This is associated with a reduction in the expression of important anti-oxidant genes (*SOD1*, *SOD2*, *HO-1*, and *NFE2L2*) in the lungs, leading to a redox imbalance that generates bioactive oxidative-stress mediators (e.g., OxPC). E06, a neutralizing antibody, can reduce classical features of airway inflammation and airway hyperresponsiveness. This implicates an important role for OxPC, oxidative-stress mediators, in allergen-induced asthma pathogenesis. Legend: HDM: House dust mite, *SOD1*: Superoxide dismutase 1, *SOD2*: Superoxide dismutase 2, *HO-1*: Heme oxygenase 1, *NFE2L2*: Nuclear factor erythroid 2-related factor 2, E: Eosinophils, N: Neutrophils, AM: Alveolar macrophages, AHR: Airway hyperresponsiveness. “Created with BioRender.com".

In summary, this is a unique study in its capacity to show that neutralizing E06 mAb can reduce airway inflammation and hyperreactivity, implicating an important role for OxPC in allergen-induced lung pathophysiology (Figure 6.7). However, further research is required to conclusively determine the therapeutic potential of E06 mAb in the context of asthma and other chronic lung diseases. A pathobiological role for OxPC is consistent with our observation that HDM challenge leads to inhibition of anti-oxidation genes, likely generating redox imbalance and oxidative stress. Indeed, OxPC accumulation in the lung itself is a biomarker for oxidative stress. Overall, this study is a steppingstone for understanding the pathophysiologic role of OxPC as mediator of oxidative stress in asthma.

Chapter 7: General Summary, Significance and Future Directions

7.1 General Summary

Collectively, the studies described in this thesis were designed to investigate the pathophysiological role of OxPC in asthma using a murine model of allergic asthma, and in particular to uncover mechanistic insights for their two functional roles in ASM pathophysiology; (1) procontractile effect on ASM that contributes to AHR, and (2) impaired β_2AR signaling in ASM that results in poor responses to frontline bronchodilator therapy. Our findings open the door for future studies to further evaluate the targeting of OxPC as a novel therapeutic approach and/or complement to conventional therapies for the treatment of asthma.

Oxidized phosphatidylcholines (OxPC) are generated during periods of oxidative stress in response to biological and chemical factors, and involved in the pathophysiology of several inflammatory diseases including those affecting the lung. Our recent groundbreaking studies link OxPC to asthma pathobiology as they accumulate in the human lung after an allergen challenge and their levels associate with the degree of AHR [176]. These findings are an important starting point in unravelling the complex role of oxidative stress effectors in asthma. Our research continued by investigating the direct impact of OxPC on airway structural cells such as ASM and epithelial cells, both of which are major drivers of asthma pathogenesis [58, 322]. ASM cells represent the principal cell determining AHR, possess immunomodulatory functions, and are subject to dysfunction in response to oxidative stress and/or its mediators [76, 323]. Epithelial cells form the epithelial barrier, which constitutes the first-line of defense against inhaled external insults in the lungs [43]. We have demonstrated that OxPC selectively induce the production of pro-inflammatory cytokines and oxylipins in ASM cells [176], and can cause multiple functional defects in epithelial cells [178]. Thus, those studies identified OxPC as important effectors of

oxidative stress in the lungs and indicated they may have a multifaceted impact in disease pathogenesis and progression.

Our preliminary work showed that OxPC can directly cause airway narrowing in murine thin-cut lung slices; this is consistent with our previous observation that OxPC levels correlate with clinically diagnosed AHR in human subjects [1]. However, the mechanisms of OxPC-induced airway contraction remained unclear at that time. This led to the studies outlines in **chapter 4**, where we investigated signaling pathways that are involved in OxPC-mediated ASM contraction. Our results indicated that OxPC directly induce elevation of intracellular Ca^{2+} in HASM cells, leading to ASM contraction and airway narrowing. OxPC mediate transient and sustained increases in cytosolic Ca^{2+} via two mutually exclusive pathways that involve intracellular RyR and plasma membrane TRPA1 channels (Figure 7.1). Interestingly, both are required for OxPC-induced airway contraction, as selective pharmacologic inhibition of either pathway is sufficient to prevent OxPC-induced ASM contraction. These novel observations uncover that OxPC can activate TRPA1 and reveal new spatiotemporal regulatory mechanisms for ASM contraction (Figure 7.1). These effects are distinct from classical GPCR pathways and are not targeted by current available therapy [8]. Of note, a small molecule TRPA1 inhibitor is currently being assessed as a new clinical therapy for allergic inflammation and bronchoconstriction [9, 10], suggesting a more central role of TRPA1 in asthma pathophysiology. Our observation that OxPC activate TRPA1 in ASM provides novel insights into the complex signaling that drives airway contraction. Although the exact interaction between OxPC and TRPA1 has not been fully explored, a recent study revealed that covalent binding to cysteine and lysine residues on the N-terminal of the channel protein is required for OxPC agonistic activity [11, 12]. Studies to unravel OxPC-TRPA1 signaling in airway fibroblasts, a different subset of airway mesenchymal cells than ASM

that also play an important role in asthma, have also been initiated. Our preliminary work indicates that OxPC-induced TRPA1 signaling is involved in pro-inflammatory gene expression by airway fibroblasts [13]. This implicates OxPC-TRPA1 signaling in multiple structural cell types of airways, which may importantly contribute to asthma pathophysiology.

β_2 adrenergic receptor (β_2AR)-agonists are a frontline therapy for relieving asthma symptoms and they principally act by relaxing ASM [92]; however, a large subgroup of patients develop desensitization or are refractory to this treatment [114, 115]. ROS has been reported to regulate β_2AR function and contribute to β_2AR insensitivity [324, 325]; however, the underlying mechanisms are incompletely understood. Thus, **chapter 5** features our studies on the impact of OxPC on β_2AR agonist-induced ASM relaxation. To this aim, we employed cultured HASM cells, *ex vivo* murine tracheal rings and thin-cut lung slices, and *in vivo* murine lung function assessment. Results using these multiple models consistently showed that OxPC selectively attenuate airway relaxation in response to β_2AR-agonists, effects that correlate with reduced cAMP signaling in HASM cells. Further mechanistic insights from this study revealed that OxPC uncouple the β_2AR from downstream signaling via PKC activation (Figure 7.1) and that is without impacting cell surface receptor levels. This body of work provides evidence that OxPC impair the bronchodilator response in ASM and, as such, may directly contribute to bronchodilator insensitivity, a common phenotype of poorly controlled asthma. Thus, our findings identify the OxPC-PKC signaling axis as an important signaling hub that not only perpetuates an inflammatory ASM phenotype [176], but also causes defective ASM relaxation.

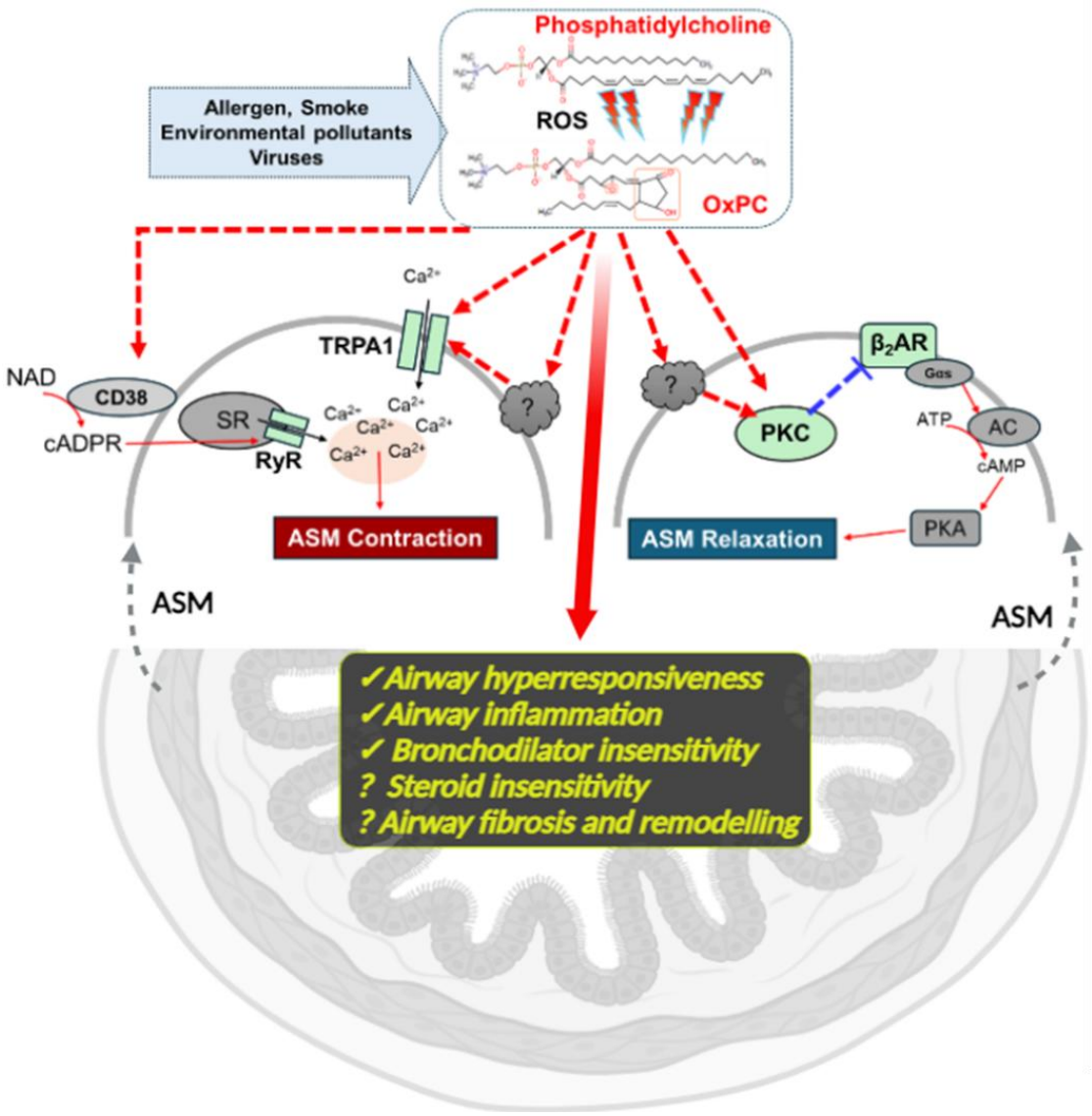

Figure 7.1: Schematic overview of the pathobiological effects of OxPC in the airways.
Various biological and chemical factors cause redox imbalance that leads to increase ROS in the lungs, which results in the oxidation of biomolecules (e.g., phosphatidylcholine) and generation of a myriad of OxPC variants. In human ASM cells, OxPC trigger concomitant but mutually exclusive activation of the RyR receptor and TRPA1 (via direct and indirect pathways) that mediates cytoplasmic Ca^{2+} flux from intra- and extracellular stores, respectively, resulting increased in intracellular Ca^{2+}. These phases of Ca^{2+} mobilization work cooperatively to induce ASM contraction and airway narrowing. OxPC can also activate PKC (via yet to be identified mechanism) that leads to inhibition of β_2AR function. This results in reduced cAMP signaling and impaired airway relaxation in response to β_2AR agonists (*e.g.*, Albuterol), providing a novel OxPC-PKC-mediated regulatory mechanism of bronchodilator insensitivity. Using a murine model of allergic asthma, we demonstrated distinct roles of OxPC (as oxidative-stress mediators) in cardinal features of asthma pathobiology. Figure 7.1 was created with BioRender.com.

Allergen-induced airway inflammation and AHR are the most common hallmarks of asthma [301, 302]. To further evaluate the pathobiological role(s) of OxPC, we used a well-established murine model of HDM-induced allergic asthma, which exhibits clinically relevant features of airway inflammation and AHR [269, 303]. The studies described in **chapter 6** demonstrate that HDM challenge causes a redox imbalance that results in an augmented oxidative burden and OxPC accumulation in the lungs. The latter corresponds with our prior observations in human asthmatics [176]. Most importantly, the profile of OxPC in the lungs of human asthmatics [299], share >90% homology with OxPC profile that is identified in HDM-challenged mice. Thus, providing the first insights about unique profile of OxPC moieties that are generated by allergen exposure. To determine the functional impact of these OxPC moieties on features of allergic asthma in our model, we subjected the mice to prophylactic treatment with E06, a natural IgM antibody that selectively neutralizes OxPC bioactivities. Intranasal administration of E06 rendered significant therapeutic benefits by significantly preventing the development of airway inflammation and small airway hyperresponsiveness. These *in vivo* findings further underline the functional importance of OxPC as mediators of oxidative stress in allergic lung pathophysiology and suggest that therapeutic interference with OxPC accumulation and/or signaling holds promise for the treatment of asthma.

7.2 Study significance and limitations

The studies described in this thesis employed *in vitro*, *ex vivo* and *in vivo* experimental approaches to provide preclinical proof-of-concept for the functional involvement of OxPC in asthma pathogenesis. We were able to conclusively demonstrate that OxPC induce ASM dysfunction. Thus, we identified signaling pathways triggered by OxPC that promote ASM contraction and impair relaxation by β_2AR-agonists (cornerstone asthma therapeutics). These are important findings as no current asthma therapies specifically target OxPC or their associated signaling pathways. This suggests that OxPC as oxidative stress mediators could offer novel tangible therapeutic target for asthma, as previous attempts to therapeutically implement broad anti-oxidant interventions were unsuccessful [121, 323, 326]. Collectively, our results suggest that specifically targeting OxPC could represent a novel approach to prevent or counteract the effects of oxidative stress in the treatment of asthma.

Although our observations are promising, we have to acknowledge the limitations of our studies that are outlined below.

- Because we used a mixture of OxPC moieties (OxPAPC) for the studies described in chapters 4 and 5, it remains unclear which specific bioactive constituent(s) of OxPC induce signaling pathway(s) in ASM cells. Identification of these moieties will favor the development of highly specific rather than broader therapeutic strategies that target OxPC.
- In chapter 4, my work also provides a need for additional mechanistic studies to identify how OxPC exposure leads to TRPA1 activation, and CD38 activation that leads to cADPR production and RyR opening, and the precise pharmacomechanical coupling mechanisms that determine a need for both TRPA1 and RyR Ca^{2+} pools to elicit contraction.

- Similarly in chapter 5, we also require additional research to identify the exact mechanisms (receptor or non-receptor) of OxPC-mediated PKC activation. In addition, assessing the specific isoform(s) of PKC involved in the inhibition of β_2AR function would provide valuable mechanistic insights. To this aim, we would consider a proteomic technique to detect specific site phosphorylation of the β2AR protein.
- It is also important to determine if any cross-talk exists between Ca^{2+} pools from TRPA1/RyR and PKC activity, as the activity of some PKC isoforms is dependent on cytoplasmic Ca^{2+} levels [327]. Such future endeavors will provide a more comprehensive understanding of the role of OxPC and associated PKC signaling in ASM dysfunction in asthma.
- The high cost of the E06 mAb limited dose optimization via intranasal delivery *in vivo* (Chapter 6). Initially, we planned to use E06-scFv TG mice for this study; these animals express sustained plasma and BALF E06 expression at concentration levels that exhibit protective effects against various inflammatory diseases [162, 204, 328]. Unfortunately, the pandemic (COVID-19)-imposed restrictions made it impossible to procure these mice. Our observations from this preclinical study suggest a strong need to study the effects of HDM challenge under conditions of sustained lung expression of E06 at higher concentrations to conclusively determine if OxPC are required for allergen-induced airway inflammation and AHR.

7.3 Future Directions

The work outlined in the thesis contributes to a growing body of evidence suggesting that OxPC, generated as the result of oxidative stress in the lung, play a pleiotropic role in allergic asthma and ASM pathophysiology. Our past and ongoing research efforts are focused on dissecting the impact of OxPC on various structural cells of the airway. Our results thus far suggest that OxPC constitute a component of persistent inflammation and AHR that prevents optimized control by conventional therapy. In this light, fully exploring the pathobiological effects of OxPC may yield some promising new avenues for future therapeutic approaches. For example, the contribution of OxPC to the development and progression of airway fibrosis and remodeling is yet to be evaluated. Our recent preliminary work showing that the OxPC-TRPA1 signaling axis is involved in pro-inflammatory gene expression in airway fibroblast is encouraging in this regard [329]. Importantly, OxPC accumulation is also evident to associate with inflammation in murine model of lung fibrosis and that OxPC-neutralizing E06 antibody improves survival and reduces fibrosis [328, 330]. These observations are in line with the demonstrated therapeutic efficacy of CAL102 (Calluna Pharma), another mAb targeting oxidized phospholipids, in several preclinical disease models of inflammation and fibrosis. Collectively, these data suggest that OxPC could indeed be involved in driving airway fibrosis and remodeling in asthma.

Furthermore, oxidative stress is strongly linked to corticosteroid insensitivity in asthma [122], which is the mainstay controller therapy for asthma. The impact of OxPC as mediators of oxidative stress on steroid insensitivity is unknown. Our next groundbreaking collaborative research programs have already begun to assess this potential impact. Our pivotal work shows that OxPC are sufficient to selectively inhibit glucocorticoid receptor function in airway epithelial cells *in*

vitro, suggesting a role for OxPC in the development of steroid resistance and persistent inflammation [331].

Overall, data presented in this thesis indicate a multifaceted impact of OxPC on key features of allergic asthma. In addition, our studies pave the way for further pre-clinical and clinical investigations on the therapeutic benefits of targeting OxPC (*e.g.*, E06 mAb) for the treatment of chronic inflammatory diseases such as asthma that are characterized by oxidative stress.

Chapter 8: References

1. Erle, D.J. and D. Sheppard, The cell biology of asthma. J Cell Biol, 2014. 205(5): p. 621-31.

2. Sakula, A., Sir John Floyer's A Treatise of the Asthma (1698). Thorax, 1984. 39(4): p. 248-54.

3. Salter, H., On Asthma: Its Pathology and Treatment. 1860, London: John Churchill.

4. Osler, W., The principles and practice of medicine. 1912: D. Appleton and Company.

5. Pavord, I.D., et al., After asthma: redefining airways diseases. Lancet, 2018. 391(10118): p. 350-400.

6. Global Initiative for Asthma. Global strategy for asthma management and prevention. Updated July 2023. Available from www.ginasthma.org. 2023.

7. Collaborators, G.C.R.D., Global burden of chronic respiratory diseases and risk factors, 1990-2019: an update from the Global Burden of Disease Study 2019. EClinicalMedicine, 2023. 59: p. 101936.

8. Shin, Y.H., et al., Global, regional, and national burden of allergic disorders and their risk factors in 204 countries and territories, from 1990 to 2019: A systematic analysis for the Global Burden of Disease Study 2019. Allergy, 2023. 78(8): p. 2232-2254.

9. Asher, M.I., et al., Worldwide trends in the burden of asthma symptoms in school-aged children: Global Asthma Network Phase I cross-sectional study. Lancet, 2021. 398(10311): p. 1569-1580.

10. Ellwood, P., et al., Global Asthma Network Phase I Surveillance: Geographical Coverage and Response Rates. J Clin Med, 2020. 9(11).

11. To, T., et al., Global asthma prevalence in adults: findings from the cross-sectional world health survey. BMC Public Health, 2012. 12: p. 204.

12. Loerbroks, A., et al., Reports of wheezing and of diagnosed asthma are associated with impaired social functioning: Secondary analysis of the cross-sectional World Health Survey data. J Psychosom Res, 2018. 105: p. 52-57.

13. Yaghoubi, M., et al., The Projected Economic and Health Burden of Uncontrolled Asthma in the United States. Am J Respir Crit Care Med, 2019. 200(9): p. 1102-1112.

14. Nurmagambetov, T., R. Kuwahara, and P. Garbe, The Economic Burden of Asthma in the United States, 2008-2013. Ann Am Thorac Soc, 2018. 15(3): p. 348-356.

15. Czira, A., et al., A systematic literature review of burden of illness in adults with uncontrolled moderate/severe asthma. Respir Med, 2022. 191: p. 106670.

16. Canada, A., Breathe Easy. 2016.

17. Mendez-Enriquez, E. and J. Hallgren, Mast Cells and Their Progenitors in Allergic Asthma. Front Immunol, 2019. 10: p. 821.

18. Mitchell, P.D. and P.M. O'Byrne, Epithelial-Derived Cytokines in Asthma. Chest, 2017. 151(6): p. 1338-1344.

19. Fahy, J.V., Type 2 inflammation in asthma--present in most, absent in many. Nat Rev Immunol, 2015. 15(1): p. 57-65.

20. Lambrecht, B.N., H. Hammad, and J.V. Fahy, The Cytokines of Asthma. Immunity, 2019. 50(4): p. 975-991.

21. Takatsu, K. and H. Nakajima, IL-5 and eosinophilia. Curr Opin Immunol, 2008. 20(3): p. 288-94.

22. Kashiwada, M., et al., IL-4-induced transcription factor NFIL3/E4BP4 controls IgE class switching. Proc Natl Acad Sci U S A, 2010. 107(2): p. 821-6.

23. Poulsen, L.K. and L. Hummelshoj, Triggers of IgE class switching and allergy development. Ann Med, 2007. 39(6): p. 440-56.

24. McBrien, C.N. and A. Menzies-Gow, The Biology of Eosinophils and Their Role in Asthma. Front Med (Lausanne), 2017. 4: p. 93.

25. Choi, Y., et al., Eosinophil extracellular traps activate type 2 innate lymphoid cells through stimulating airway epithelium in severe asthma. Allergy, 2020. 75(1): p. 95-103.

26. Lambrecht, B.N. and H. Hammad, The immunology of asthma. Nat Immunol, 2015. 16(1): p. 45-56.

27. Hammad, H. and B.N. Lambrecht, The basic immunology of asthma. Cell, 2021. 184(6): p. 1469-1485.

28. Persson, E.K., et al., Protein crystallization promotes type 2 immunity and is reversible by antibody treatment. Science, 2019. 364(6442).

29. Svenningsen, S. and P. Nair, Persistent Airway Plugs: A Call for Clinical Recognition and Novel Therapies. Am J Respir Crit Care Med, 2022. 205(9): p. 977-978.

30. Wenzel, S.E., et al., Evidence that severe asthma can be divided pathologically into two inflammatory subtypes with distinct physiologic and clinical characteristics. Am J Respir Crit Care Med, 1999. 160(3): p. 1001-8.

31. Gibson, P.G., J.L. Simpson, and N. Saltos, Heterogeneity of airway inflammation in persistent asthma : evidence of neutrophilic inflammation and increased sputum interleukin-8. Chest, 2001. 119(5): p. 1329-36.

32. Wadsworth, S., D. Sin, and D. Dorscheid, Clinical update on the use of biomarkers of airway inflammation in the management of asthma. J Asthma Allergy, 2011. 4: p. 77-86.

33. Jeffery, P.K., et al., Bronchial biopsies in asthma. An ultrastructural, quantitative study and correlation with hyperreactivity. Am Rev Respir Dis, 1989. 140(6): p. 1745-53.

34. Drazen, J.M. and J.J. Fredberg, Epithelial cells crowded out in asthma. Science, 2024. 384(6691): p. 30-31.

35. Varricchi, G., et al., Airway remodelling in asthma and the epithelium: on the edge of a new era. Eur Respir J, 2024. 63(4).

36. Ordoñez, C.L., et al., Mild and moderate asthma is associated with airway goblet cell hyperplasia and abnormalities in mucin gene expression. Am J Respir Crit Care Med, 2001. 163(2): p. 517-23.

37. Ward, C., et al., Airway inflammation, basement membrane thickening and bronchial hyperresponsiveness in asthma. Thorax, 2002. 57(4): p. 309-16.

38. Roche, W.R., et al., Subepithelial fibrosis in the bronchi of asthmatics. Lancet, 1989. 1(8637): p. 520-4.

39. Burgess, J.K., et al., The extracellular matrix - the under-recognized element in lung disease? J Pathol, 2016. 240(4): p. 397-409.

40. Ito, J.T., et al., Extracellular Matrix Component Remodeling in Respiratory Diseases: What Has Been Found in Clinical and Experimental Studies? Cells, 2019. 8(4).

41. Ebina, M., et al., Cellular hypertrophy and hyperplasia of airway smooth muscles underlying bronchial asthma. A 3-D morphometric study. Am Rev Respir Dis, 1993. 148(3): p. 720-6.

42. James, A.L., et al., Airway Smooth Muscle Hypertrophy and Hyperplasia in Asthma. American Journal of Respiratory and Critical Care Medicine, 2012. 185(10): p. 1058-1064.

43. Heijink, I.H., et al., Epithelial cell dysfunction, a major driver of asthma development. Allergy, 2020. 75(8): p. 1902-1917.

44. Carroll, N., et al., The structure of large and small airways in nonfatal and fatal asthma. Am Rev Respir Dis, 1993. 147(2): p. 405-10.

45. James, A.L., P.D. Paré, and J.C. Hogg, The mechanics of airway narrowing in asthma. Am Rev Respir Dis, 1989. 139(1): p. 242-6.

46. Xiao, C., et al., Defective epithelial barrier function in asthma. J Allergy Clin Immunol, 2011. 128(3): p. 549-56.e1-12.

47. de Boer, W.I., et al., Altered expression of epithelial junctional proteins in atopic asthma: possible role in inflammation. Can J Physiol Pharmacol, 2008. 86(3): p. 105-12.

48. Barbato, A., et al., Epithelial damage and angiogenesis in the airways of children with asthma. Am J Respir Crit Care Med, 2006. 174(9): p. 975-81.

49. Turner, J., et al., Goblet cells are derived from a FOXJ1-expressing progenitor in a human airway epithelium. Am J Respir Cell Mol Biol, 2011. 44(3): p. 276-84.

50. Schmidt, H., et al., IL-13 Impairs Tight Junctions in Airway Epithelia. Int J Mol Sci, 2019. 20(13).

51. Boxall, C., S.T. Holgate, and D.E. Davies, The contribution of transforming growth factor-beta and epidermal growth factor signalling to airway remodelling in chronic asthma. Eur Respir J, 2006. 27(1): p. 208-29.

52. Halwani, R., et al., Role of Transforming Growth Factor–β in Airway Remodeling in Asthma. American Journal of Respiratory Cell and Molecular Biology, 2011. 44(2): p. 127-133.

53. Stewart, A., More Muscle in Asthma, but Where Did It Come From? American Journal of Respiratory and Critical Care Medicine, 2012. 185(10): p. 1035-1037.

54. O'Byrne, P.M. and M.D. Inman, Airway hyperresponsiveness. Chest, 2003. 123(3 Suppl): p. 411S-6S.

55. Cockcroft, D.W., Direct challenge tests: Airway hyperresponsiveness in asthma: its measurement and clinical significance. Chest, 2010. 138(2 Suppl): p. 18S-24S.

56. Cockcroft, D.W. and B.E. Davis, Mechanisms of airway hyperresponsiveness. J Allergy Clin Immunol, 2006. 118(3): p. 551-9; quiz 560-1.

57. Hargreave, F.E., et al., The origin of airway hyperresponsiveness. J Allergy Clin Immunol, 1986. 78(5 Pt 1): p. 825-32.

58. An, S.S., et al., Airway smooth muscle dynamics: a common pathway of airway obstruction in asthma. Eur Respir J, 2007. 29(5): p. 834-60.

59. Chapman, D.G. and C.G. Irvin, Mechanisms of airway hyper-responsiveness in asthma: the past, present and yet to come. Clin Exp Allergy, 2015. 45(4): p. 706-19.

60. Wiggs, B.R., et al., On the mechanism of mucosal folding in normal and asthmatic airways. Journal of Applied Physiology, 1997. 83(6): p. 1814-1821.

61. Lambert, R.K., et al., Functional significance of increased airway smooth muscle in asthma and COPD. J Appl Physiol (1985), 1993. 74(6): p. 2771-81.

62. Slats, A.M., et al., Expression of smooth muscle and extracellular matrix proteins in relation to airway function in asthma. J Allergy Clin Immunol, 2008. 121(5): p. 1196-202.

63. Ma, X., et al., Changes in biophysical and biochemical properties of single bronchial smooth muscle cells from asthmatic subjects. Am J Physiol Lung Cell Mol Physiol, 2002. 283(6): p. L1181-9.

64. Jiang, H., et al., Bronchial smooth muscle mechanics of a canine model of allergic airway hyperresponsiveness. J Appl Physiol (1985), 1992. 72(1): p. 39-45.

65. Finucane, K.E. and H.J. Colebatch, Elastic behavior of the lung in patients with airway obstruction. J Appl Physiol, 1969. 26(3): p. 330-8.

66. Macklem, P.T., A theoretical analysis of the effect of airway smooth muscle load on airway narrowing. American Journal of Respiratory and Critical Care Medicine, 1996. 153(1): p. 83-89.

67. Chen, H., et al., TNF-[alpha] modulates murine tracheal rings responsiveness to G-protein-coupled receptor agonists and KCl. J Appl Physiol (1985), 2003. 95(2): p. 864-72; discussion 863.

68. Tliba, O., et al., IL-13 enhances agonist-evoked calcium signals and contractile responses in airway smooth muscle. Br J Pharmacol, 2003. 140(7): p. 1159-62.

69. Perkins, C., et al., Selective stimulation of IL-4 receptor on smooth muscle induces airway hyperresponsiveness in mice. J Exp Med, 2011. 208(4): p. 853-67.

70. Brightling, C.E., et al., Mast-cell infiltration of airway smooth muscle in asthma. N Engl J Med, 2002. 346(22): p. 1699-705.

71. Drake, M.G., et al., Eosinophils increase airway sensory nerve density in mice and in human asthma. Sci Transl Med, 2018. 10(457).

72. Zhou, J., et al., Local small airway epithelial injury induces global smooth muscle contraction and airway constriction. J Appl Physiol (1985), 2012. 112(4): p. 627-37.

73. Sterk, P. and E. Bel, Bronchial hyperresponsiveness: the need for a distinction between hypersensitivity and excessive airway narrowing. European Respiratory Journal, 1989. 2(3): p. 267-274.

74. Mitzner, W., Airway smooth muscle: the appendix of the lung. Am J Respir Crit Care Med, 2004. 169(7): p. 787-90.

75. Tan, L.D., et al., Bronchial Thermoplasty: A Decade of Experience: State of the Art. J Allergy Clin Immunol Pract, 2019. 7(1): p. 71-80.

76. Bourke, J.E., et al., Smooth Muscle Cells☆, in Encyclopedia of Respiratory Medicine (Second Edition), S.M. Janes, Editor. 2022, Academic Press: Oxford. p. 37-51.

77. Sanders, K.M., Invited review: mechanisms of calcium handling in smooth muscles. J Appl Physiol (1985), 2001. 91(3): p. 1438-49.

78. Billington, C.K. and R.B. Penn, Signaling and regulation of G protein-coupled receptors in airway smooth muscle. Respir Res, 2003. 4: p. 2.

79. Wright, D.B., et al., Regulation of GPCR-mediated smooth muscle contraction: implications for asthma and pulmonary hypertension. Pulm Pharmacol Ther, 2013. 26(1): p. 121-31.

80. Pozzan, T., et al., Molecular and cellular physiology of intracellular calcium stores. Physiological Reviews, 1994. 74(3): p. 595-636.

81. Chen, J. and M.J. Sanderson, Store-operated calcium entry is required for sustained contraction and Ca(2+) oscillations of airway smooth muscle. J Physiol, 2017. 595(10): p. 3203-3218.

82. Koopmans, T., et al., Ca2+ handling and sensitivity in airway smooth muscle: emerging concepts for mechanistic understanding and therapeutic targeting. Pulm Pharmacol Ther, 2014. 29(2): p. 108-20.

83. Anaparti, V., et al., NMDA receptors mediate contractile responses in human airway smooth muscle cells. Am J Physiol Lung Cell Mol Physiol, 2015. 308(12): p. L1253-64.

84. Prakash, Y.S., et al., Role of cyclic ADP-ribose in the regulation of [Ca2+]i in porcine tracheal smooth muscle. Am J Physiol, 1998. 274(6): p. C1653-60.

85. Seow, C.Y., An introduction to smooth muscle mechanics. 2020: Cambridge Scholars Publishing.

86. Chiba, Y. and M. Misawa, The role of RhoA-mediated Ca2+ sensitization of bronchial smooth muscle contraction in airway hyperresponsiveness. J Smooth Muscle Res, 2004. 40(4-5): p. 155-67.

87. Kitazawa, T., et al., Agonists trigger G protein-mediated activation of the CPI-17 inhibitor phosphoprotein of myosin light chain phosphatase to enhance vascular smooth muscle contractility. J Biol Chem, 2000. 275(14): p. 9897-900.

88. Yasuda, Y., et al., Rho-Kinase Inhibition of Active Force and Passive Tension in Airway Smooth Muscle: A Strategy for Treating Airway Hyperresponsiveness in Asthma. Biology, 2024. 13(2): p. 115.

89. Schaafsma, D., et al., Inhalation of the Rho-kinase inhibitor Y-27632 reverses allergen-induced airway hyperresponsiveness after the early and late asthmatic reaction. Respir Res, 2006. 7(1): p. 121.

90. Sassone-Corsi, P., The cyclic AMP pathway. Cold Spring Harb Perspect Biol, 2012. 4(12).

91. Pera, T. and R.B. Penn, Bronchoprotection and bronchorelaxation in asthma: New targets, and new ways to target the old ones. Pharmacol Ther, 2016. 164: p. 82-96.

92. Billington, C.K., R.B. Penn, and I.P. Hall, beta2 Agonists. Handb Exp Pharmacol, 2017. 237: p. 23-40.

93. Liu, G., et al., Assembly of a Ca2+-dependent BK channel signaling complex by binding to beta2 adrenergic receptor. Embo j, 2004. 23(11): p. 2196-205.

94. Xiong, D.J.P., J.G. Martin, and A.M. Lauzon, Airway smooth muscle function in asthma. Front Physiol, 2022. 13: p. 993406.

95. Yang, C.L., et al., Canadian Thoracic Society 2021 Guideline update: Diagnosis and management of asthma in preschoolers, children and adults. Canadian Journal of Respiratory, Critical Care, and Sleep Medicine, 2021. 5(6): p. 348-361.

96. FitzGerald, J.M., et al., Recognition and management of severe asthma: A Canadian Thoracic Society position statement. Canadian Journal of Respiratory, Critical Care, and Sleep Medicine, 2017. 1(4): p. 199-221.

97. Walters, E.H., J.A. Walters, and P.W. Gibson, Regular treatment with long acting beta agonists versus daily regular treatment with short acting beta agonists in adults and children with stable asthma. Cochrane Database Syst Rev, 2002. 2002(4): p. Cd003901.

98. Nwaru, B.I., et al., Overuse of short-acting β₂-agonists in asthma is associated with increased risk of exacerbation and mortality: a nationwide cohort study of the global SABINA programme. European Respiratory Journal, 2020. 55(4): p. 1901872.

99. McIvor, E.R. and R.A. McIvor, The evolving role of tiotropium in asthma. J Asthma Allergy, 2017. 10: p. 231-236.

100. Barnes, P.J., Inhaled Corticosteroids. Pharmaceuticals (Basel), 2010. 3(3): p. 514-540.

101. Chauhan, B.F. and F.M. Ducharme, Anti-leukotriene agents compared to inhaled corticosteroids in the management of recurrent and/or chronic asthma in adults and children. Cochrane Database Syst Rev, 2012. 2012(5): p. Cd002314.

102. Zazzali, J.L., et al., Risk of corticosteroid-related adverse events in asthma patients with high oral corticosteroid use. Allergy Asthma Proc, 2015. 36(4): p. 268-74.

103. Fajt, M.L. and S.E. Wenzel, Asthma phenotypes and the use of biologic medications in asthma and allergic disease: the next steps toward personalized care. J Allergy Clin Immunol, 2015. 135(2): p. 299-310; quiz 311.

104. Castro, M., et al., Dupilumab Efficacy and Safety in Moderate-to-Severe Uncontrolled Asthma. New England Journal of Medicine, 2018. 378(26): p. 2486-2496.

105. O'Byrne, P.M., et al., Development of an inhaled anti-TSLP therapy for asthma. Pulm Pharmacol Ther, 2023. 78: p. 102184.

106. Johnston, S.L., Macrolide antibiotics and asthma treatment. J Allergy Clin Immunol, 2006. 117(6): p. 1233-6.

107. Miller, J.D., et al., A prospective feasibility study of bronchial thermoplasty in the human airway. Chest, 2005. 127(6): p. 1999-2006.

108. Chung, K.F., et al., International ERS/ATS guidelines on definition, evaluation and treatment of severe asthma. Eur Respir J, 2014. 43(2): p. 343-73.

109. Barnes, P.J., Scientific rationale for inhaled combination therapy with long-acting beta2-agonists and corticosteroids. Eur Respir J, 2002. 19(1): p. 182-91.

110. Park, H.J., et al., Comparative efficacy of inhalers in mild-to-moderate asthma: systematic review and network meta-analysis. Sci Rep, 2022. 12(1): p. 5949.

111. McGrath, K.W., et al., A large subgroup of mild-to-moderate asthma is persistently noneosinophilic. Am J Respir Crit Care Med, 2012. 185(6): p. 612-9.

112. Woodruff, P.G., et al., T-helper type 2-driven inflammation defines major subphenotypes of asthma. Am J Respir Crit Care Med, 2009. 180(5): p. 388-95.

113. Tan, R., et al., Promises and challenges of biologics for severe asthma. Biochemical Pharmacology, 2020. 179: p. 114012.

114. Peters, S.P., et al., Real-world Evaluation of Asthma Control and Treatment (REACT): findings from a national Web-based survey. J Allergy Clin Immunol, 2007. 119(6): p. 1454-61.

115. Liu, L., et al., Reduced bronchodilator reversibility correlates with non-type 2 high asthma and future exacerbations: A prospective cohort study. Respir Med, 2022. 200: p. 106924.

116. Yawn, B.P., Factors accounting for asthma variability: achieving optimal symptom control for individual patients. Prim Care Respir J, 2008. 17(3): p. 138-47.

117. Penn, R.B., R.A. Bond, and J.K. Walker, GPCRs and arrestins in airways: implications for asthma. Handb Exp Pharmacol, 2014. 219: p. 387-403.

118. Yim, R.P. and A.C. Koumbourlis, Tolerance & resistance to β_2-agonist bronchodilators. Paediatr Respir Rev, 2013. 14(3): p. 195-8.

119. Matsunaga, K., et al., Progression of Irreversible Airflow Limitation in Asthma: Correlation with Severe Exacerbations. J Allergy Clin Immunol Pract, 2015. 3(5): p. 759-64.e1.

120. Durrani, S.R., R.K. Viswanathan, and W.W. Busse, What effect does asthma treatment have on airway remodeling? Current perspectives. J Allergy Clin Immunol, 2011. 128(3): p. 439-48; quiz 449-50.

121. Sahiner, U.M., et al., Oxidative stress in asthma. World Allergy Organ J, 2011. 4(10): p. 151-8.

122. Lewis, B.W., et al., Oxidative Stress Promotes Corticosteroid Insensitivity in Asthma and COPD. Antioxidants (Basel), 2021. 10(9).

123. Pizzino, G., et al., Oxidative Stress: Harms and Benefits for Human Health. Oxid Med Cell Longev, 2017. 2017: p. 8416763.

124. Bayr, H., Reactive oxygen species. Critical Care Medicine, 2005. 33(12).

125. Juan, C.A., et al., The Chemistry of Reactive Oxygen Species (ROS) Revisited: Outlining Their Role in Biological Macromolecules (DNA, Lipids and Proteins) and Induced Pathologies. Int J Mol Sci, 2021. 22(9).

126. Liguori, I., et al., Oxidative stress, aging, and diseases. Clin Interv Aging, 2018. 13: p. 757-772.

127. Binder, C.J., N. Papac-Milicevic, and J.L. Witztum, Innate sensing of oxidation-specific epitopes in health and disease. Nat Rev Immunol, 2016. 16(8): p. 485-97.

128. Alic, L., C.J. Binder, and N. Papac-Milicevic, The OSE complotype and its clinical potential. Front Immunol, 2022. 13: p. 1010893.

129. Erzurum, S.C., New Insights in Oxidant Biology in Asthma. Ann Am Thorac Soc, 2016. 13 Suppl 1: p. S35-9.

130. Al-Harbi, N.O., et al., Oxidative airway inflammation leads to systemic and vascular oxidative stress in a murine model of allergic asthma. Int Immunopharmacol, 2015. 26(1): p. 237-45.

131. Mishra, V., J. Banga, and P. Silveyra, Oxidative stress and cellular pathways of asthma and inflammation: Therapeutic strategies and pharmacological targets. Pharmacol Ther, 2018. 181: p. 169-182.

132. Kleniewska, P. and R. Pawliczak, The participation of oxidative stress in the pathogenesis of bronchial asthma. Biomed Pharmacother, 2017. 94: p. 100-108.

133. Aldakheel, F.M., et al., Relationships between adult asthma and oxidative stress markers and pH in exhaled breath condensate: a systematic review. Allergy, 2016. 71(6): p. 741-57.

134. Wood, L.G., P.G. Gibson, and M.L. Garg, Biomarkers of lipid peroxidation, airway inflammation and asthma. European Respiratory Journal, 2003. 21(1): p. 177-186.

135. Wang, Z., et al., Urinary total conjugated 3-bromotyrosine, asthma severity, and exacerbation risk. Am J Physiol Lung Cell Mol Physiol, 2022. 323(5): p. L548-l557.

136. Hanazawa, T., S.A. Kharitonov, and P.J. Barnes, Increased nitrotyrosine in exhaled breath condensate of patients with asthma. Am J Respir Crit Care Med, 2000. 162(4 Pt 1): p. 1273-6.

137. Pascoe, C.D., J. Vaghasiya, and A.J. Halayko, Oxidation specific epitopes in asthma: New possibilities for treatment. Int J Biochem Cell Biol, 2020. 129: p. 105864.

138. Gibellini, F. and T.K. Smith, The Kennedy pathway--De novo synthesis of phosphatidylethanolamine and phosphatidylcholine. IUBMB Life, 2010. 62(6): p. 414-28.

139. Cole, L.K., J.E. Vance, and D.E. Vance, Phosphatidylcholine biosynthesis and lipoprotein metabolism. Biochim Biophys Acta, 2012. 1821(5): p. 754-61.

140. Han, S. and R.K. Mallampalli, The Role of Surfactant in Lung Disease and Host Defense against Pulmonary Infections. Ann Am Thorac Soc, 2015. 12(5): p. 765-74.

141. Bochkov, V.N., et al., Generation and biological activities of oxidized phospholipids. Antioxid Redox Signal, 2010. 12(8): p. 1009-59.

142. Yin, H., L. Xu, and N.A. Porter, Free radical lipid peroxidation: mechanisms and analysis. Chem Rev, 2011. 111(10): p. 5944-72.

143. Leibundgut, G., et al., Determinants of binding of oxidized phospholipids on apolipoprotein (a) and lipoprotein (a). J Lipid Res, 2013. 54(10): p. 2815-30.

144. Solati, Z. and A. Ravandi, Lipidomics of Bioactive Lipids in Acute Coronary Syndromes. Int J Mol Sci, 2019. 20(5).

145. Bochkov, V., et al., Pleiotropic effects of oxidized phospholipids. Free Radical Biology and Medicine, 2017. 111: p. 6-24.

146. Stamenkovic, A., G.N. Pierce, and A. Ravandi, Oxidized lipids: not just another brick in the wall (1). Can J Physiol Pharmacol, 2019. 97(6): p. 473-485.

147. Karki, P. and K.G. Birukov, Oxidized Phospholipids in Healthy and Diseased Lung Endothelium. Cells, 2020. 9(4): p. 981.

148. Oskolkova, O.V., et al., Oxidized phospholipids are biomarkers, drug targets, and drug leads. Frontiers in Drug Discovery, 2022. 2.

149. Dong, Y. and V.W. Yong, Oxidized phospholipids as novel mediators of neurodegeneration. Trends in Neurosciences, 2022. 45(6): p. 419-429.

150. Oehler, B., et al., Pain Control by Targeting Oxidized Phospholipids: Functions, Mechanisms, Perspectives. Front Endocrinol (Lausanne), 2020. 11: p. 613868.

151. Morissette, M.C., et al., Disruption of pulmonary lipid homeostasis drives cigarette smoke-induced lung inflammation in mice. European Respiratory Journal, 2015. 46(5): p. 1451-1460.

152. Podrez, E.A., et al., A novel family of atherogenic oxidized phospholipids promotes macrophage foam cell formation via the scavenger receptor CD36 and is enriched in atherosclerotic lesions. J Biol Chem, 2002. 277(41): p. 38517-23.

153. Podrez, E.A., et al., Identification of a novel family of oxidized phospholipids that serve as ligands for the macrophage scavenger receptor CD36. J Biol Chem, 2002. 277(41): p. 38503-16.

154. Moore, K.J., F.J. Sheedy, and E.A. Fisher, Macrophages in atherosclerosis: a dynamic balance. Nat Rev Immunol, 2013. 13(10): p. 709-21.

155. Solati, Z., et al., Increase in Plasma Oxidized Phosphatidylcholines (OxPCs) in Patients Presenting With ST-Elevation Myocardial Infarction (STEMI). Front Med (Lausanne), 2021. 8: p. 716944.

156. Ravandi, A., et al., Release and capture of bioactive oxidized phospholipids and oxidized cholesteryl esters during percutaneous coronary and peripheral arterial interventions in humans. J Am Coll Cardiol, 2014. 63(19): p. 1961-71.

157. Yeang, C., et al., Reduction of myocardial ischaemia-reperfusion injury by inactivating oxidized phospholipids. Cardiovasc Res, 2019. 115(1): p. 179-189.

158. Stamenkovic, A., et al., Abstract 12366: Intracoronary Delivery of E06 Antibody Directed to Oxidized Phospholipids Decreases Infarct Size in a Porcine Model of Ischemia/Reperfusion Injury. Circulation, 2021. 144(Suppl_1): p. A12366-A12366.

159. Kiechl, S., et al., Oxidized phospholipids, lipoprotein(a), lipoprotein-associated phospholipase A2 activity, and 10-year cardiovascular outcomes: prospective results from the Bruneck study. Arterioscler Thromb Vasc Biol, 2007. 27(8): p. 1788-95.

160. Tsimikas, S., et al., Oxidation-specific biomarkers, prospective 15-year cardiovascular and stroke outcomes, and net reclassification of cardiovascular events. J Am Coll Cardiol, 2012. 60(21): p. 2218-29.

161. Solati, Z., et al., Oxidized phosphatidylcholines are produced in renal ischemia reperfusion injury. PLOS ONE, 2018. 13(4): p. e0195172.

162. Que, X., et al., Oxidized phospholipids are proinflammatory and proatherogenic in hypercholesterolaemic mice. Nature, 2018. 558(7709): p. 301-306.

163. Qin, J., et al., Oxidized phosphatidylcholine is a marker for neuroinflammation in multiple sclerosis brain. J Neurosci Res, 2007. 85(5): p. 977-84.

164. Oehler, B., et al., Inflammatory pain control by blocking oxidized phospholipid-mediated TRP channel activation. Scientific Reports, 2017. 7.

165. Liu, B., et al., Oxidized Phospholipid OxPAPC Activates TRPA1 and Contributes to Chronic Inflammatory Pain in Mice. PLoS One, 2016. 11(11): p. e0165200.

166. Imai, Y., et al., Identification of oxidative stress and Toll-like receptor 4 signaling as a key pathway of acute lung injury. Cell, 2008. 133(2): p. 235-49.

167. Akpınar, S., et al., The role of oxidized phospholipids in COVID-19-associated hypercoagulopathy. Eur Rev Med Pharmacol Sci, 2021. 25(16): p. 5304-5309.

168. Ke, Y., et al., Elevated truncated oxidized phospholipids as a factor exacerbating ALI in the aging lungs. FASEB J, 2019. 33(3): p. 3887-3900.

169. Ryu, M., et al., Oxidized Phosphatidylcholine in Human Airways Upon Exposure to Allergen and/or Diesel Exhaust. Am J Respir Crit Care Med, 2017. 195: p. A6834-A6834.

170. Thayaparan, D., et al., Induction of pulmonary antibodies against oxidized lipids in mice exposed to cigarette smoke. Respir Res, 2016. 17(1): p. 97.

171. Romero, F., et al., A pneumocyte-macrophage paracrine lipid axis drives the lung toward fibrosis. Am J Respir Cell Mol Biol, 2015. 53(1): p. 74-86.

172. Hou, X., et al., Lipid Uptake by Alveolar Macrophages Drives Fibrotic Responses to Silica Dust. Sci Rep, 2019. 9(1): p. 399.

173. Kwak, D., et al., CD36/Lyn kinase interactions within macrophages promotes pulmonary fibrosis in response to oxidized phospholipid. Respir Res, 2023. 24(1): p. 314.

174. Venosa, A., et al., Regulation of Macrophage Foam Cell Formation During Nitrogen Mustard (NM)-Induced Pulmonary Fibrosis by Lung Lipids. Toxicological Sciences, 2019. 172(2): p. 344-358.

175. Godzien, J., et al., Exploration of oxidized phosphocholine profile in non-small-cell lung cancer. Front Mol Biosci, 2023. 10: p. 1279645.

176. Pascoe, C.D., et al., Allergen inhalation generates pro-inflammatory oxidised phosphatidylcholine associated with airway dysfunction. European Respiratory Journal, 2021. 57(2): p. 2000839.

177. Vaghasiya, J., et al., Oxidized Phosphatidylcholines Trigger TRPA1 and Ryanodine Receptor Dependent Airway Smooth Muscle Contraction. Am J Respir Cell Mol Biol, 2023.

178. Pascoe, C.D., et al., Oxidized phosphatidylcholines induce multiple functional defects in airway epithelial cells. Am J Physiol Lung Cell Mol Physiol, 2021. 321(4): p. L703-L717.

179. Li, X.M., et al., Conformation of an endogenous ligand in a membrane bilayer for the macrophage scavenger receptor CD36. Biochemistry, 2007. 46(17): p. 5009-17.

180. Greenberg, M.E., et al., The lipid whisker model of the structure of oxidized cell membranes. J Biol Chem, 2008. 283(4): p. 2385-96.

181. Stremler, K.E., et al., An oxidized derivative of phosphatidylcholine is a substrate for the platelet-activating factor acetylhydrolase from human plasma. J Biol Chem, 1989. 264(10): p. 5331-4.

182. Stremler, K.E., et al., Human plasma platelet-activating factor acetylhydrolase. Oxidatively fragmented phospholipids as substrates. J Biol Chem, 1991. 266(17): p. 11095-103.

183. Dennis, E.A., et al., Phospholipase A2 enzymes: physical structure, biological function, disease implication, chemical inhibition, and therapeutic intervention. Chem Rev, 2011. 111(10): p. 6130-85.

184. Burke, J.E. and E.A. Dennis, Phospholipase A2 structure/function, mechanism, and signaling. J Lipid Res, 2009. 50 Suppl(Suppl): p. S237-42.

185. Endo, Y., M. Fujita, and K. Ikewaki, HDL Functions—Current Status and Future Perspectives. Biomolecules, 2023. 13(1): p. 105.

186. Emert, B., et al., HDL inhibits the effects of oxidized phospholipids on endothelial cell gene expression via multiple mechanisms. J Lipid Res, 2014. 55(8): p. 1678-92.

187. Navab, M., et al., A cell-free assay for detecting HDL that is dysfunctional in preventing the formation of or inactivating oxidized phospholipids. J Lipid Res, 2001. 42(8): p. 1308-17.

188. Brites, F., et al., Antioxidative activity of high-density lipoprotein (HDL): Mechanistic insights into potential clinical benefit. BBA Clin, 2017. 8: p. 66-77.

189. Mastorikou, M., M. Mackness, and B. Mackness, Defective metabolism of oxidized phospholipid by HDL from people with type 2 diabetes. Diabetes, 2006. 55(11): p. 3099-103.

190. Wolska, A., et al., Apolipoprotein Mimetic Peptides: Potential New Therapies for Cardiovascular Diseases. Cells, 2021. 10(3).

191. Van Lenten, B.J., et al., Anti-inflammatory apoA-I-mimetic peptides bind oxidized lipids with much higher affinity than human apoA-I. J Lipid Res, 2008. 49(11): p. 2302-11.

192. Yao, X., et al., Emerging Roles of Apolipoprotein E and Apolipoprotein A-I in the Pathogenesis and Treatment of Lung Disease. Am J Respir Cell Mol Biol, 2016. 55(2): p. 159-69.

193. Palinski, W., et al., Cloning of monoclonal autoantibodies to epitopes of oxidized lipoproteins from apolipoprotein E-deficient mice. Demonstration of epitopes of oxidized low density lipoprotein in human plasma. J Clin Invest, 1996. 98(3): p. 800-14.

194. Friedman, P., et al., Correlation of antiphospholipid antibody recognition with the structure of synthetic oxidized phospholipids. Importance of Schiff base formation and aldol condensation. J Biol Chem, 2002. 277(9): p. 7010-20.

195. Hörkkö, S., et al., Monoclonal autoantibodies specific for oxidized phospholipids or oxidized phospholipid-protein adducts inhibit macrophage uptake of oxidized low-density lipoproteins. J Clin Invest, 1999. 103(1): p. 117-28.

196. Yao, X., et al., Apolipoprotein mimetic peptides: a new approach for the treatment of asthma. Front Pharmacol, 2012. 3: p. 37.

197. Jha, A., et al., Inhaled Simvastatin Concomitantly Prevents Generation of Oxidized Phosphatidylcholine, Airway Inflammation, and Hyperresponsiveness in Allergen-Challenged Mice. Am J Respir Crit Care Med, 2016. 193: p. A1263.

198. Jha, A., et al., Inhibition of Oxidized Phosphatidylcholine Formation in the Lung of Allergen-Challenged Mice: Comparison of Effects for Inhaled Simvastatin and Corticosteroid Treatment. Am J Respir Crit Care Med, 2016. 193: p. A2463.

199. Oesterle, A., U. Laufs, and J.K. Liao, Pleiotropic Effects of Statins on the Cardiovascular System. Circulation Research, 2017. 120(1): p. 229-243.

200. Palmieri, M., et al., A Neutralizing Antibody Targeting Oxidized Phospholipids Promotes Bone Anabolism in Chow-Fed Young Adult Mice. Journal of Bone and Mineral Research, 2021. 36(1): p. 170-185.

201. Upchurch, C.M., et al., Targeting oxidized phospholipids by AAV-based gene therapy in mice with established hepatic steatosis prevents progression to fibrosis. Science Advances, 2022. 8(28): p. eabn0050.

202. Ambrogini, E., et al., Oxidation-specific epitopes restrain bone formation. Nature Communications, 2018. 9(1): p. 2193.

203. Sun, X., et al., Neutralization of Oxidized Phospholipids Ameliorates Non-alcoholic Steatohepatitis. Cell Metab, 2020. 31(1): p. 189-206 e8.

204. Sajti, E., et al., Oxidized Phospholipid Neutralizing Antibody Ameliorates Hyperoxia-Induced Lung Injury. Am J Respir Crit Care Med, 2022. 205: p. A5648.

205. Thimmulappa, R.K., et al., Oxidized phospholipids impair pulmonary antibacterial defenses: Evidence in mice exposed to cigarette smoke. Biochemical and Biophysical Research Communications, 2012. 426(2): p. 253-259.

206. Mohammadi, M., et al., Antinociception by the anti-oxidized phospholipid antibody E06. British Journal of Pharmacology, 2018. 175(14): p. 2940-2955.

207. Dong, Y., et al., Oxidized phosphatidylcholines found in multiple sclerosis lesions mediate neurodegeneration and are neutralized by microglia. Nature Neuroscience, 2021. 24(4): p. 489-503.

208. Eva, B., et al., Oxidative Damage and Bronchial Asthma, in Respiratory Diseases, D.M. Ghanei, Editor. 2012.

209. Holguin, F., Oxidative stress in airway diseases. Ann Am Thorac Soc, 2013. 10 Suppl: p. S150-7.

210. Hubbard, R. and A. Fogarty, The developing story of antioxidants and asthma. Thorax, 2004. 59(1): p. 3-4.

211. Milos, J., Z. Maria, and B. Eva, Oxidative Stress and Bronchial Asthma in Children—Causes or Consequences? Frontiers in Pediatrics, 2017. 5: p. 8.

212. Marwick, J.A., et al., Oxidative stress and steroid resistance in asthma and COPD: pharmacological manipulation of HDAC-2 as a therapeutic strategy. Expert Opinion on Therapeutic Targets, 2007. 11(6): p. 745-755.

213. Vasconcelos, L.H.C., et al., Uncovering the Role of Oxidative Imbalance in the Development and Progression of Bronchial Asthma. Oxid Med Cell Longev, 2021. 2021: p. 6692110.

214. Lin, J., et al., Acute cigarette smoke or extract exposure rapidly activates TRPA1-mediated calcium influx in primary human airway smooth muscle cells. Scientific Reports, 2021. 11(1).

215. Balestrini, A., et al., A TRPA1 inhibitor suppresses neurogenic inflammation and airway contraction for asthma treatment. Journal of Experimental Medicine, 2021. 218(4).

216. Gupta, R., et al., Structural basis of TRPA1 inhibition by HC-030031 utilizing species-specific differences. Sci Rep, 2016. 6: p. 37460.

217. Oka, T., et al., Xestospongin C, a novel blocker of IP3 receptor, attenuates the increase in cytosolic calcium level and degranulation that is induced by antigen in RBL-2H3 mast cells. British Journal of Pharmacology, 2002. 135(8): p. 1959-1966.

218. Gafni, J., et al., Xestospongins: potent membrane permeable blockers of the inositol 1,4,5-trisphosphate receptor. Neuron, 1997. 19(3): p. 723-33.

219. Hyvelin, J.M., et al., Human isolated bronchial smooth muscle contains functional ryanodine/caffeine-sensitive Ca-release channels. Am J Respir Crit Care Med, 2000. 162(2 Pt 1): p. 687-94.

220. Prakash, Y.S., M.S. Kannan, and G.C. Sieck, Regulation of intracellular calcium oscillations in porcine tracheal smooth muscle cells. Am J Physiol, 1997. 272(3 Pt 1): p. C966-75.

221. Bai, Y. and M.J. Sanderson, Modulation of the Ca2+ sensitivity of airway smooth muscle cells in murine lung slices. Am J Physiol Lung Cell Mol Physiol, 2006. 291(2): p. L208-21.

222. White, T.A., M.S. Kannan, and T.F. Walseth, Intracellular calcium signaling through the cADPR pathway is agonist specific in porcine airway smooth muscle. FASEB J, 2003. 17(3): p. 482-4.

223. Sharma, P., et al., Expression of the dystrophin-glycoprotein complex is a marker for human airway smooth muscle phenotype maturation. Am J Physiol Lung Cell Mol Physiol, 2008. 294(1): p. L57-68.

224. Burgess, J.K., et al., Phenotype and Functional Features of Human Telomerase Reverse Transcriptase Immortalized Human Airway Smooth Muscle Cells from Asthmatic and Non-Asthmatic Donors. Sci Rep, 2018. 8(1): p. 805.

225. Naureckas, E.T., et al., Bronchoalveolar lavage fluid from asthmatic subjects is mitogenic for human airway smooth muscle. Am J Respir Crit Care Med, 1999. 160(6): p. 2062-6.

226. Tran, T., et al., Laminin-binding integrin alpha7 is required for contractile phenotype expression by human airway myocytes. Am J Respir Cell Mol Biol, 2007. 37(6): p. 668-80.

227. Bai, Y., M. Zhang, and M.J. Sanderson, Contractility and Ca2+ signaling of smooth muscle cells in different generations of mouse airways. Am J Respir Cell Mol Biol, 2007. 36(1): p. 122-30.

228. Ray, A., et al., Current concepts of severe asthma. J Clin Invest, 2016. 126(7): p. 2394-403.

229. Pulfer, M.K. and R.C. Murphy, Formation of biologically active oxysterols during ozonolysis of cholesterol present in lung surfactant. J Biol Chem, 2004. 279(25): p. 26331-8.

230. Sabatini, K., et al., Characterization of two oxidatively modified phospholipids in mixed monolayers with DPPC. Biophys J, 2006. 90(12): p. 4488-99.

231. Fruhwirth, G.O., A. Loidl, and A. Hermetter, Oxidized phospholipids: from molecular properties to disease. Biochim Biophys Acta, 2007. 1772(7): p. 718-36.

232. Miller, Y.I., et al., Oxidation-specific epitopes are danger-associated molecular patterns recognized by pattern recognition receptors of innate immunity. Circ Res, 2011. 108(2): p. 235-48.

233. Lee, S., et al., Role of phospholipid oxidation products in atherosclerosis. Circ Res, 2012. 111(6): p. 778-99.

234. Lichtman, A.H., et al., Adaptive immunity in atherogenesis: new insights and therapeutic approaches. J Clin Invest, 2013. 123(1): p. 27-36.

235. Bochkov, V.N., et al., Oxidized phospholipids stimulate tissue factor expression in human endothelial cells via activation of ERK/EGR-1 and Ca(++)/NFAT. Blood, 2002. 99(1): p. 199-206.

236. Vaghasiya, J., et al., Oxidized Phosphatidylcholine Induces Release of Intracellular Ca2+ in Human Airway Smooth Muscle Cells. Am J Respir Crit Care Med, 2020. 201.

237. Vaghasiya, J., et al., Oxidized Phosphatidylcholines Mediate Airway Narrowing by Inducing Cytoplasmic Ca2+ Flux in Airway Smooth Muscle Cells. Am J Respir Crit Care Med, 2021. 203(9).

238. Grynkiewicz, G., M. Poenie, and R.Y. Tsien, A new generation of Ca2+ indicators with greatly improved fluorescence properties. J Biol Chem, 1985. 260(6): p. 3440-50.

239. Nemati, S., et al., Long-term self-renewable feeder-free human induced pluripotent stem cell-derived neural progenitors. Stem Cells Dev, 2011. 20(3): p. 503-14.

240. Tomishima, M., Neural induction – Dual SMAD inhibition., in Stembook. 2008.

241. Chambers, S.M., et al., Highly efficient neural conversion of human ES and iPS cells by dual inhibition of SMAD signaling. Nat Biotechnol, 2009. 27(3): p. 275-80.

242. Sutherland, D.P., et al., Canadian lung tissue biobank with associated clinical data supporting respiratory research for four decades. Canadian Journal of Respiratory, Critical Care, and Sleep Medicine, 2022. 6(1): p. 49-57.

243. Nassini, R., et al., Transient receptor potential ankyrin 1 channel localized to non-neuronal airway cells promotes non-neurogenic inflammation. PLoS One, 2012. 7(8): p. e42454.

244. Su, Y., et al., Identification of lung innervating sensory neurons and their target specificity. Am J Physiol Lung Cell Mol Physiol, 2022. 322(1): p. L50-L63.

245. Deshpande, D.A., et al., CD38/cyclic ADP-ribose signaling: role in the regulation of calcium homeostasis in airway smooth muscle. Am J Physiol Lung Cell Mol Physiol, 2005. 288(5): p. L773-88.

246. Deshpande, D.A., et al., CD38/cyclic ADP-ribose-mediated Ca2+ signaling contributes to airway smooth muscle hyper-responsiveness. FASEB J, 2003. 17(3): p. 452-4.

247. Prakash, Y.S., Airway smooth muscle in airway reactivity and remodeling: what have we learned? Am J Physiol Lung Cell Mol Physiol, 2013. 305(12): p. L912-33.

248. Prakash, Y.S., Emerging concepts in smooth muscle contributions to airway structure and function: implications for health and disease. Am J Physiol Lung Cell Mol Physiol, 2016. 311(6): p. L1113-l1140.

249. Jude, J.A., et al., Calcium signaling in airway smooth muscle. Proc Am Thorac Soc, 2008. 5(1): p. 15-22.

250. JE Bourke, et al., Smooth Muscle Cells, in Encyclopedia of Respiratory Medicine (Second Edition),, S.M. Janes, Editor. 2022, Academic Press,. p. 37-51.

251. Fruhwirth, G., A. Loidl, and A. Hermetter, Oxidized phospholipids: From molecular properties to disease. Biochimica Et Biophysica Acta-Molecular Basis of Disease, 2007. 1772(7): p. 718-736.

252. Li, R., et al., Identification of prostaglandin E2 receptor subtype 2 as a receptor activated by OxPAPC. Circ Res, 2006. 98(5): p. 642-50.

253. Al-Shawaf, E., et al., Short-term stimulation of calcium-permeable transient receptor potential canonical 5-containing channels by oxidized phospholipids. Arterioscler Thromb Vasc Biol, 2010. 30(7): p. 1453-9.

254. Caceres, A.I., et al., A sensory neuronal ion channel essential for airway inflammation and hyperreactivity in asthma. Proc Natl Acad Sci U S A, 2009. 106(22): p. 9099-104.

255. Jha, A., et al., A role for transient receptor potential ankyrin 1 cation channel (TRPA1) in airway hyper-responsiveness? Can J Physiol Pharmacol, 2015. 93(3): p. 171-6.

256. Bolz, S.S., et al., Oxidized LDL increases the sensitivity of the contractile apparatus in isolated resistance arteries for Ca(2+) via a rho- and rho kinase-dependent mechanism. Circulation, 2000. 102(19): p. 2402-10.

257. Ahn, T.Y., et al., Enhanced contractility of rabbit corpus cavernosum smooth muscle by oxidized low density lipoproteins. Int J Impot Res, 1999. 11(1): p. 9-14.

258. Liu, C., T. Tazzeo, and L.J. Janssen, Isoprostane-induced airway hyperresponsiveness is dependent on internal Ca2+ handling and Rho/ROCK signaling. Am J Physiol Lung Cell Mol Physiol, 2006. 291(6): p. L1177-84.

259. Galle, J., E. Bassenge, and R. Busse, Oxidized low density lipoproteins potentiate vasoconstrictions to various agonists by direct interaction with vascular smooth muscle. Circ Res, 1990. 66(5): p. 1287-93.

260. Sanderson, M.J., Exploring lung physiology in health and disease with lung slices. Pulm Pharmacol Ther, 2011. 24(5): p. 452-65.

261. Waldeck, B., Beta-adrenoceptor agonists and asthma--100 years of development. Eur J Pharmacol, 2002. 445(1-2): p. 1-12.

262. Walker, J.K., et al., New perspectives regarding β(2) -adrenoceptor ligands in the treatment of asthma. Br J Pharmacol, 2011. 163(1): p. 18-28.

263. Penn, R.B., Embracing emerging paradigms of G protein-coupled receptor agonism and signaling to address airway smooth muscle pathobiology in asthma. Naunyn Schmiedebergs Arch Pharmacol, 2008. 378(2): p. 149-69.

264. Fatani, S.H., Biomarkers of oxidative stress in acute and chronic bronchial asthma. J Asthma, 2014. 51(6): p. 578-84.

265. Kwon, H.S., et al., Hyperoxidized peroxiredoxins in peripheral blood mononuclear cells of asthma patients is associated with asthma severity. Life Sci, 2012. 90(13-14): p. 502-8.

266. Marwick, J.A., et al., Oxidative stress modulates theophylline effects on steroid responsiveness. Biochem Biophys Res Commun, 2008. 377(3): p. 797-802.

267. Sharma, P., et al., Epithelium-dependent modulation of responsiveness of airways from caveolin-1 knockout mice is mediated through cyclooxygenase-2 and 5-lipoxygenase. Br J Pharmacol, 2012. 167(3): p. 548-60.

268. McGovern, T.K., et al., Evaluation of respiratory system mechanics in mice using the forced oscillation technique. J Vis Exp, 2013(75): p. e50172.

269. Jha, A., et al., Prophylactic benefits of systemically delivered simvastatin treatment in a house dust mite challenged murine model of allergic asthma. Br J Pharmacol, 2018. 175(7): p. 1004-1016.

270. Butt, E., et al., cAMP- and cGMP-dependent protein kinase phosphorylation sites of the focal adhesion vasodilator-stimulated phosphoprotein (VASP) in vitro and in intact human platelets. J Biol Chem, 1994. 269(20): p. 14509-17.

271. Nayak, A.P., et al., Regulation of ovarian cancer G protein-coupled receptor-1 expression and signaling. Am J Physiol Lung Cell Mol Physiol, 2019. 316(5): p. L894-l902.

272. Addison, K.J., et al., A Novel in vivo System to Test Bronchodilators. J Infect Pulm Dis, 2017. 3(1).

273. Bates, J.H., et al., Oscillation mechanics of the respiratory system. Compr Physiol, 2011. 1(3): p. 1233-72.

274. Cattani-Cavalieri, I., et al., Real-Time cAMP Dynamics in Live Cells Using the Fluorescent cAMP Difference Detector In Situ. JoVE, 2024(205): p. e66451.

275. Tewson, P.H., et al., New DAG and cAMP Sensors Optimized for Live-Cell Assays in Automated Laboratories. J Biomol Screen, 2016. 21(3): p. 298-305.

276. Boterman, M., et al., Potentiation of beta-adrenoceptor function in bovine tracheal smooth muscle by inhibition of protein kinase C. Eur J Pharmacol, 2005. 516(1): p. 85-92.

277. Boterman, M., et al., Protein kinase C potentiates homologous desensitization of the beta(2)-adrenoceptor in bovine tracheal smooth muscle. Eur J Pharmacol, 2006. 529(1-3): p. 151-156.

278. Van Ly, D., et al., Characterising the mechanism of airway smooth muscle β2 adrenoceptor desensitization by rhinovirus infected bronchial epithelial cells. PLoS One, 2013. 8(2): p. e56058.

279. Yadav, S., et al., Autocrine regulation of airway smooth muscle contraction by diacylglycerol kinase. Journal of Cellular Physiology, 2022. 237(1): p. 603-616.

280. Nayak, A.P., et al., Cooperativity between β-agonists and c-Abl inhibitors in regulating airway smooth muscle relaxation. FASEB J, 2021. 35(7): p. e21674.

281. Koziol-White, C., et al., Budesonide enhances agonist-induced bronchodilation in human small airways by increasing cAMP production in airway smooth muscle. Am J Physiol Lung Cell Mol Physiol, 2020. 318(2): p. L345-L355.

282. Meurs, H., et al., Regulation of the beta-receptor-adenylate cyclase system in lymphocytes of allergic patients with asthma: possible role for protein kinase C in allergen-induced nonspecific refractoriness of adenylate cyclase. J Allergy Clin Immunol, 1987. 80(3 Pt 1): p. 326-39.

283. Rex, E.B., et al., Identification of RanBP 9/10 as interacting partners for protein kinase C (PKC) gamma/delta and the D1 dopamine receptor: regulation of PKC-mediated receptor phosphorylation. Mol Pharmacol, 2010. 78(1): p. 69-80.

284. Bansal, S.K., et al., Increased levels of protein kinase C in lymphocytes in asthma: possible mechanism of regulation. Eur Respir J, 1997. 10(2): p. 308-13.

285. Busse, W.W., et al., The Inhaled Steroid Treatment As Regular Therapy in Early Asthma (START) study 5-year follow-up: effectiveness of early intervention with budesonide in mild persistent asthma. J Allergy Clin Immunol, 2008. 121(5): p. 1167-74.

286. Barisione, G., et al., Beta-Adrenergic Agonists. Pharmaceuticals (Basel), 2010. 3(4): p. 1016-1044.

287. Scelo, G., et al., Analysis of comorbidities and multimorbidity in adult patients in the International Severe Asthma Registry. Ann Allergy Asthma Immunol, 2023.

288. Sood, A., et al., Effect of allergen inhalation on airway oxidant stress, using exhaled breath condensate 8-isoprostane, in mild asthma. J Asthma, 2013. 50(5): p. 449-56.

289. van der Vliet, A., Y.M.W. Janssen-Heininger, and V. Anathy, Oxidative stress in chronic lung disease: From mitochondrial dysfunction to dysregulated redox signaling. Mol Aspects Med, 2018. 63: p. 59-69.

290. To, T., et al., Does early life exposure to exogenous sources of reactive oxygen species (ROS) increase the risk of respiratory and allergic diseases in children? A longitudinal cohort study. Environ Health, 2022. 21(1): p. 90.

291. Vasconcelos, L.H.C., et al., Uncovering the Role of Oxidative Imbalance in the Development and Progression of Bronchial Asthma. Oxid Med Cell Longev, 2021. 2021: p. 6692110.

292. Erzurum, S.C., New Insights in Oxidant Biology in Asthma. Ann Am Thorac Soc, 2016. 13 Suppl 1(Suppl 1): p. S35-9.

293. Nadeem, A., A. Masood, and N. Siddiqui, Oxidant--antioxidant imbalance in asthma: scientific evidence, epidemiological data and possible therapeutic options. Ther Adv Respir Dis, 2008. 2(4): p. 215-35.

294. Vincenzo, S.D., et al., Oxidative Stress, Environmental Pollution, and Lifestyle as Determinants of Asthma in Children. Biology (Basel), 2023. 12(1).

295. Usui, K., et al., Site-specific modification of Alzheimer's peptides by cholesterol oxidation products enhances aggregation energetics and neurotoxicity. Proc Natl Acad Sci U S A, 2009. 106(44): p. 18563-8.

296. Jha, A., et al., Peroxidation of Phosphatidylcholine: A Signature for Allergen-Induced Airway Responses and Allergen Specificity. Am J Respir Crit Care Med, 2017. 195: p. A7338.

297. Yeang, C., et al., Reduction of myocardial ischaemia–reperfusion injury by inactivating oxidized phospholipids. Cardiovascular Research, 2018. 115(1): p. 179-189.

298. Pascoe, C.D., et al., The importance of reporting house dust mite endotoxin abundance: impact on the lung transcriptome. American Journal of Physiology-Lung Cellular and Molecular Physiology, 2020. 318(6): p. L1229-L1236.

299. Jha, A., Effect of simvastatin on airway inflammation, remodelling and hyperreactivity in a house dust mite challenged murine model of allergic asthma. 2018, University of Manitoba. p. 234.

300. Raemdonck, K., et al., $CD4^+$ and $CD8^+$ T cells play a central role in a HDM driven model of allergic asthma. Respir Res, 2016. 17: p. 45.

301. Lopuhaä, C.E., et al., Allergen-induced bronchial inflammation in house dust mite-allergic patients with or without asthma. Clin Exp Allergy, 2002. 32(12): p. 1720-7.

302. Lukawska, J.J., et al., Imaging Inflammation in Asthma: Real Time, Differential Tracking of Human Neutrophil and Eosinophil Migration in Allergen Challenged, Atopic Asthmatics in Vivo. EBioMedicine, 2014. 1(2-3): p. 173-80.

303. Wang, L., et al., Single-cell transcriptomic analysis reveals the immune landscape of lung in steroid-resistant asthma exacerbation. Proc Natl Acad Sci U S A, 2021. 118(2).

304. Smith, L.J., et al., Reduced superoxide dismutase in lung cells of patients with asthma. Free Radic Biol Med, 1997. 22(7): p. 1301-7.

305. Comhair, S.A. and S.C. Erzurum, Redox control of asthma: molecular mechanisms and therapeutic opportunities. Antioxid Redox Signal, 2010. 12(1): p. 93-124.

306. Dong, Y. and V.W. Yong, Oxidized phospholipids as novel mediators of neurodegeneration. Trends Neurosci, 2022. 45(6): p. 419-429.

307. Haider, L., et al., Oxidative damage in multiple sclerosis lesions. Brain, 2011. 134(Pt 7): p. 1914-24.

308. Qin, J., et al., Oxidized phosphatidylcholine formation and action in oligodendrocytes. J Neurochem, 2009. 110(5): p. 1388-99.

309. Dunigan-Russell, K., et al., Scavenger receptor BI attenuates oxidized phospholipid-induced pulmonary inflammation. Toxicology and Applied Pharmacology, 2023. 462: p. 116381.

310. Ozaras, R., et al., Changes in malondialdehyde levels in bronchoalveolar fluid and serum by the treatment of asthma with inhaled steroid and beta2-agonist. Respirology, 2000. 5(3): p. 289-92.

311. Handa, J.T., et al., Lipoprotein(A) with An Intact Lysine Binding Site Protects the Retina From an Age-Related Macular Degeneration Phenotype in Mice (An American Ophthalmological Society Thesis). Trans Am Ophthalmol Soc, 2015. 113: p. T5.

312. Buga, G.M., et al., D-4F reduces EO6 immunoreactivity, SREBP-1c mRNA levels, and renal inflammation in LDL receptor-null mice fed a Western diet. J Lipid Res, 2008. 49(1): p. 192-205.

313. Gowdy, K.M., et al., Novel Mechanisms of Ozone-Induced Pulmonary Inflammation and Resolution, and the Potential Protective Role of Scavenger Receptor BI. Res Rep Health Eff Inst, 2021. 2021(204): p. 1-49.

314. Wyatt, T.A., et al., Malondialdehyde-acetaldehyde-adducted protein inhalation causes lung injury. Alcohol, 2012. 46(1): p. 51-9.

315. Li, Y., et al., Elevated Expression of IL-33 and TSLP in the Airways of Human Asthmatics In Vivo: A Potential Biomarker of Severe Refractory Disease. The Journal of Immunology, 2018. 200(7): p. 2253-2262.

316. Préfontaine, D., et al., Increased expression of IL-33 in severe asthma: evidence of expression by airway smooth muscle cells. J Immunol, 2009. 183(8): p. 5094-103.

317. Marshall, C., et al., IFNγ-mediated IL-33 production is dependent on the aryl hydrocarbon receptor in human bronchial epithelial cells. Cytokine, 2023. 172: p. 156414.

318. Ouyang, W. and A. O'Garra, IL-10 Family Cytokines IL-10 and IL-22: from Basic Science to Clinical Translation. Immunity, 2019. 50(4): p. 871-891.

319. Coomes, S.M., et al., CD4(+) Th2 cells are directly regulated by IL-10 during allergic airway inflammation. Mucosal Immunol, 2017. 10(1): p. 150-161.

320. HOHLFELD, J.M., et al., Dysfunction of Pulmonary Surfactant in Asthmatics after Segmental Allergen Challenge. American Journal of Respiratory and Critical Care Medicine, 1999. 159(6): p. 1803-1809.

321. Lewis, B.W., et al., Chronic Allergen Challenge Induces Corticosteroid Insensitivity With Persistent Airway Remodeling and Type 2 Inflammation. Front Pharmacol, 2022. 13: p. 855247.

322. Crystal, R.G., et al., Airway epithelial cells: current concepts and challenges. Proc Am Thorac Soc, 2008. 5(7): p. 772-7.

323. Saunders, R.M., et al., Stressed out - The role of oxidative stress in airway smooth muscle dysfunction in asthma and COPD. Free Radical Biology and Medicine, 2022. 185: p. 97-119.

324. Teyani, R.L., F. Moghaddam, and N.H. Moniri, ROS-mediated regulation of β2AR function: Does oxidation play a meaningful role towards β2-agonist tachyphylaxis in airway obstructive diseases? Biochem Pharmacol, 2024. 226: p. 116403.

325. Rambacher, K.M. and N.H. Moniri, Cysteine redox state regulates human β2-adrenergic receptor binding and function. Sci Rep, 2020. 10(1): p. 2934.

326. Barnes, P.J., Oxidative Stress in Chronic Obstructive Pulmonary Disease. Antioxidants (Basel), 2022. 11(5).

327. Webb, B.L., S.J. Hirst, and M.A. Giembycz, Protein kinase C isoenzymes: a review of their structure, regulation and role in regulating airways smooth muscle tone and mitogenesis. Br J Pharmacol, 2000. 130(7): p. 1433-52.

328. Tang, W., et al., Oxidized Phospholipid Neutralizing Antibody Ameliorates Pulmonary Fibrosis. Am J Respir Crit Care Med, 2024. 209: p. A3266.

329. Pandey, D., et al., Requirement of TRPA1 in Oxidized Phosphatidylcholine Induced Pro-inflammatory Gene Expression by Human Airway Fibroblasts. Am J Respir Crit Care Med, 2024. 209: p. A5254.

330. O'Callaghan, M., et al., Comparing the Effects of Oxidised and Non-oxidised Lipids on Fibrogenesis in IPF. Am J Respir Crit Care Med, 2024. 209: p. A2617.

331. Dalvand, A., et al., Oxidized Phospholipids Suppress Glucocorticoid Transactivation and Transrepression Regulation of Gene Transcription in Airway Epithelial Cells. Am J Respir Crit Care Med, 2024. 209: p. A3270.